VALIDATING THE MOUSE MODEL FOR OCULAR SURFACE RESREACH AND ASSESSING MORPHOLOGICAL CHANGES IN THE DRY EYE PALPEBRAL CONJUNCTIVA

VALIDATING THE MOUSE MODEL FOR OCULAR SURFACE RESEARCH AND ASSESSING MORPHOLOGICAL CHANGES IN THE DRY EYE PALPEBRAL CONJUNCTIVA

By

Johanna Tukler Henriksson, BS Opt.

DISSERTATION

In partial satisfaction of the requirements for the degree of

DOCTOR OF PHILOSOPHY

in

PHYSIOLOGICAL OPTICS

Presented to the Graduate Faculty of the

College of Optometry
University of Houston

May 2011

Approved:

_____
Jan P.G. Bergmanson, OD, PhD, PhD hc, D Sc (Chair)

_____
Peter J. Gierow, PhD

_____
Alison M. McDermott, PhD

_____
William L. Miller, OD, PhD

_____
Stephen C. Pflugfelder, MD

Committee in Charge

Dedication

Till min morfar,

Som varit min största supporter så länge jag kan minas. Tyvärr fick du inte uppleva den här dagen, men jag vet precis hur stolt du hade varit.

To my Grandfather,

For always believing in me and encouraging me to follow my dreams. Unfortunately you never got a chance to experience this day, but I know how proud my accomplishments would have made you.

Acknowledgements

Dissertation Advisor/Committee Chair:

Jan P.G. Bergmanson, OD, PhD

I owe a special thank you to my dissertation advisor Dr Bergmanson, who introduced me to this opportunity nine years ago when I came over to Houston as an exchange student. Thank you for your tremendous encouragement, support and guidance throughout this journey. I will be forever grateful for everything you have done for me over the last five years.

Chefen – Tusen tack för fem fantastiska år som jag aldrig kommer att glömma!

I would like to extend my warmest thank you to:

My Dissertation Committee:

Peter J. Gierow, PhD
Alison M. McDermott, PhD
William L. Miller, OD, PhD
Stephen C. Pflugfelder, MD

My Co-authors:

Jan P.G. Bergmanson OD, PhD
Anthony J. Bron, BSc
Alan R. Burns, PhD
Cintia S. De Paiva, MD
William Farley
Alison M. McDermott, PhD
Stephen C. Pflugfelder, MD
James E. Walsh, PhD

Dean of the Graduate Program:

Laura J. Frishman, PhD

Graduate Student Administration:

Michele Murphy

Audio Visual Department:

Special thank you to Sze Quan and Kim Thompson

Funding:

NEI Core Grant P30 EY007551 to University of Houston College of Optometry
Optikbranschen (Stockholm, Sweden)
Texas Eye Research and Technology Center (TERTC)
2009 William C Ezell Fellowship sponsored by Bausch and Lomb
2010 William C Ezell Fellowship sponsored by Vistakon

Last but not least I would like to thank my family, who over the last five years has come to love Texas as much as I do, for all your support and numerous visits. I could not have done it without you!

By

Johanna Tukler Henriksson, BS Opt

DISSERTATION

In partial fulfillment of requirements of the degree of

DOCTOR OF PHILOSOHPY

in

PHYSIOLOGICAL OPTICS

Presented to the
Graduate faculty

of the

College of Optometry
University of Houston

May, 2011

General Abstract

Purpose: The young adult mouse has become the preferred animal model in many areas of ophthalmic research. For this reason, there is a need to validate its use in different experimental settings and to assess its applicability to the human. The purpose of this research was to firstly, evaluate the normal mouse cornea and conjunctiva, secondly to utilize the mouse as an animal model, to investigate structural changes occurring in the dry eye and thirdly to investigate ocular UVR transmittance of this small eye.

Methods: A total of 45 animals were utilized for these experiments. Ocular dryness was induced in 16 by administration of scopolamine hydrobromide (0.5mg/0.2ml) QID, and exposure to a dry environment for 5 (DS5) or 10 (DS10) days. After euthanization the corneas or eye lids were fixed either in 2% glutaraldehyde and processed according to an established histology protocol for light- (LM) and transmission electron microscopy (TEM) or in 10% formalin and embedded in paraffin. Counts or measurements were obtained utilizing well defined specific reference points allowing the observer to conduct accurate and repeatable intra-corneal or intra-conjunctival measurements. Goblet cell density was investigated both on resin and paraffin embedded tissues with a variety stains and histological protocols.

UVR transmittance of the whole mouse eye, the cornea and the crystalline lens was also investigated. Immediately after euthanization the mouse eye was placed under a 0.2 mm diameter detecting fiber optic illuminated by an Oceans Optics deuterium/halogen source (DT-MINI-2-GS). The data were recorded and analyzed with an Ocean Optics spectrometer (USB4000) and analyzed in Matlab.

Results: The mouse epithelium contributed to 1/3 and the stroma to 2/3 of the total corneal thickness. A statistically significant ($P < 0.001$) decrease in overall thickness was found in the periphery compared to the center. The central cornea had an average of 50 ± 2 lamellae with an average thickness of 2.1 µm versus 36 ± 3 and 1.8 µm peripherally ($P < 0.005$). The mouse did not possess an anterior limiting lamina (ALL).

Near the junction between the lid margin and the normal palpebral conjunctiva the epithelium had an average thickness of 46 ± 11 µm and 9 ± 2 cell layers, versus 42 ± 7 µm and 8 ± 1 layers in the DS5 ($P > 0.05$) and 38 ± 6 µm and 7 ± 1 layers in the DS10 ($P < 0.05$). In the goblet cell populated palpebral region the normal conjunctival epithelium averaged 24 ± 4 µm and was significantly ($P < 0.05$) thicker than in the DS5 (18 ± 3 µm) and the DS10 (19 ± 3 µm). In the control 43% of the goblet cells had epithelial coverage, compared to 58% for the DS5 and 63% for the DS10 ($P < 0.05$). Some stains indicated a decreased number of goblet cells in the dry eye (PAS and Alcian blue), while (MUC5AC, histology) did not.

The mouse had a UVR transmittance cut off at 280 nm for the cornea and 310 nm for the crystalline lens. 50% absorption of UVR was achieved at 330 nm and 375 nm by the cornea and crystalline lens respectively. The combined transmittance spectra of the cornea and the lens compared well with the total UVR transmittance for the whole eye and, thus, supported the validity of our findings.

Conclusions: The mouse cornea becomes significantly thinner towards the periphery and this was explained by a decreased thickness of both the epithelium and the stroma. Stromal thinning was caused by a reduction in number of lamellae towards the periphery.

This finding suggests that not all lamellae cross the cornea limbus to limbus. A notable difference between the mouse and the human cornea is the absence of an ALL in the former.

The palpebral conjunctival epithelium decreased in thickness in the dry eye and the goblet cell access to the surface appears to be inhibited by surrounding epithelial cells, which potentially may slow down their migration to the surface. Goblet cell density differed depending on stain used for evaluation of mucous secreting cells, suggesting that there may be different subtypes of goblet cells on the ocular surface or may be PAS and Alcian blue are mucin specific and not goblet cell specific.

It is important to be aware of the ultrastructural and dimensional differences between the mouse and the human cornea when utilizing the mouse as a model. The mouse conjunctival epithelium has a structure similar to the human and appears to be viable model for conjunctival and dry eye research. However, due to the differences between the mouse and human in UVR transmittance, it is concluded that the mouse is not an ideal model for UVR experiments.

Table of Contents

List of Figures

List of Tables

List of Abbreviations

ALL: Anterior limiting lamina

ANOVA: One way analysis of variance

BSS: Basic salt solution

DAB: Diaminobenzidine

SD: Standard deviation

SEM: Standard error of the mean

DS10: Experimental ocular surface desiccating stress, 10 days

DS5: Experimental ocular surface desiccating stress, 5 days

EDF: Electron dense formation

LM: Light microscope

PAS: Periodic acid-schiff stain

PLL: Posterior limiting lamina

QID: Four times per day

SURS: Systematic random uniform sampling

Sv: Surface density

TEM: Transmission electron microscopy

UT: Untreated

UVR: Ultraviolet radiation

Vv: Volume fraction

Chapter 1 - General Introduction

Introduction

The cornea, conjunctiva and limbus form the ocular surface. The human cornea has an average diameter of 11.7 mm horizontally and 10.6 mm vertically [1]. In the human, the cornea is thinner centrally where it measures approximately 535 µm compared to 657 µm at the thicker periphery [2]. It is a transparent avascular tissue that is responsible for two thirds (40D) of the eyes' refractive power and is composed of five layers, epithelium, anterior limiting lamina (ALL), stroma, posterior limiting lamina (PLL) and endothelium.

The epithelium is the outermost layer. It has an average thickness of 50 µm and makes up 10% of the corneal thickness in the human. It is composed of five to seven cell layers of cells that have undergone different stages of differentiation. The basal cells are tall, columnar and form the most internal layer of the epithelium. These cells attach to their basement membrane via hemidesmosomes. Above the basal cells there are two layers of intermediate sized cells, wing cells, which attach to each other by desmosomes.

Outermost, the cornea has two to four layers of flattened squamous cells held together by desmosomes. Tight junctions (zonula occludentes) are present between the superficial cells and function as a barrier by preventing fluid to leak into the cornea. Additional functions of the epithelium include being a physical barrier against microorganisms, contributing to an optically smooth surface by its smooth outline and by secreting mucins to the tear film and assisting in ultraviolet (UVR) absorption.

The ALL is approximately 8 µm thick and located internal the epithelial basement membrane. It is acellular, except for perforating nerve fibers and is composed of randomly oriented type I collagen fibrils. One function of the ALL is to provide attachments for the epithelial basement membrane by collagen VII fibrils. These collagen

VII fibrils fuse with the epithelial basement membrane anteriorly and attach to anchorning plaques found in the ALL posteriorly.

The stroma with its approximate 500 μm thickness makes up 90% of the thickness of the cornea and consists primarily of collagenous extracellular matrix, with nerve fibers and scattered keratocytes and immune cells. The keratocytes are the most abundant cell type in the stroma, they reside mainly between the lamellae and are responsible for synthesis and maintenance of collagen and proteoglycans. Collagens are a family of proteins, composed of three collagen polypeptide α-chains, that form a superhelix. Collagen polypeptide chains are synthesized on membrane bound ribosomes in the keratocyte and dispensed into the endoplasmic reticulum as pro-α chains. Each chain is subsequently hydroxylated, glycosylated and combined with two others to form a hydrogen-bonded, triple stranded molecule, procollagen. The procollagen molecule is secreted into the extracellular matrix and the propeptides are removed by enzymes. This step converts the procollagen molecule to a mature collagen molecule, which self assemble into collagen fibrils [3]. The main component of the stroma, collagen type I, contributes to physical strength, stability of corneal shape and transparency. Collagen type III is involved in stromal repair, type IV is the major component of the lamina densa of the corneal basement membranes. Collagen types V, VI are also present. In the corneal stroma the collagen fibrils are organized into flattened sheets, lamellae. The human cornea has an average of 242 ± 4 lamellae [4]. The distribution of corneal lamellae differs between the anterior and posterior stroma. The anterior stroma has 50% more lamellae and these anterior lamellae are thinner and more intertwined compared to the posterior stroma where the lamellae are thicker and arranged in flattened sheets running parallel to

the PLL [4]. Most studies report that the corneal lamellae bridge from limbus to limbus, however a recent study showed evidence that this might not be the case [5].

The second largest group of proteins in the corneal stroma is the proteoglycans. They consist of a core protein, namely lumican, keratocan, mimecan or decorin, and one or more glycosaminoglycan side chains e.g keratan- or dermatan sulfate. The proteoglycans are present between the collagen fibrils, and their function is to maintain regular spacing between the collagen fibrils which is necessary for corneal transparence [6].

The PLL, the basement membrane of the corneal endothelium is composed of collagen type IV. The material in this layer is synthesized by the corneal endothelial cells. The PLL increases in thickness from 3 µm at birth with approximately 1 µm being added per decade and is comprised of a thin banded pre-natal region and a thicker non-banded post-natal region [7].

The endothelium is a 5 µm thick layer of single flat predominantly hexagonal cells that do not regenerate. These cells have a high metabolic activity as seen by the presence of an abundance of organelles. Tight junctions are present to restrict fluid flow between cells and gap junctions aid in cell to cell communication. The main function of the endothelium is to maintain the transparency of the cornea by regulating the passage of fluid in both directions [7].

The rabbit has for many years been the preferred animal model for studies of the mammalian ocular surface. Recently, the young (6-8 weeks) adult mouse has become widely utilized in research on the cornea and conjunctiva as well as studies involving other ocular regions such as the retina or the crystalline lens [8-9]. The main reason for the increased utilization of the mouse is that its genome has been sequenced and there are

many different transgenic and knockouts available for different types of research. Additional advantages with the mouse include that it is easy to breed, it grows rapidly and it is cost effective [10-12].

Although the mouse is a widely used model, current literature contains incomplete data in several areas of mouse ocular surface research and, therefore, its human applicability is not assured. Mouse corneal morphology and its dimensions are one area where the current literature contains limited data. To date, there are only a few reports regarding the overall central corneal and central stromal thickness available. Discrepancies are found among these reports, which may be related to variations in measuring techniques, strains and ages of mice used [12-15]. In addition to these disagreements, available literature only provides central corneal measurements and no information is available about the mouse peripheral cornea. Similar to the human cornea and that of other mammals, the mouse cornea is reported to contain five corneal layers (epithelium, anterior limiting lamina, stroma, posterior limiting lamina and endothelium) as described by [9], although, the presence of an anterior limiting lamina has been disputed [16-17].

The **first aim** of this dissertation was designed to investigate the **hypothesis that the shape, relative dimension and morphology of the overall mouse cornea and its components are similar to the human cornea both centrally and peripherally**. The purpose of this study was to assess and validate the mouse as a mammalian model for corneal research by using a histological approach and to provide needed dimensional and morphological information on the cornea in the three most commonly used strains of mice (chapter 3).

Over the last century several studies have utilized different methodologies to measure the human corneal thickness centrally and peripherally. These studies have all reached the same conclusion, that the human cornea is thinner centrally and thicker peripherally [18-23]. However, an explanation of this thickness difference has yet to be offered. Increased understanding of corneal stromal architecture will aid in understanding the effects of stromal thinning occurring in for example keratoconus (KC), but also to better predict outcomes of surgical procedures involving the stroma.

Most studies concerning the structure of the mammalian cornea state that the stromal lamellae bridge limbus to limbus [24-27] but a recent report provided evidence that this may not be the case [5]. In this study, electron dense formations are described and these appear to be lamellar terminations within the central corneal region and, therefore, contradicting the general belief that lamellae stretch from one side of the cornea to the other. This discovery raises the question whether the peripheral and central cornea have the same number of lamellae in a transverse section.

Keratocytes are the principal cells of the corneal stroma and it has been estimated that the adult cornea has 2.4 million keratocytes [28-30]. When these cells are observed in a transverse section by TEM they are primarily noted to be located between lamellae [31-33]. Is it therefore possible, that the number of keratocytes, present in a transverse section, may provide an indication of lamellar contribution to the corneal thickness at a particular corneal location?

One purpose of the **second aim** of this dissertation was to utilize the mouse as an animal model **to examine the general belief that corneal stromal lamellae span from limbus to limbus**. Another question this aim intended to investigate was **whether a**

keratocyte count in a transverse section can give an indication of number of lamellae present at a specific corneal location (chapter 4).

The conjunctiva is another tissue forming the ocular surface. This tissue is comprised of three regions, the palpebral, fornix and bulbar conjunctiva. It is composed of two different layers, the epithelium and the stroma. The conjunctival epithelium is stratified non-keratinized, has two to four layers of cells and contains goblet cells. In the human, the goblet cells are present in all three regions; however they are more numerous in the fornix and the palpebral parts. Goblet cells are mucin secreting cells. Mucins are a group of large heavily glycosylated glycoproteins with 50-80% of their weight comprised of carbohydrates. The mucin monomers are synthesized and N-glycosylated in the rough endoplasmic reticulum where they form disulfide linked dimers before they are transported to the Golgi complex. In the Golgi complex the mucin precursors are O-glycosylated and packaged for secretion [34]. The mucins can be membrane spanning, gel forming or small soluble. Currently 11 mucins have been detected on the ocular surface [35-36]. Most of the mucins including MUC 1, 2, 4, 13, 15, 16, 17, 19, 20 are produced by the corneal and conjunctival epithelium, however MUC5AC is produced by the goblet cells and MUC7 by the lacrimal gland. The membrane spanning mucins such as MUC 1,4 and 16 make up the glycocalyx which extends from the tips of the microplicae on the outside of the corneal and conjunctival epithelial cells. The functions of the mucins are to act as a wetting agent to spread the tears over the ocular surface and/or to be disadhesive to prevent e.g. pathogens from adhering to the ocular surface.

The conjunctival stroma resides below the epithelium and consists of the adenoid and the deep fibrous layer. The adenoid layer is the most superficial layer and it contains

capillaries, nerves and lymphatics. The deep fibrous layer is comprised of larger blood vessels, nerves and dense collagen fibers that provide strength. In the palpebral conjunctiva the deep fibrous layer is replaced by the tarsal plate. In the human, the tarsal plate of the superior lid houses the accessory palpebral lacrimal gland.

Nerves of both sensory and autonomic origin innervate the conjunctival epithelium and stroma. The sensory innervation derives from the trigeminal nerve (CN V), with the ophthalmic division innervating the superior- and the maxillary division the inferior conjunctiva. Over 60 % of the conjunctival blood vessels receive dual autonomic innervation, sympathetic fibers from (superior cervical ganglion) and parasympathetic from (pterygopalatine ganglion CN VII) [37]. In addition, parasympathetic innervation has been reported to regulate goblet cell secretion [38].

Dry eye or keratoconjunctivitis sicca is a disease that affects both the cornea and the conjunctiva. 'Dry eye is defined as a multifactorial disease of the tears and ocular surface that results in symptoms of discomfort, visual disturbance and tear film instability with potential damage to the ocular surface. It is accompanied by increased osmolarity of the tear film and inflammation of the ocular surface'[39]. Almost 5 million Americans, 50 years or older - 3.23 million women and 1.68 million men – have dry eyes [40-41]. However, the DEWS report suggested that tens of millions more have less severe symptoms, which may become manifest only during stressful conditions for the ocular surface. These conditions include, for instance, contact lens wear, airline travel, dry atmosphere working conditions etc [42].

Human specimens are not practical to use for ethical reasons. As a consequence, studies into the pathology of the dry eye have required animal models, and

currently most studies have utilized rats or mice [43-45]. The development of the mouse dry eye model has proved useful in assessing several tear functions and properties [43 45-47].

The palpebral conjunctival epithelium is another area along the ocular surface where the literature surprisingly has limited histological information to offer, both in humans and in mice [9 48]. Current literature have reported decreased amounts of MUC5AC mRNA [49] and a decreased number of goblet cells in the dry eye when these cells have been stained and counted with PAS and Alcian Blue [43 46 50]. However, these findings have never been confirmed ultrastructurally. The literature also contains sparse information with regards to morphological alterations occurring due to a change in the tears and their ability to provide for a wet and healthy ocular surface. What morphologically happens to the conjunctival epithelium and to its goblet cells in the dry eye is not clearly understood. Ultrastructural studies evaluating the normal and the dry eye conjunctiva therefore are needed. By studying morphological changes of the palpebral conjunctival epithelium in a well established dry eye model, my understanding of the dry eye can be enhanced.

The **third aim** of this dissertation was to investigate the **hypothesis that there will be a decrease in goblet cell size, density and epithelial dimensions in the palpebral conjunctiva of the dry eyed mouse compared to the normal mouse of the same strain**. The purpose was to include a rigorous morphometric assessment and description of the palpebral conjunctiva in both the normal and in the established dry eye mouse model (chapter 5).

Since the young (6-8 weeks) adult mouse has become an increasingly popular model in ophthalmic research there is an urgent need to enhance our understanding of the mouse eye, and to validate its use in different experimental settings. One important role

of the cornea and the crystalline lens is to protect the retina from toxic solar and artificial ultraviolet radiation (UVR), with solar radiation being the primary source of UVR for humans and animals. The level of UVR irradiance at various positions in the eye depends on the ocular media anterior to a particular point and the species investigated. In most species that perceive visible light with wavelengths from 400 to 760 nm, such as humans and rabbits, the cornea and the crystalline lens accomplish almost all of the absorption and have spectral transmittance curves blocking the majority of UV-B and UV-A wavelengths [51-52]. In contrast, both the aqueous and the vitreous are relatively transparent to the entire solar UVR waveband [51 53]. Eyes from animals such as dogs, cats, horses, cows, guinea pigs, hamsters, rats and mice transmit some UVR due to a decreased UVR filter in the lens [54-55]. Interestingly, rodents, including mice have photoreceptors sensitive to the transmitted UVR and, as a consequence the mouse could potentially utilize the transmitted UVR for enhanced vision [56].

There are a number of studies that quantify the spectral transmittance of the rabbit eye in particular [53 57-58] but there are relatively few publications on the transmittance of the mouse eye and its individual components [59-60]. It is important to precisely determine the contribution of each ocular component in the overall ocular UVR filter for any chosen test species so that the effects of UVR exposure can be predicted and related to the spectral sensitivity of the retina for the species in question. The transmittance of the whole mouse eye and its individual components has not yet been investigated. As a consequence, a study investigating the transmittance of the mouse eye was needed.

The **fourth aim** of this dissertation was to investigate the **hypothesis that the mouse eye will not be an applicable model for the human eye in regards to ultraviolet radiation transmittance** (chapter 6).

The mouse is today one of the most commonly used models in ophthalmic research; however the similarities or differences between the mouse anterior segment and the human is poorly understood. The four experiments included in this dissertation represent the first attempts to validate the mouse as an animal model for studies of the anterior segment or provide limitations to such investigation. The purpose of this research was therefore, firstly to assess the normal structure of the mouse cornea and conjunctiva to determine its human applicability. Secondly, my clinical need for improved ways to diagnose the dry eye can benefit from an enhanced understanding of changes in the conjunctival morphology from dryness. Thirdly, it is of interest to establish the part of the UVR spectrum transmitted to the retina in the mouse eye.

My knowledge of the mouse corneal structure and its similarities and differences to the human will be enhanced by this research. This knowledge is of interest and importance when utilizing the mouse as an animal model for corneal research and when applying the results to the human. The second aim of this research makes an attempt to explain the central to peripheral thickness difference in the cornea by counting and measuring thickness of lamellae in a transverse section. The conclusions from this study provides an enhanced understanding of corneal stromal architecture, which is essential for further understanding of structural changes occurring in stromal diseases such as keratoconus or stromal changes occurring after surgery e.g. LKP, LASIK. Thirdly, the ultrastructural investigation of the normal conjunctiva provides needed normative data in

an area where the literature is lacking information both in the human and in the mouse. What happens morphologically to the palpebral conjunctival epithelium is not clearly understood and this research will enhance our understanding of ultrastructural changes occurring in the dry eye, which is essential when diagnosing and treating this condition clinically. Lastly, the UVR transmittance of the mouse eye and its individual components has never been investigated. Thus, this research will increase our understanding of the mouse in yet another experimental setting. This knowledge is of importance when utilizing the mouse cornea and crystalline lens in transmittance studies and cataract studies.

Chapter 2 - Methods

Methods

All experiments were conducted in accordance with the ARVO Statement for the Use of Animals in Ophthalmic and Vision Research and all protocols have been approved by the Institutional Animal Care and Use Committee of the University of Houston or by the Baylor College of Medicine Center for Comparative Medicine.

2.1 Histological preparation of tissue (Chapter 3, 4 and 5)

Adult mice, 6-8 weeks of age were euthanized and a few drops of 2% glutaraldehyde in 80mM sodium cacodylate buffer, 330mOsm/kg fixative [61] was immediately applied to the cornea and the eye lids. The eyes with surrounding eye lids were removed and immersed in fixative for 4-6 hours to ensure proper cross linking and preservation of the tissue.

The tissue processing protocol that was utilized in the present study has shown that a fixative maintaining near physiological osmolality values, produced minimal tissue shrinkage with a resultant undistorted, natural contour of the tissue preserved [4].

The fixed corneas or eye lids were dissected into small pieces (1 x 1.5 mm) and washed three times in sodium cacodylate buffer pH 7.4 at room temperature and left 10 minutes in each wash. Subsequently, the samples were immersed in a freshly prepared 1 % solution of osmium tetroxide in 100mM sodium cacodylate buffer for 1 hour under subdued light. The samples were once again washed several times in sodium cacodylate buffer and left 10 minutes in each wash. A Leica EM TP tissue processor was used for the following steps: dehydration, transition, infiltration and embedding. First the tissue samples were dehydrated through a graded alcohol series (30% - 100% in 6 steps) at room temperature. Next the tissue samples were infiltrated with propylene oxide.

Embedding with agitation was achieved through an initial mixture of propylene oxide and Araldite resin 2:1 for 3 hours followed by overnight immersion in a 1:1 mixture of propylene oxide and Araldite resin. Thereafter, the tissue samples were immersed in propylene oxide and Araldite resin 1:3 for 4-8 hours before lastly being transferred to 100 % Araldite resin overnight. The tissue samples were then oriented in embedding molds and left 12 hours for polymerization in an oven at 60º C.

An ultramicrotome (Research Manufacturing Co. Inc MT-7000) was used to cut thick (0.5 – 1 µm) and ultrathin (60-100 nm) transverse sections. The thick sections were stained with 1 % toluidine blue for examination with an Olympus BX51 light microscope. For morphological analysis ultrathin sections were mounted on parallel bar copper grids (200MP, Cat # G200P, Electron Microscopy Sciences) or oval slot (2x1 mm) formvar carbon coated copper grids (FCF2010-Cu, Electron Microscopy Sciences). These sections were double stained, first, in 3.5 % uranyl acetate for 20 minutes at 60º C, followed by Reynold's lead citrate for 10 minutes at room temperature. The grids were examined in a Tecnai G2 Bio Twin Spirit (FEI Company, USA) transmission electron microscope (TEM) and images captured digitally.

2.2 Methodology Chapter 3

After fixation, before tissue processing (section 2.1), measurements of the corneal diameter were obtained under a dissecting microscope (Olympus SZ60) for increased magnification on one eye per animal, utilizing a pair of digital calipers. The corneal diameter was measured from limbus to limbus in triplicate using the easily visualized (at 25X magnification) corneo-scleral junction to define the limit of the cornea.

The corneal diameter measurements were obtained on fixed eyes for consistency with the corneal thickness measurements. The average corneal radius (diameter/2) was used to identify the location where the central corneal measurements were made. After tissue processing (Section 2.1) digital images were captured at 40X and 200X of two thick toluidine stained corneal sections, cut from two levels of the same block separated by approximately 200 µm. Peripheral measurements were taken at the extremity of the cornea, defined histologically as immediately central (anterior) to limbal capillaries and central to the anterior edge of the trabecular meshes (Figure 2.1). Central corneal measurements were taken at a distance, half the corneal diameter from the peripheral measurements where the cornea has its natural contour, took up stain in a uniform manner and was free of artifacts. All measurements were made in triplicate with NIH Image Software, at the same location centrally and peripherally.

The layers of epithelial cells forming the epithelium were counted from electron- micrographs taken from both the central and peripheral regions. Cells were counted in a straight line from the basement membrane to the corneal surface and did not have to display a nucleus in the plane of the section.

Analysis

An unpaired student's t-test was used to compare the two corneal sections cut from two levels of the same block, separated by approximately 200 μm to ensure no difference throughout the tissue sample. An unpaired student's t-test was also used to compare the average central with the average peripheral corneal measurements for three mice from three different strains (129/SVJ, C57BL/6 and BALB/c). The statistical significance was set to ($P < 0.05$).

2.3 Methodology Chapter 4

Following tissue processing (Section 2.1), the grids were examined in a Tecnai G2 Bio Twin Spirit (FEI Company, USA) TEM and consecutive slightly overlapping micrographs were captured digitally at 890X magnification across the total thickness of the cornea centrally and peripherally. Micrographs were assembled into montages using image assembly software, PanaVue ImageAssebler 3 (Sharelt Inc, USA) and printed (Roland FJ-52) at a final magnification of 5000X.

All measurements were carried out by one investigator (JTH) following strict, preset criteria. According to these criteria the distinction between adjacent lamellae was based on an obvious difference in contrast between collagen bundles generated by different fiber orientations [4]. If obvious branching was noticed within the micrograph care was taken not to double-count such lamellae. Presence of a keratocyte or its cytoplasmic projection as an indication of a lamellar border and lamellae thinner than 0.2 µm were not included in the count.

For analysis, the corneal stroma was divided into anterior, middle and posterior thirds, to investigate differences in the number of lamellae per unit length between the regions. After the lamellae were counted their individual width was measured using a millimeter ruler. According to the magnification used, one millimeter was equal to 0.2 µm.

Keratocytes were counted in the antero-posterior plane on digital images of one representative, thick toluidine blue stained, LM section, from each cornea, at 200X magnification. In addition, lamellar width and numbers were measured on TEM sections at a magnification of 890X. Peripheral counts were made at the extremity of the cornea,

defined histologically as immediately central to the limbal capillaries and to the anterior edge of the trabecular meshwork (Figure 2.1). The morphometry was conducted in triplicate, at the same location, within a defined anterior-posterior, 10 µm wide axial band, at the corneal apex and periphery. Central corneal counts were carried out 1300 µm from the peripheral extreme of the cornea and were based on the corneal diameter for the C57BL/6 mouse established and published previously [62]. Keratocyte and lamellae counts, individual lamellar thicknesses and epithelial thickness were measured by a single observer (JTH) using specified criteria to minimize inter-observer differences. A single observer was used, based on a previous study, which showed that the coefficient of variation between trained observers was 1% when determining the number of lamellae present in the human stroma [4].

Keratocytes were counted if they did not possess a basement membrane, a lobulated nucleus or dense staining granules. If more than one keratocyte appeared at the same level within the defined 10 µm band, only one was counted. To be included in the count the keratocytes also had to measure 4 µm horizontally and 0.2 µm vertically. Furthermore, full stromal thicknesses were also measured.

Analysis

A matched pair t-test was used to compare the average central with the average peripheral corneal counts and measurements. The statistical significance was set to ($P < 0.05$).

2.4 Methodology Chapter 5

6-8 week old C57BL/6 mice of both genders were utilized for this experiment. Untreated (UT) C57BL/6 mice (control) were used for morphometric assessment and description of the normal palpebral conjunctiva. The data obtained from the UT mice were compared to data obtained from the palpebral conjunctiva of 16 mice, 8 per group who were exposed to experimental ocular surface desiccating stress (DS) for 5 or 10 days (DS5 and DS10). DS was created by injection of scopolamine hydrobromide (0.5mg/0.2ml) QID, alternating between the left and right flanks [43]. Mice (up to 5 per cage) were exposed to a constant air draft for 16hr/day from a fan placed 6" away from a side of their cage. Room humidity was maintained at 35-40% and temperature at 80°F. Aqueous tear production/volume was assessed using cotton thread (Quick Zone Thread; Oasis)[63]. Following euthanization, eyes with surrounding eyelids were dissected, the right eyes processed for histology (Section 2.1) and the left eyes for histovhemistry and immunohistochemistry (Please see below).

Histochemistry

The eyes with surrounding eyelids were fixed in 10% buffered formalin over night and embedded in paraffin. 5 μm thick serial sections from each sample were cut with a microtome (Microm HM 340E). The sections were deparaffinized and stained with 0.5% periodic acid-schiff (PAS) stain, Alcian blue (pH 2.5) or with MUC5AC antibody (SC-20118 Santa Cruz) for identification of goblet cells. Digital images of four sections, (eight eye lids), from 3 animals per group were captured (DXM, 1200; Nikon) and evaluated (NIS Elements, Nikon). The number of positively stained goblet cells was

counted and the length of the basement membrane between the first and last goblet cell measured. In addition the MUC5AC positive area was also measured. The data are presented as the average number of goblet cells and total goblet cells/mm per eye lid.

MUC5AC Immunohistochemical staining

After deparaffinization, heat induced antigen retrieval was performed for 20 minutes in sodium citrate buffer (10mM sodium citrate, 0.05% Tween 20, pH 6.0). Subsequently, the sections were treated with 0.3% H_2O_2 in PBS to quench the endogenous peroxidase activity and then incubated with an avidin-biotin block (Vector Laboratories) for 10 minutes each. After blocking with 20% normal goat serum in PBS for 30 minutes, the rabbit polyclonal primary antibody, SC-20118 Santa Cruz (1:200) diluted in 5% goat serum was applied and incubated for 60 minutes at room temperature. Next, the secondary antibody (rabbit polyclonal BD Pharmingen CN 550338, 1:50) in 5% goat serum was applied for 30 minutes also at room temperature. The tissue was then incubated in an ABC solution (Vectastain Elite ABC Kit, Vector Laboratories) which is an immunoperoxidase procedure where the antibody is visualized through a peroxidase-catalyzed reaction, and stained with a diaminobenzidine (DAB) solution (NovaRed substate kit, Vector, CN-4800, red stain) for 2 minutes. The reaction was terminated in distilled water, the sections counterstained with Mayer's Hematoxylin, rinsed in tap water, dehydrated, cleared and mounted with 1-2 drops of Permount (SP15-100, Fisher Chemicals). Normal rabbit serum concentration (1:200) was substituted for the primary antibody as an irrelevant control.

Light (LM) and Transmission Electron Microscopy (TEM)

Subsequent tissue processing (Section 2.1), the thickness of the conjunctival palpebral epithelium was measured in triplicate using NIH Image Software and the number of cell layers counted in the marginal, central and peripheral palpebral conjunctiva (Figure 2.2). Slightly overlapping digital images were captured with the LM at 100X, montages assembled using PanaVue ImageAssembler 3 (Sharelt Inc, USA) and printed (Roland FJ-52). On the printed montages the number of goblet cells was counted based on histological criteria. Cells meeting one or more of the following criteria, a triangular shaped nucleus, cytoplasm packed with secretory granules or a bloated or ballooning cell body, were classified and counted as goblet cells. Their location within the epithelium (basal or superficial) was also determined.

Morphometry

Stereology is a widely used biological technique utilized to obtain three dimensional data from sampling in two dimensions (e.g from tissue sections) [64]. Statistical analysis was used to determine that 10 goblet cells from each sample were sufficient for accurate morphometric analysis; a random number generator and systematic random uniform sampling (SURS) were used for unbiased selection of 10 goblet cells from each sample to include in the data analysis.

To determine surface density (Sv) of the goblet cell and volume fraction (Vv) of granules per goblet cell [65-66] the point counting method was used, by randomly placing a cycloid grid oriented perpendicular over the goblet cell of interest, Surface density (Sv) was calculated by the formula, $Sv = (2*\Sigma I)/ (l/p *\Sigma P)$ where I = the number cycloid

intersects with the goblet cell plasma membrane or granule plasma membrane, P = points falling on the entire goblet cell or on granules and l/p equals a constant corrected for linear magnification [64 67]. The volume fraction (Vv) was calculated by counting all dots falling on granules and dividing by all dots falling on the goblet cell. To investigate the volume fraction (Vv) of goblet cells per palpebral conjunctival epithelium a point counting grid was used. (Vv) was computed by counting all dots falling on goblet cells and dividing by the total number of dots falling on the palpebral conjunctival epithelium. The average area per goblet cell in each of the three conditions was also measured.

Statistical Analysis

One way analysis of variance (ANOVA) with Dunnett post hoc testing was performed to compare morphometry, palpebral conjunctival epithelial thickness measurements and counts between the three conditions (UT, DS5 and DS10). Statistical significance was set to ($P < 0.05$). Data is presented as mean ± SD. Prism 4.0 software (GraphPad Software Inc., San Diego CA) was utilized for the statistical analysis.

2.5 Methodology Chapter 6

Adult C57BL/6 mice were euthanized and the intact eyes were carefully enucleated. To determine the spectral transmittance of the whole mouse eye a small disc of sclera was removed from the posterior pole to provide an anterior to posterior ocular optical path. The cornea with a scleral rim and the crystalline lens were subsequently removed by dissection and measured independently. Before corneal transmittance measurements were obtained, the effects of post mortem optical deterioration of the tissue was investigated to determine the time frame that corneal clarity may be maintained. Earlier work has shown that the rabbit cornea will produce increased light scatter with time and there is a 20 minute period immediately post mortem during which the cornea remained clear [51]. This immediate post mortem period is essential for an *in vivo* approximation of spectral transmittance. Corneal clarity can be prolonged with careful handling during dissection and mounting and by irrigating with Alcon BSS (Alcon, Fort Worth Texas)[51]. The crystalline lens is an isolated organ completely enclosed and protected by its own basement membrane and more resistant than the cornea to changes in its environment. Therefore, the transparency of this tissue is maintained for a long period of time after removal from the whole eye allowing measurements to be obtained without concerns for a change in light scatter produced by its components.

To test the period of post-excision corneal clarity in mice a series of spectra were recorded over a 90 minute period. One additional mouse cornea from the same species (C57BL/6) was utilized and spectra obtained as soon as possible post mortem. Spectra were initially recorded as rapidly as possible and periodically thereafter over a

period of 90 minutes. During the experiment the excised tissue was kept artificially hydrated by Alcon BSS to prevent dehydration and distortion of the tissue. For the remainder of the data, the whole eye and component media were tested immediately post mortem to minimize any optical deterioration. To ensure repeatability, transmittance spectra were rapidly recorded at five test points near the center of each whole mouse eye, cornea and crystalline lens. To minimize the decay in optical clarity post mortem, the enucleated whole mouse eye, dissected cornea and dissected crystalline lens were sampled within 10, 15 and 20 minutes respectively. In addition, left and right eyes were measured to give intra-mouse consistency and inter-mouse variations by sampling four mice in total, giving a total final value of n = 8 for each ocular component tested.

Spectral transmittance of the samples was measured using a non-cuvette based fiber USB4000 optic spectrometer system (Ocean Optics, Dunedin FA), with a spectral range of 200-800 nm. Samples were illuminated by an Ocean Optics DT-Mini-2-GS deuterium-halogen light source, with a 200-2000 nm output spectral range. All media were illuminated from the front with a collimated beam from a 400 μm diameter fiber optic fitted with 10 mm focal length collimating lens that were coupled to the light source. The bare front end of the 200 μm diameter detecting fiber was placed immediately behind the test medium, with the other end coupled to the 5 μm input slit of the spectrometer that provided a spectral resolution of less than 3 nm [51]. The overall set-up is shown schematically and pictorially in (Figure 2.3) and the basic principles of the system have previously been calibrated, tested and proven on contact lenses of known transmittance [68-69] and on rabbit eyes as well as on its various media components [51 70].

After the spectrometer dark current and the reference spectra were established transmittance spectra were computed and recorded in a few milliseconds. The rapid data collection from the spectrometer CCD detector and the small aperture on the illuminating and detecting fiber optics allow for transmittance of small tissue samples such as the whole mouse eye, its cornea and crystalline lens to be recorded. The reference spectrum is simply the spectrometer observing the lamp through the empty sample holder, which is effectively the 100% transmittance baseline. The tissue transmittance is observed when a specific sample is carefully placed normal to the light beam.

Intra-mouse, left versus right eye, as well as inter-mouse transmittance curves were recorded to test homogeneity and variation throughout our sample eyes. Placement variations will be greatly reduced by normalizing all spectra in the visible at 600 nm where the test media have high transmittance and no absorption feature of note [51 68].

In addition, the spectral transmittance of a drop of Alcon BSS was determined to ensure that it does not absorb any UVR in the region of interest. After testing whole eyes, the individual corneas and crystalline lenses were carefully excised and placed in the test beam for measurements, with less placement error than the whole eyes due to their relative optical simplicity.

Analysis

The whole eye, the cornea and crystalline lens spectra were normalized based on the mean of the five spectra taken on each of the eight test eyes. The relative thickness of each test medium was incorporated and the amount of surface or Fresnel reflection was

accounted for in the analysis. Transmittance data were saved using Ocean Optics software and analyzed using Matlab (MathWorks).

2.6 Figures

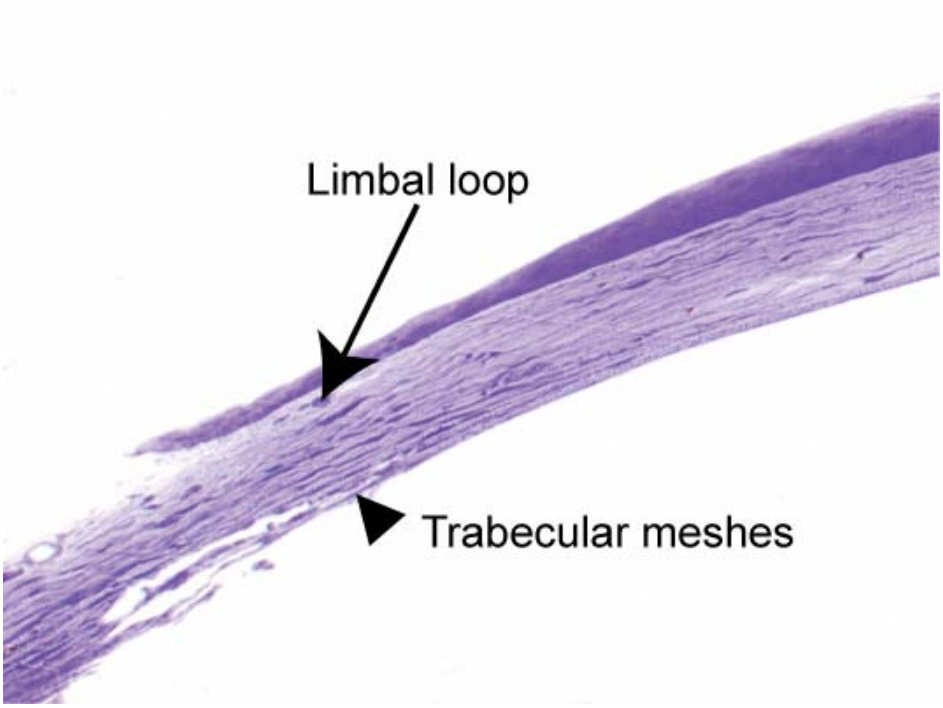

Figure 2.1 Peripheral cornea

Peripheral measurements were taken immediately central (anterior) to limbal loops and central to the anterior edge of the trabecular meshes (Magnification 100X).

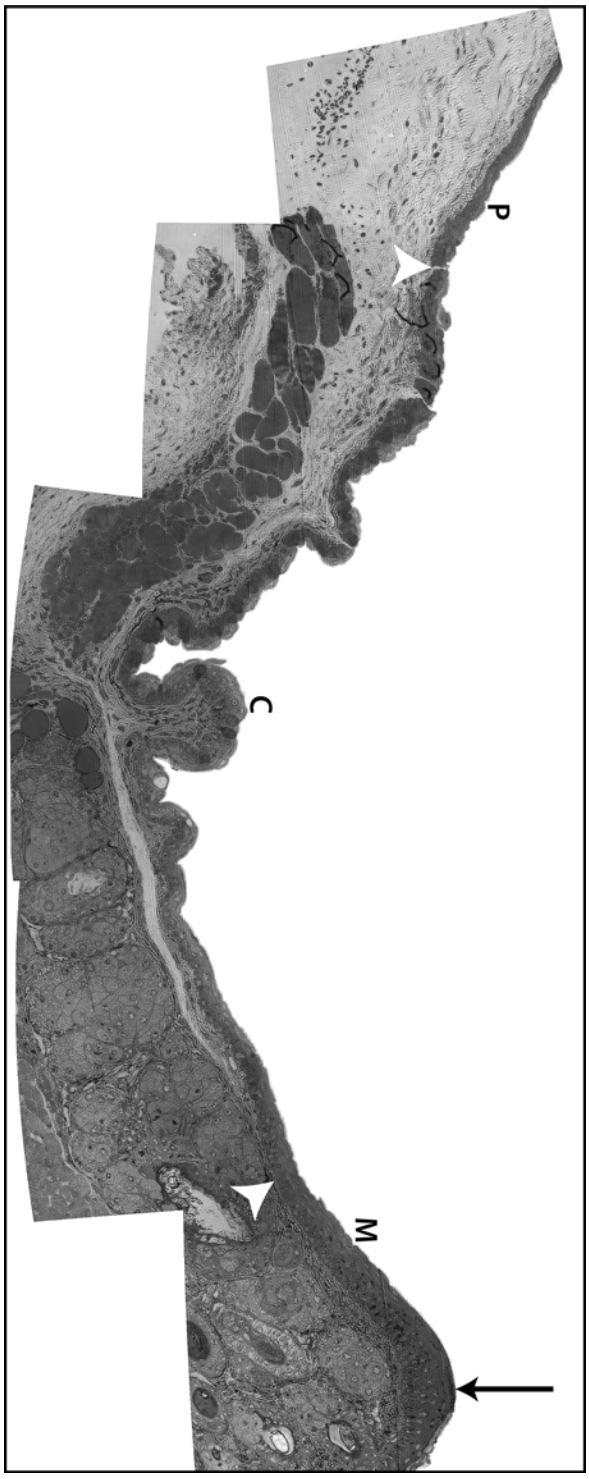

Figure 2.2 Normal palpebral conjunctiva

Normal palpebral conjunctiva illustrating its three regions. M=Marginal, C=Central and P=Peripheral. Close to the lid margin (arrow) is the stratified multi-layered epithelium thickest and devoid of goblet cells. The region where goblet cells are present is indicated between the two white arrow heads. (Magnification 100X).

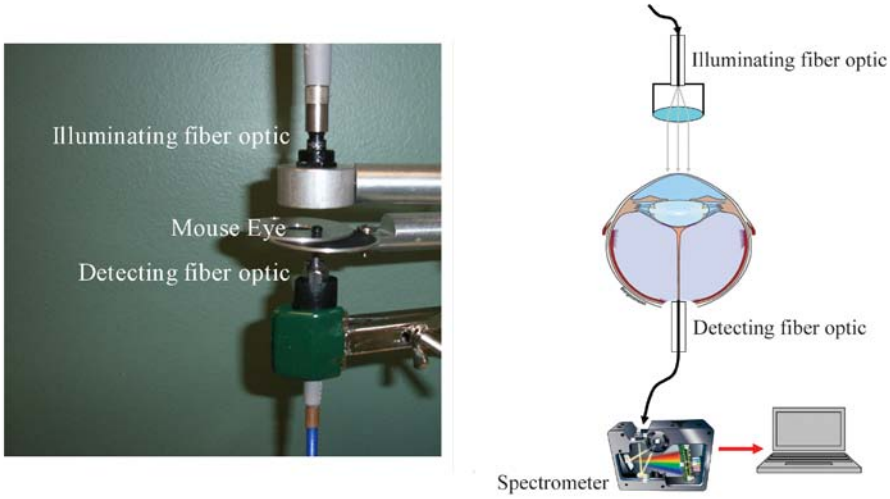

Figure 2.3 Spectrometer set up

Photograph of instrumentation set up (A) explained by schematic diagram (B).

Chapter 3 - Dimensions and Morphology of the Cornea in Three Strains of Mice

Johanna Tukler Henriksson BS Opt, Alison M. McDermott PhD, Jan P.G Bergmanson OD, PhD, PhD h.c., DSc, Texas Eye Research and Technology Center, University of Houston College of Optometry, Houston, Texas

As published in: Investigate Ophthalmology and Visual Science 2009:50(8):3648-54

3.1 Abstract

Purpose: To use a histological approach to provide dimensional and morphological information on the cornea in three commonly used strains of mice.

Methods: Adult mice (three each of 129/SVJ, C57BL/6, BALB/c) were euthanized the eyes enucleated, immersed in 2% glutaraldehyde fixative and prepared for light- and transmission electron microscopy. The full corneal, epithelial, stromal and posterior limiting lamina (PLL) with endothelium thicknesses were measured at the same location centrally and peripherally.

Results: All three strains showed a statistically significant ($P < 0.001$) decrease in overall thickness in peripheral compared to central cornea. This was due to a decreased thickness of both epithelium and stroma. The stroma and epithelium contributed to approximately 2/3 and 1/3 of the total corneal thickness respectively. The epithelium had the classic stratified layout, and consisted of 13.00 ± 1.41 layers centrally versus 10.33 ± 1.37 peripherally. Some adaptation of stromal tissue immediately adjacent to the epithelial basement membrane was found, but a clearly defined anterior limiting lamina did not exist. The stroma was organized into lamellae but lacked the anterior branching and interweaving reported in humans and had unmyelinated nerve fibers within microns from the endothelium. The PLL was 2.17 ± 0.3 µm thick and was divided into pre- and post-natal layers, with striated bodies in the post-natal portion.

Conclusions: This study demonstrated that in the three strains of mice examined, the cornea becomes significantly thinner towards the periphery. Dimensionally, proportionally and anatomically the three strains used appear to be similar. However morphological differences were observed compared to other mammals and awareness of these differences is important when using the mouse as an animal model applicable to the human.

3.2 Introduction

For many years the rabbit was generally the preferred animal model for ophthalmic research but recently the mouse has become widely utilized in corneal research and studies involving other ocular regions such as the retina or the crystalline lens [8 11]. The main reason for the increased utilization of the mouse is that its genome has been sequenced and there are many different transgenic and knockout strains available for different types of research. Additional advantages with the mouse include that it is easy to breed, it grows rapidly and it is cost effective [9-10 12].

An obvious disadvantage with the mouse as a model is that its corneal diameter is much smaller than that of the human cornea. However, the mouse cornea contains five corneal layers (epithelium, anterior limiting lamina, stroma, posterior limiting lamina and endothelium) as described by Smith *et al*. [9], although the presence of an anterior limiting lamina has been disputed [16-17]. The literature also contains conflicting data on the dimensions of the mouse cornea. For instance, there are large discrepancies between different reports on the overall central corneal thickness and central stromal thickness which may be related to variations in the measuring techniques and strains of mice used. Zhang *et al*. reported a central corneal thickness of 170 µm in the BALB/c mouse utilizing a confocal microscope (Hund/Wetzlar). Zhang *et al*. also reported a central epithelial thickness of 51 µm and a central stromal thickness of 119 µm. These measurements were obtained from cryostat sections photographed with an Olympus Photomicroscope OM-2 (Olympus/Japan)[12]. In contrast Schulz *et al*. based their thickness assessment on optical low coherence reflectometry and reported the central corneal thickness to be 106 ± 3.45 µm in the same strain of mice, the BALB/c [14]. Jester *et al*. used

yet another technique, *in vivo* confocal microscopy by a Tandem Scanning Confocal Microscope (Tandem Scanning Corporation, Reston, VA) to determine corneal thickness and reported a central corneal thickness of 112.9 ± 7.0 µm in wild type littermates of PEPCK- TGFβ1 transgenic mice [13]. Song *et al.* also utilized the same *in vivo* confocal microscope to measure the central epithelial and stromal thickness in the wild type CD1 mouse and reported values of 49.3 ± 5.7 µm and 81.5 ± 10.7 µm respectively [15].

In addition to these discrepancies available literature only provides central corneal measurements and no information is available about the mouse peripheral cornea. An understanding of the normal corneal structure together with normative data is desirable for future comparisons when using the mouse as a model for anterior segment research.

The purpose of this study was to use a histological approach to provide needed normative morphometric data on the dimensions of the overall cornea and its components, both centrally and peripherally, while also assessing the mouse corneal morphology in three commonly used strains of mice, the BALB/c, C57BL/6 and 129/SVJ.

3.3 Materials and Methods

All experiments were conducted in accordance with the ARVO Statement for the Use of Animals in Ophthalmic and Vision Research. Nine adult mice, 6-8 weeks of age, (three 129/SVJ, three C57BL/6 and three BALB/c) were euthanized and a few drops of 2% glutaraldehyde in 80mM sodium cacodylate buffer, 330mOsm/kg fixative [61] were immediately applied to the cornea after resection of the eye lids. The whole eyes were carefully enucleated and immersed in fixative for 4-6 hours to ensure proper cross linking and preservation of the tissue.

After fixation corneal diameter measurements were obtained on one eye per animal under a dissecting microscope (Olympus SZ60) for increased magnification. A pair of digital calipers with sensitivity down to 0.1 mm was used to obtain measurements from all eyes. The corneal diameter was measured from limbus to limbus using the easily visualized (at 25X magnification) corneo-scleral junction to define the limit of the cornea. The corneal limbus to sclera transitional zone is very narrow at approximately 0.1 mm and was for this reason not considered separately. The mouse cornea was found to be circular, not oval like the human cornea, and, therefore, the measurements do not differ in the horizontal and vertical meridians. All three measurements on the same cornea were obtained along the same meridian and the corneal diameter measurements were performed on fixed eyes for consistency with the other measurements. The tissue processing protocol utilized in the present study has shown that a fixative maintaining near physiological osmolality values produced minimal tissue shrinkage with a resultant undistorted, natural contour of the tissue preserved [61]. The average corneal radius

(diameter/2) was used to identify the location where the central corneal measurements were made.

The fixed corneas were bisected and small pieces (1x 1.5 mm) were cut from the central region. The corneal pieces were washed three times in sodium cacodylate buffer pH 7.4 at room temperature and left 10 minutes in each wash. Subsequently the samples were immersed in a freshly prepared 1 % solution of osmium tetroxide in 100mM sodium cacodylate buffer for 1 hour under subdued light. The samples were once again washed several times in sodium cacodylate buffer and left 10 minutes in each wash. A Leica EM TP tissue processor was used for the following steps: dehydration, transition, infiltration and embedding. First the tissue samples were dehydrated through a graded alcohol series (30% - 100% in 6 steps) at room temperature. Next the tissue samples were infiltrated with propylene oxide. Embedding with agitation was achieved through an initial mixture of propylene oxide and Araldite resin 2:1 for 3 hours followed by overnight immersion in a 1:1 mixture of propylene oxide and Araldite resin. Thereafter the tissue samples were immersed in propylene oxide and Araldite resin 1:3 for 4-8 hours before lastly being transferred to 100 % Araldite resin overnight. The tissue samples were then oriented in embedding molds and left 12 hours for polymerization in an oven at 60º C.

An ultramicrotome (Research Manufacturing Co. Inc MT-7000) was used to cut thick transverse sections (0.5 – 1 µm). These sections were stained with 1 % toluidine blue for examination with an Olympus BX51 light microscope. For morphological analysis ultrathin sections were obtained and mounted on parallel bar copper grids (200MP, Cat # G200P, Electron Microscopy Sciences). The sections were double stained,

first, in 3.5 % uranyl acetate for 20 minutes at 60º C, followed by Reynold's lead citrate for 10 minutes at room temperature. The grids were examined in a Tecnai G2 Bio Twin Spirit (FEI Company, USA) transmission electron microscope and images captured digitally.

Digital images were captured at 40X and 200X of two thick toluidine stained corneal sections, cut from two levels of the same block separated by approximately 200 µm. Peripheral measurements were taken at the extremity of the cornea, defined histologically as immediately central (anterior) to limbal capillaries and central to the anterior edge of the trabecular meshes (Figure 3.1).

Measurements for central cornea were taken at a distance, half the corneal diameter ± 14 % from the peripheral measurements where the cornea had its natural contour, taken up stain in a uniform manner and was free of artifacts. All measurements were made with NIH Image Software and done in triplicate, at the same location centrally and peripherally.

The layers of epithelial cells forming the epithelium were counted from electron- micrographs taken from both the central and peripheral regions. Cells were counted in a straight line from the basement membrane to the corneal surface and did not have to display a nucleus in the plane of the section.

An unpaired student's t-test was used to compare the two corneal sections cut from two levels of the same block but separated by approximately 200 µm to ensure no difference throughout the tissue sample. An unpaired student's t-test was also used to compare the average central with the average peripheral corneal measurements for three mice within the same strain. The statistical significance was set to ($P < 0.05$).

3.4 Results

The averages of three measurements per mouse for the three strains (129/SVJ, BALB/c and C57BL/6) tested in this study are presented in (Table 3.1). The corneal diameter for the 129/SVJ mice measured 2.3 mm and was slightly smaller than the diameter for the BALB/c and the C57BL/6 mice that both measured 2.6 mm. All three strains of mice showed a statistically significant difference ($P < 0.001$) between the total central corneal thickness compared to the periphery, with the periphery being thinner compared to the center (Table 3.1, Figure 3.2 and 3.3).

All three strains of mice showed a similar dimensional relationship between the stroma and the epithelium with the center being thicker than the periphery (Table 3.1, Figure 3.4). In none of the strains did the endothelium with PLL measurement vary between the central and peripheral cornea. The stroma contributed to approximately 2/3 of the total corneal thickness with the epithelium accounting for approximately 1/3.

Morphologically the epithelium had the classic stratified layout. Centrally it consisted of 13 layers (Figure 3.5) while peripherally the epithelium was reduced by approximately 3 layers (Figure 3.6). The increased number of layers compared to the primate was attributable to the addition of multiple layers of squamous cells. The epithelial cells were tightly packed and adhered to its neighbors through numerous desmosomes and to its basement membrane through hemidesmosomes.

There was scant evidence of an ALL. However, collagen fibers oriented and appearing like Type VII were in place at the epithelial basement membrane and at intervals there were individual or a few collagen fibrils that departed from the characteristics of the stromal lamellar organization (Figure 3.7).

The substantia propria or the stroma was essentially organized into lamellae, which anteriorly did not show the extensive and complex interweaving seen in the human cornea. No electron dense formations suggesting mid-corneal lamellar terminations were recorded (Figure 3.8). Posteriorly lamellae followed the human like layered arrangement. Scattered across the cornea were keratocytes in a density that approximates that of the primate. Gap junctions between adjacent keratocyte processes were noted (Figure 3.9).

Measurements and morphological analysis of the PLL and endothelium individually were made from electron micrographs. The animals examined were all young adults and the PLL measured on average 2.17 ± 0.3 μm in crossection. The mouse PLL did not possess the distinct banded and non-banded division seen in the primate cornea but had a thin anterior layer facing the stroma that appeared to correlate to the banded fetal portion. It had a texture that was different with a tendency towards banding compared to the underlying and presumably post-natal basement membrane. Scattered within the posterior portion of the basement membrane were numerous bodies with collagen like cross striations. The endothelium, measuring on average 2.15 ± 0.4 μm in thickness, provided full corneal coverage all the way to the trabeculum and had a smooth anterior and posterior outline. The lateral sides showed intimate interdigitation with its neighbors and a lateral flap extending from one cell to bridge the narrow gap between two cells. This junction between two cells contained a zonula occludens (Figure 3.10).

An interesting departure from the primate pattern was the distribution of corneal nerves. Stromal nerve fibers were observed throughout the full corneal thickness. Unmyelinated nerve fiber bundles were regularly seen within a few microns of the PLL and the endothelium, where they often exhibited axon varicosities (Figure 3.11).

3.5 Discussion

The present study qualitatively and morphometrically assessed the corneal anatomy of three strains of mice. With minor variations all strains of mice showed the same general structural arrangement and dimensions, while also possessing features distinct to this species.

Little information is available concerning the dimensions of the BALB/c and the 129/SVJ and C57BL/6 mouse cornea. As noted in the introduction the existing data show a large discrepancy between central corneal thickness measurements (106.00 ± 3.45 µm versus 170 µm) [12 14]. This difference is likely to be due to the different methodologies used to obtain the measurements. The protocol followed in the present study eliminated shrinkage and tissue distortion, which, together with the presence of histologically well defined reference points, allowed the observer to conduct accurate intra-corneal measurements [61].

Schultz *et al.* used optical low coherence reflectometry, which is a type of noncontact pachymeter to obtain the measurements [14]. To use this technique the refractive index of the cornea has to be accurately known. The refractive index used in Schultz's study was based on a rat schematic eye reported by Massof *et al*., which might be similar but not exactly corresponding to the refractive index of the mouse cornea [71]. Another drawback with using optical low coherence reflectometry is that accurate calibration of this type of instrument is known to be difficult [72].

Zhang *et al*., on the other hand, used a 'Hund/Wetzlar' confocal microscope on one animal to arrive at a 170 µm central corneal thickness value for the mouse [12]. In addition to a small sample (n=1), this confocal instrument, of nondescript technical

specification, may not have had the precision to make such an assessment. The corneal diameter ranged from 2.3 to 2.6 mm in the three strains assessed in the present study. Zhang *et al*. made a measurement on one BALB/c mouse eye and found a corneal diameter of 3.5 mm, which is substantially larger than the measurements on our BALB/c mice or the other strains used in this study [12]. The reason for this discrepancy may be the age of the animals, 6 to 8 weeks versus 6 months and likely also the methodology utilized for this measurement. Higher magnification and resolution through the use of a high quality dissection microscope, in conjunction with a precision caliper allowed our measurement to be very precise. We also found a good agreement between the different strains. Zhang *et al*., [12] also determined the stromal and the epithelial proportions towards the total corneal thickness with cryosections, which have known disadvantages such as poor morphological preservation and limited resolution [73]. Both Jester *et al*. and Song *et al*. utilized *in vivo* confocal microscopy to obtain their measurements and the drawback with this method is its poor reproducibility due to the difficulty in locating the appropriate area for the assessment [13 15].

Another issue to consider relates to how the central cornea was defined in the before mentioned studies. Schultz *et al*. defined the central cornea by the visual corneal apex, [14] whereas Zhang *et al*. did not state any criteria to locate the central cornea [12]. In the present study both the central and the peripheral measurements were taken from clearly defined corneal zones. Therefore, we would like to argue that our measurements are likely to be accurate for each of the three strains.

The data showed that there was a significant decrease ($P < 0.001$) in thickness between the central and peripheral cornea in the 129/SVJ, C57BL/6 and the BALB/c

mice. The cornea thinned between 55 to 66 % going from center to periphery depending on mouse strain. The decreased thickness of the mouse cornea towards the periphery appeared mainly to be due to tissue thinning of the stroma and the epithelium but some compacting of the tissue may also occur towards the periphery**.**

It is also interesting to note the difference in shape between the human and the mouse cornea. The average human cornea measures 535 ± 20 μm in the center compared to 657 ± 71 μm in the periphery [2]. Thus the human cornea is thinner in the center than periphery making it a negative meniscus lens. In contrast, the mouse cornea is thicker in the center and thinner in the periphery and could, therefore, be described as having the shape of a positive meniscus lens. For comparison, the rabbit cornea maintains a uniform thickness across its width and is therefore, similar to a plano lens [74]. The thinning of the mouse cornea towards the periphery is a new discovery, and the structural cause to the thinning has yet to be explained. One possible explanation for this thickness difference may be that the peripheral cornea is formed by fewer stromal lamellae. Alternatively the cornea may have the same number of lamellae centrally and peripherally but with the peripheral lamellae being thinner. Further ultrastructural histological studies are needed and under way in our laboratory to uncover the structural reason for this corneal thickness variation which might also explain the non-uniform thickness of the human cornea.

It was also concluded in the current study that the epithelium contributes approximately 30% percent and the stroma approximately 70% to the total central and peripheral corneal thicknesses. In contrast, corneal epithelium represents approximately only 10% and the stroma 90% of the total corneal thickness in humans [75]. As an experimental model it is important to be aware of the greater relative contribution of the

epithelium towards the overall corneal thickness in the mouse compared to the human. Such differences are likely to have an impact when relating corneal wound healing studies on the mouse to the human. For the mouse epithelium to heal and to return to full thickness, may take longer compared to the primate, since the mouse epithelium is formed by more layers of cells. Ultraviolet radiation experiments on the cornea are another example where a species variation will make interspecies comparisons more uncertain, since the epithelium and the stroma have different absorption characteristics [51].

The stratified layout of the murine corneal epithelium is consistent with the description of this epithelium in the mammalian cornea, such as rat, rabbit, cat and man [8 28 76-78]. Compared to the human the mouse epithelium consisted of approximately double the number of layers of cells and the increased number of cells was due to a comparative elevation in the number of squamous cells [1 79]. The average of 13 cell layers in the epithelium was a consistent finding in our specimens, as was the thinning of the epithelium by approximately 3 layers in the peripheral cornea. Other epithelial features, such as desmosomal junctions, hemidesmosomes and basement membrane were present in numbers and a form similar to that described for the primate [79].

The presence or absence of an ALL in a cornea of a particular species is going to vary according to how this layer is defined. If the criteria for the presence of an ALL include a layer of primate-like thickness of 8 to 10 μm, clearly the mouse does not possess one. However, if some Type VII collagen fibers and one or a few Type I fibers not strictly following the lamellar pattern of stroma proper is all that is required, then it may be argued that the mouse has an ALL. However, we would propose that the ALL in the primate is a distinct and separate layer sandwiched between the epithelium and the

stroma. In the mouse there is no such layer but there is some adaptation of stromal tissue immediately adjacent to the epithelial basement membrane. This is what other authors [9 80] may have elected to call an ALL but to do so will only cause confusion because there is no resemblance between the primate ALL and the same region in the mouse. In this respect we are in agreement with Rehbinder, who also concluded that the mouse does not possess an ALL [17].

The mouse corneal stroma was organized into lamellae crossing each other at various angles while remaining parallel to the ocular surface, as is also the case in the human cornea [1 78]. However, the anterior interweaving and branching lamellae reported in humans [4-5 79] were not present in mice and electron dense formations recently described in humans were also absent [5]. Therefore, significant differences between the anterior stroma of the human and the mouse exist. In the mouse the anterior stromal layout consisted essentially of lamellae parallel to the corneal surface and laid down on top of each other at different angles. The architecture of the mouse anterior stroma was similar to the human mid and posterior stroma.

Keratocytes were present primarily between the lamellae and had a morphology similar to that reported in man and rabbit [28 31]. They seemed to be there in sufficient numbers and possessed gap junctions to permit the intra-corneal network suggested by Watsky [81].

The PLL consists of a fetal and a post-natal portion, [1 9 79] which in the case of the human cornea divides the membrane into a distinctly banded and a more uniformly textured portion. Our observations suggest that the mouse PLL had a similar but less distinct organization into pre- and post-natal layers, perhaps because of the relatively

shorter gestation period in mice. The presence of striated bodies in the PLL post-natal portion was also noted by Smith *et al*. and pictured but not commented on by Rehbinder [9] [17]. This feature may be peculiar to mice. Interestingly, similar features were observed in the human PLL in a patient with Fuchs Endothelial Dystrophy but in this case the bodies were located in the posterior collagenous layer, which is formed by the abnormal basement membrane material pathologically produced by the endothelium in this disease [82]. The function and exact composition of these collagen like bodies are not yet known. The termination of the PLL at the trabeculum resembled the primate and the rabbit.

The structure of the mouse corneal endothelium closely resembled both the human [1] [79] and the rabbit [8] [61]. However, the mouse endothelium at 2.1 μm in transverse section is thinner than the rabbit (2.6 μm) and human (5 μm) endothelia [61] [83]. The general shape and outline, the extensive interdigitation of the lateral sides and the position of junctions showed striking similarity between the two species and presumably also provided the same functions.

The distribution of the mouse corneal nerve fibers was at variance with the primate. In the primate cornea nerve fibers are not found deeper than 50 μm from the epithelium, especially in the central cornea where most stromal fibers will be within 25 μm of the epithelium [79] [84]. However, the mouse cornea contained unmyelinated nerves in the deeper layers of the cornea within microns of the endothelium. Some of these fibers harbored terminals and must, therefore, be carrying out their functions at this posterior location. The mouse cornea, being a relatively thin one, may permit these terminals to respond to stimuli from an anterior direction. Alternatively, the posterior corneal nerve

fibers may have other functions than those associated with the primate corneal innervation.

Dimensionally, proportionally and anatomically all three strains of mice used for this experiment appear to be similar, and this may be true for other strains of mice as well. However, significant dimensional differences exist between mice and other mammals including human. Some noticeable variations were demonstrated ultrastructurally. Overall the mouse is a useful model for corneal research; however awareness of the morphological features peculiar to the mouse is important when using the mouse as an animal model applicable to the human.

3.6 Figures and Tables

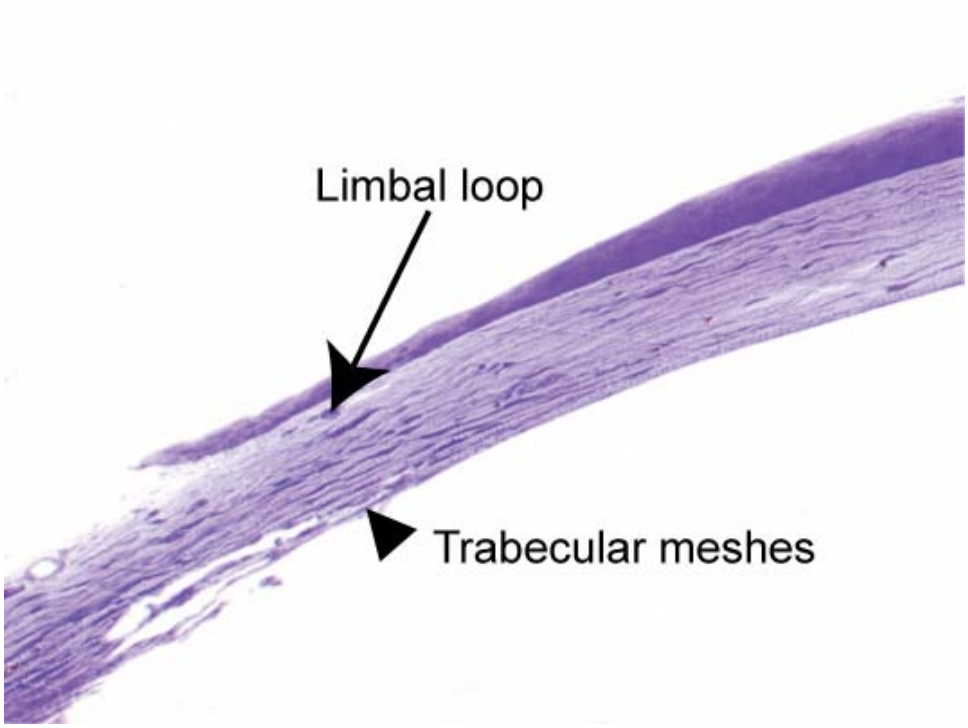

Figure 3.1 Peripheral cornea

Peripheral measurements were taken immediately central (anterior) to limbal loops and central to the anterior edge of the trabecular meshes (magnification 100X).

Figure 3.2 Mouse cornea

Thick section stained with toluidine blue showing the thickness variation between the central and peripheral mouse cornea in a C57BL/6 mouse (magnification 40X).

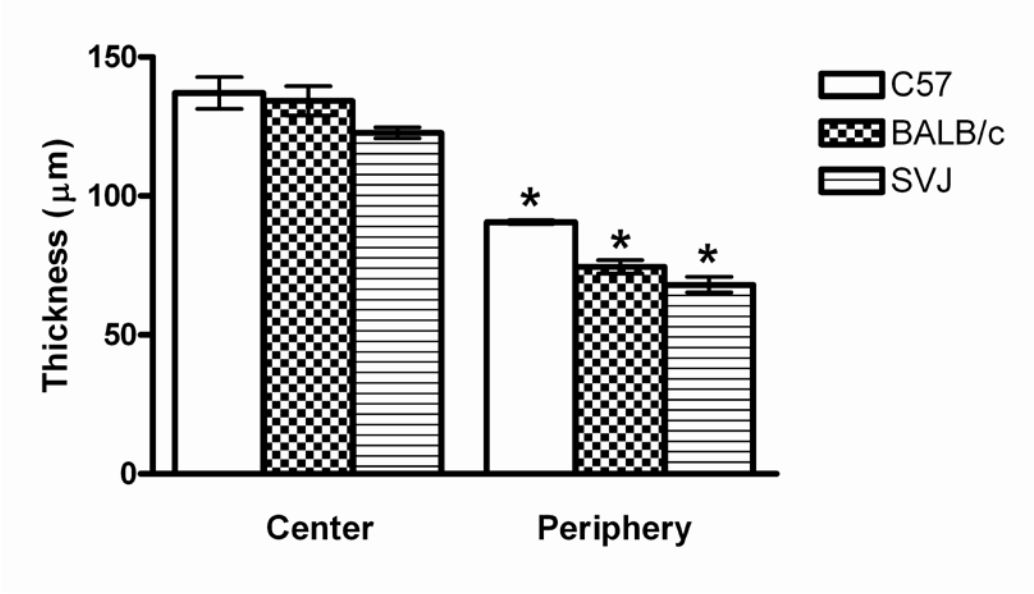

Figure 3.3 Central and peripheral corneal thickness

Average full central and peripheral corneal thickness for the BALB/c, C57BL/6 and the 129/SVJ mice. Central and peripheral corneal thickness within each strain was statistically compared using a student's t-test. Asterisk = ($P < 0.001$). Error bars show SD.

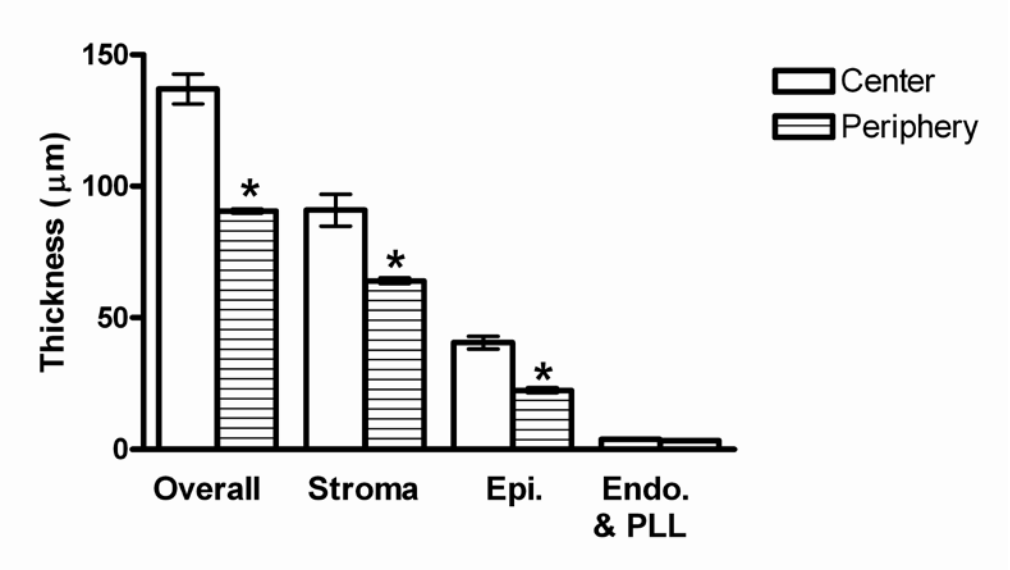

Figure 3.4 Overall thickness of corneal layers

Central and peripheral overall, stromal, epithelial and endothelial with PLL corneal thickness in the C57BL/6 mice. Central and peripheral corneal thickness of each of the corneal layers individually were statistically compared using a student's t-test. Asterisk = ($P < 0.001$). Error bars show SD.

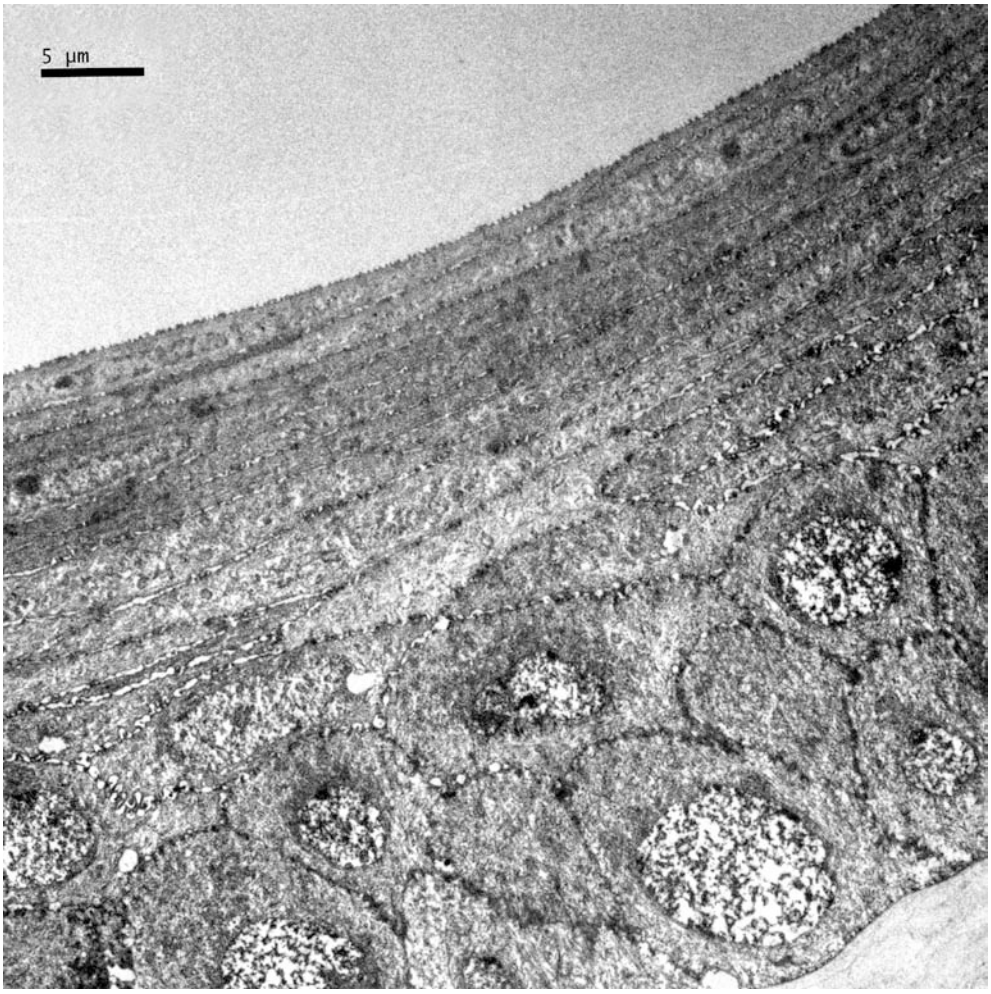

Figure 3.5 Central epithelium

The stratified epithelium is formed by 13 layers of cells and most numerous are the squamous cells. The cells are tightly packed with no obvious spaces between them.

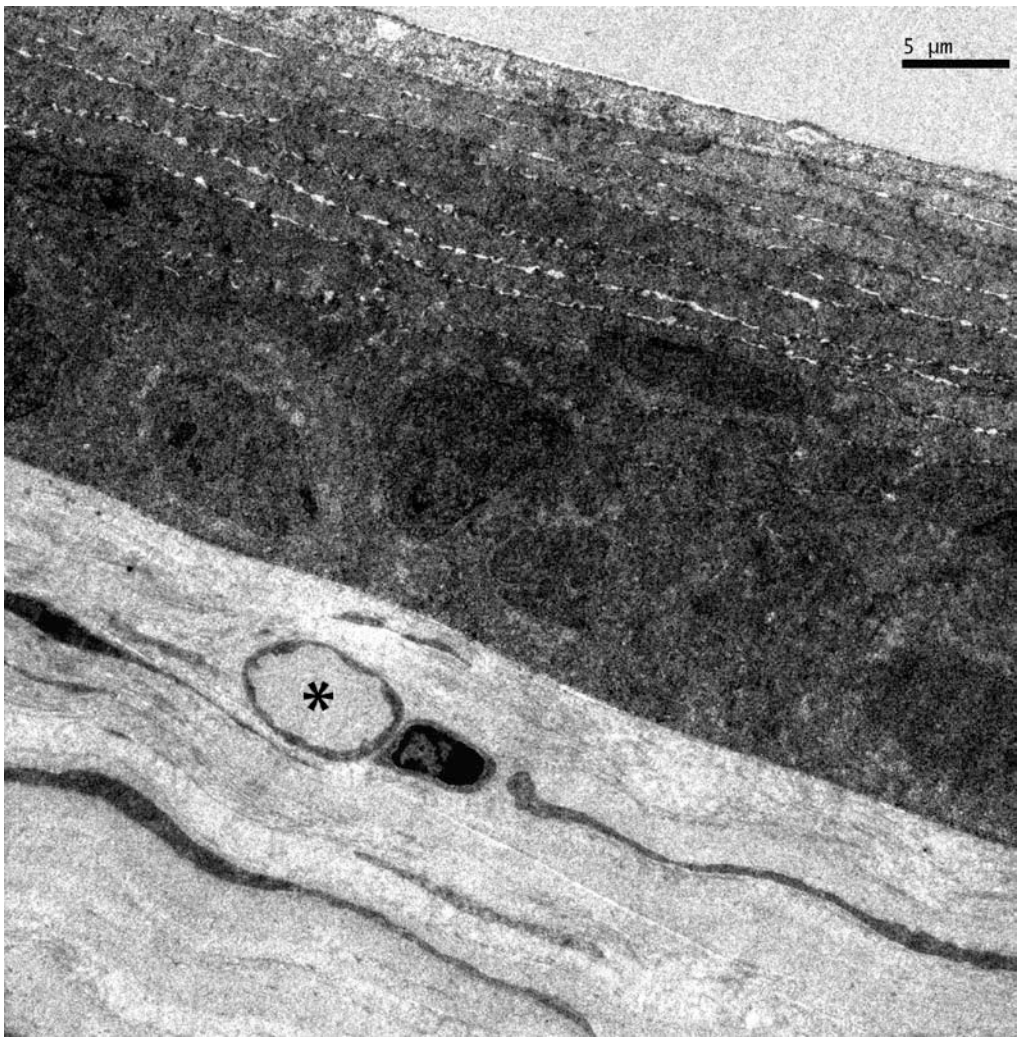

Figure 3.6 Peripheral cornea

The stratified epithelium is noticeably thinner than in the central cornea and consists here of 10 layers. Subepithelially a limbal capillary (asterisk) is in view. The stromal organization remains similar to the central cornea.

Figure 3.7 Micrograph of epithelium and stroma

The internal aspect of the epithelium is outlined by hemidesmosomes (white arrowhead) and a linear basement membrane (black arrow). Immediately internal to the basement membrane the collagen fibers are organized as stromal lamellae. An unmyelinated nervefiber bundle (asterisk) at preterminal level is present in the field of view.

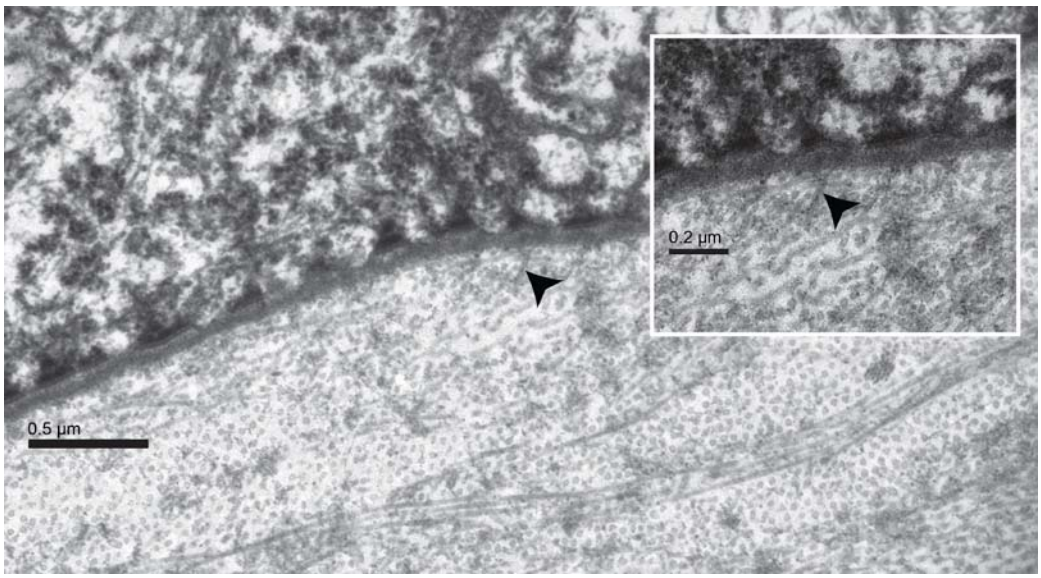

Figure 3.8 Epithelium - stroma interface

Except for apparent collagen Type Vll anchoring fibers (black arrowhead) all collagen fibers in this view are essentially parallel to the corneal surface. Inset: Higher magnification to show collagen Type Vll fibers (black arrowhead) inserting into the basement membrane.

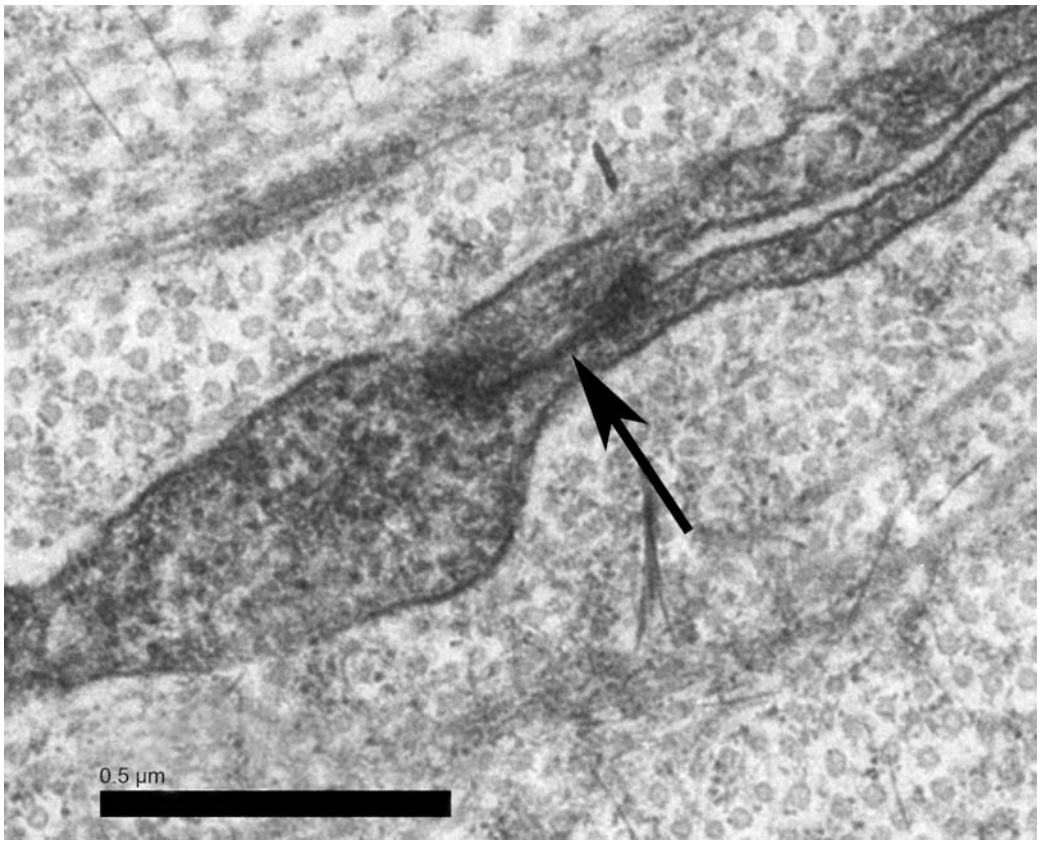

Figure 3.9 Keratocytes

Processes from two separate keratocytes form a gap junction (arrow) in the mid-stroma.

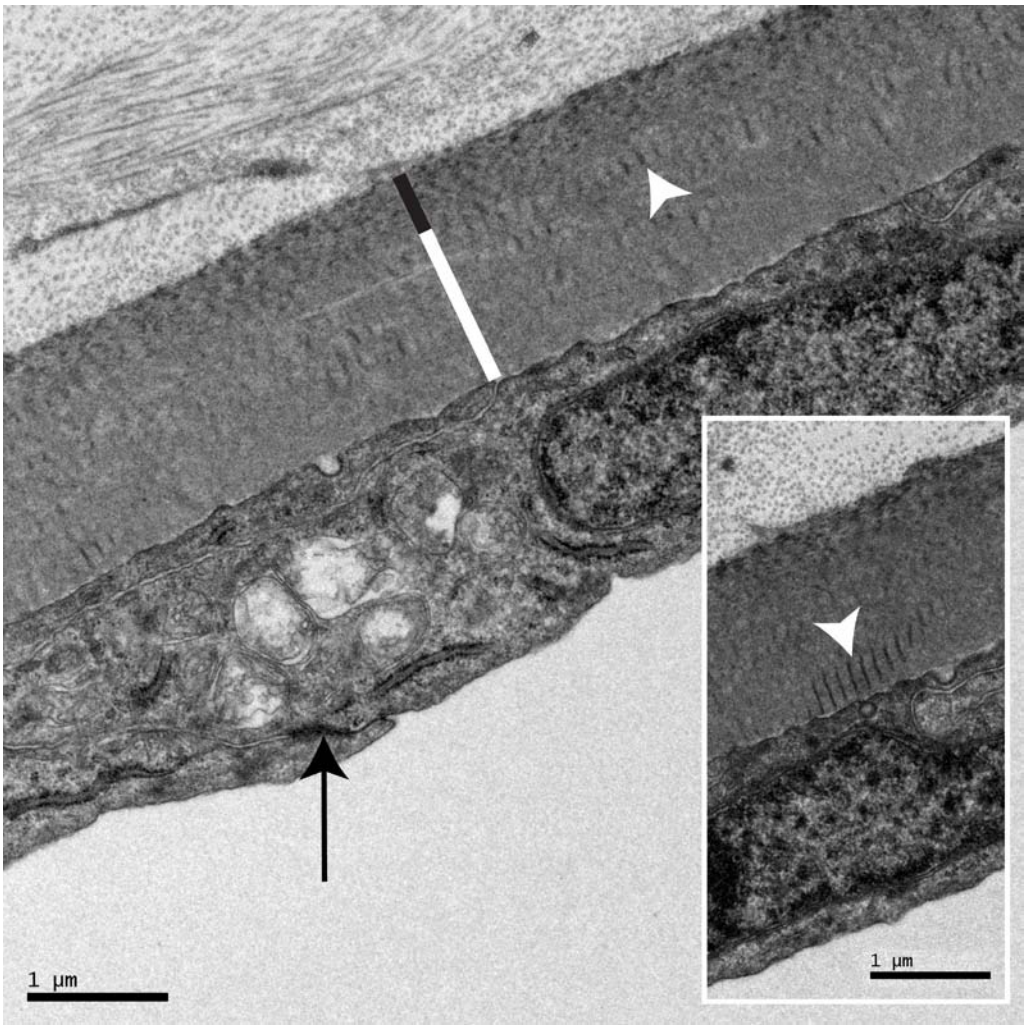

Figure 3.10 Endothelium and posterior limiting lamina

Neighboring endothelial cells are linked by a zonula occludens (black arrow), have essentially parallel apical and basal sides and are richly provided with organelles. The posterior limiting lamina has a thin banded portion (black line) and a thicker non-banded portion (white line). Collagen-like striated bodies (white arrowhead) are scattered along the non-banded portion at all levels. Inset: High magnification of posterior limiting lamina showing banded portion and striated bodies (white arrowhead) in greater detail.

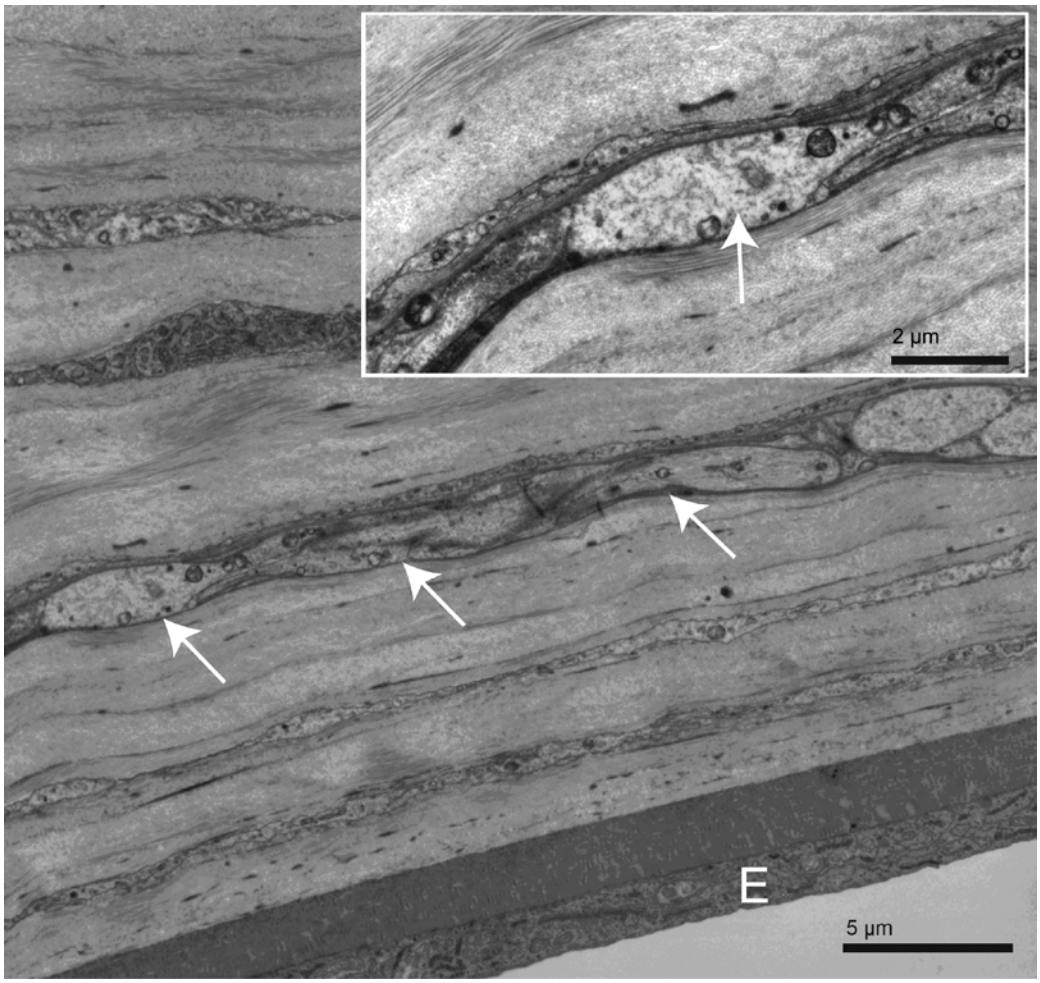

Figure 3.11 Stromal unmyelinated nervefiber bundle

Stromal unmyelinated nervefiber bundle within 10 µm of the endothelium. The nerve fiber (white arrows), here sectioned obliquely to longitudinally, runs parallel to the endothelial layer (E) and is at a preterminal to terminal stage. Inset: Higher magnification of this posterior stromal nerve fiber. One of its axons (white arrow) is forming a varicosity and at this point it is devoid of its Schwann cell wrapping.

	129/SVJ	C57BL/6	BALB/c
Corneal diameter (mm) (n= 4-5)	2.3 ± 0.1	2.6 ± 0.2	2.6 ± 0.1
Full corneal thickness (µm) (n= 3)	C: 122.7 ± 4.8 P: 68.0 ± 6.8	C: 137.0 ± 14.0 P: 90.6 ± 1.9	C: 134.2 ± 12.9 P: 74.5 ± 5.8
Stromal thickness (µm) (n= 3)	C: 80.6 ± 6.7 P: 45.4 ± 2.9	C: 90.9 ± 14.8 P: 64.1 ± 2.5	C: 81.9 ± 8.1 P: 51.7 ± 4.2
Epithelial thickness (µm) (n= 3)	C: 37.1 ± 2.3 P: 17.9 ± 6.6	C: 40.6 ± 5.8 P: 22.4 ± 2.5	C: 46.9 ± 4.9 P: 18.9 ± 4.2

Table 3.1 Corneal thickness

The mean and standard deviation of the measurements obtained from the 3 strains of mice investigated in this study. C = measurements from central cornea and P = measurements from peripheral cornea.

Chapter 4 - An Explanation for the Central to Peripheral Thickness Variation in the Mouse Cornea

Johanna Tukler Henriksson BS Opt[a], Anthony J. Bron BSc. FRCOpth FMedSci[b], Jan P.G Bergmanson OD, PhD, PhD h.c., DSc[a]

[a]Texas Eye Research and Technology Center, University of Houston College of Optometry, Houston, Texas, USA. [b]Nuffield Laboratory of Ophthalmology, University of Oxford, UK.

As submitted to: Experimental Eye Research November 2010

4.1 Abstract

The mouse corneal stroma varies in thickness across its diameter. The purpose of the present study was to explain this variation and to advance our understanding of stromal lamellar architecture in the mammalian cornea.

Eight C57BL/6 mice were euthanized, eyes enucleated, immersed in 2% glutaraldehyde fixative, processed and sectioned transversely for light (LM) and transmission electron microscopy (TEM). Keratocyte numbers were counted light microscopically and ultrastructurally, as those cells intersected along a narrow band, passing at a normal to the corneal surface at its center or in its periphery. TEM micrographs assembled into montages at 5000X magnification were used for keratocyte counts and lamellar counts and thickness assessments.

On average, 11.6 ± 0.2 keratocytes (LM) or 10.0 ± 0.6 keratocytes (TEM) were intersected and 49.8 ± 2.4 (TEM) lamellae were present centrally, averaging 2.1 µm in thickness. Peripherally 8.0 ± 0.6 keratocytes (LM) or 8.5 ± 0.6 keratocytes (TEM) were intersected, and 35.5 ± 3.0 (TEM) lamellae, averaging 1.9 µm in thickness. The central to peripheral decrease in number of keratocytes (LM), lamellae (TEM) and lamellar thickness (TEM) was statistically significant ($P < 0.005$), but statistical significance was not achieved with the ultrastructural keratocyte count.

This study demonstrated that the thickness difference between the thicker central and thinner peripheral mouse cornea is explained primarily by the number of lamellae present and that the peripheral lamellar drop out occurred in the anterior 2/3 of stroma. The decreased lamellar count towards the periphery suggested that not all lamellae cross the cornea limbus to limbus. An axial count of keratocytes with LM

provided a relative assessment of lamellae present. These findings may be relevant to the thickness variation of the human cornea.

4.2 Introduction

The structure of the human corneal stroma has many functional implications. It determines corneal refractive power [25], the distribution of water in the presence of stromal edema [85-93], the response of the cornea to refractive surgery [94-95] and the evolution of keratoconus, through a mechanism involving a loss of connective tissue adhesiveness [96-97]. The latter underlies the current treatment of keratoconus by cross-linking therapy [98-100]. Consequently it is important to understand stromal architecture and in particular, the organization of collagen across the full extent of the cornea.

The first accurate measurements of corneal thickness in the living human eye were made in the 1800s when it was concluded that, across its width, the cornea was thicker in its periphery than at its center [18]. This was supported later by a major study using optical pachometry [101] and has since been confirmed by others, using various techniques - ultrasound, [19 21-23], optical coherence tomography, [23]. None of these reports offered a formal anatomical explanation for this thickness variation although it has been suggested that it may be based on differences between the organization of the anterior and posterior stromal collagen lamellae [102].

Kokott [103], who studied the organization of collagen bundles in human cornea and sclera by teasing their fibrils apart, concluded that the lamellae had an orthogonal arrangement in the central cornea and extended without interruption from limbus to limbus, with a circular arrangement at the limbus itself. This view has been adopted in several textbook accounts of corneal structure [24-26 104]. However, there is evidence that, for a proportion of collagen bundles at least, this is not the case. Many anterior lamellae, central to the limbus, insert into the anterior limiting lamina (ALL) [104-110] or terminate

focally, subjacent to the ALL, in electron-dense formations [5]. These insertions probably make an important contribution to the asphericity of anterior corneal surface and hence to the optical power of the cornea [102]. They account too, for the greater antero-posterior interweave in the anterior third of the stroma, which, together with differences in antero-posterior stromal proteoglycan distribution (e.g. in bovine cornea - [85-86], is thought to limit the swellability of the anterior stroma considerably [87-88 93]). Their existence also indicates that, at least in the anterior third of the stroma, collagen bundles are present which are not interlimbal. In addition, narrow and wide angle X-ray diffraction studies have indicated that the lamellae of the posterior two thirds of the stroma have a predominantly orthogonal arrangement, registered on the vertical and horizontal meridian [111]. Those of the anterior stroma are more obliquely aligned. Furthermore, this work, supplemented by more recent microfocus X-ray techniques, has concluded that the annular orientation of limbal and peripheral corneal lamellae, is due to the presence of arcs of collagen bundles which traverse the sclera and enter the limbus tangentially [112-114]. In attempting to understand how the organization of collagen lamellae influences the distribution of thickness across the mammalian cornea, we have chosen to study the murine cornea, since it can be obtained in the fresh, unswollen state and has a more simple structure than that of the human cornea. In contrast to the human, we have found, in three different strains of mouse, that the thickness of the peripheral cornea is significantly less than that of the central cornea, with up to a 60 % decrease from centre to periphery [62]. This attenuation is due to a combined decrease in stromal and epithelial thickness in the periphery. Although the mouse corneal thickness variation across its meridional width is the reverse of that in the human cornea, it may serve as a model for

how such a variation is accomplished in the mammalian eye. In the present study the influence of stromal lamellar number on regional thickness variation was examined using two techniques. The first, involved direct measurement of lamellar number and thickness by TEM and the second, counting keratocyte numbers by light and electron microscopy, across the antero-posterior width of the cornea, along a narrow band at a normal to the surface. When observed in transverse sections by TEM, keratocytes are located predominantly *between* lamellae [4 7 31-33 62 83 104 115-116]. Therefore the number of keratocytes, intersected in a transverse section, could provide an indication of lamellar number and the lamellar contribution to corneal thickness.

4.3 Materials and Methods

All experiments were conducted in accordance with the ARVO Statement for the Use of Animals in Ophthalmic and Vision Research. Eight adult C57BL/6 mice, 6-8 weeks of age, were euthanized. A few drops of 2% glutaraldehyde in 80mM sodium cacodylate buffer, 330mOsm/kg fixative [61] were immediately applied to the corneas after resection of the eye lids. One intact eye was carefully enucleated from each mouse and immersed in fixative for 4-6 hours to ensure adequate tissue preservation. The tissue preparation protocol followed has been published previously [62].

Thick, transverse sections (0.5 – 1 μm) were cut from the central cornea with an ultramicrotome (Research Manufacturing Co. Inc MT-7000) and stained with 1% toluidine blue for assessment of orientation and data collection with an Olympus BX51 light microscope (LM). For morphological analysis ultrathin sections were obtained and mounted on parallel bar, copper grids (200MP, Cat # G200P, Electron Microscopy Sciences). The sections were double stained, first, in 3.5% uranyl acetate for 20 minutes at 60º C, followed by Reynold's lead citrate for 10 minutes at room temperature. The grids were examined in a Tecnai G2 Bio Twin Spirit (FEI Company, USA) TEM and consecutive slightly overlapping micrographs were captured digitally at 890X magnification across the total thickness of the cornea centrally and peripherally. Micrographs were assembled into montages using image assembly software, PanaVue ImageAssembler 3 (Sharelt Inc, USA) and printed (Roland FJ-52) at a final magnification of 5000X. All measurements were carried out by one investigator (JTH) following strict, preset criteria. According to these criteria the distinction between adjacent lamellae was based on an obvious difference in contrast between collagen bundles generated by

different fiber orientations [4]. If obvious branching was noticed within the micrograph care was taken not to double-count such lamellae. Presence of a keratocyte or its cytoplasmic projection as an indication of a lamellar border and lamellae thinner than 0.2 µm were not included in the count.

For analysis, the corneal stroma was divided precisely, into anterior, middle and posterior thirds, to investigate differences in the number of lamellae per unit length between the regions. After the lamellae were counted their individual width was measured using a millimeter ruler.

Keratocytes were counted in the antero-posterior plane on digital images of one representative, thick toluidine blue stained, LM section, from each cornea, at X200 magnification. In addition, lamellar width and numbers were measured on TEM sections at a magnification of X890. Peripheral counts were made at the extremity of the cornea, defined histologically as immediately central to the limbal capillaries and to the anterior edge of the trabecular meshwork. The morphometry was conducted in triplicate, at the same location, within a defined anterior-posterior, 10 µm wide axial band, at the corneal apex and periphery. Central corneal counts were carried out 1300 µm from the peripheral extreme of the cornea and were based on the corneal diameter for this species established and published previously [62]. Keratocyte and lamellae counts, individual lamellar thicknesses and epithelial thickness were measured by a single observer (JTH) using specified criteria to minimize inter-observer differences. A single observer was used, based on a previous study, which showed that the coefficient of variation between trained observers was 1% when determining the number of lamellae present in the human stroma [4].

Keratocytes were counted if they did not possess a basement membrane, a lobulated nucleus or dense staining granules. If more than one keratocyte appeared at the same level within the defined 10 µm band, only one was counted. To be included in the count the keratocytes also had to measure 4 µm horizontally and 0.2 µm vertically. Furthermore, full stromal thicknesses were also measured.

A paired t-test was used to compare the average central with the average peripheral corneal counts and measurements. The statistical significance was set to ($P < 0.05$). Data are presented as mean ± SEM.

4.4 Results

Under TEM, the stroma was found to be composed of collagen fibrils organized into lamellae, most of which were well-demarcated and arranged as flattened sheets running parallel to the surfaces of the cornea (Figure 4.1, 4.2). As in many other non-primate, mammalian corneas, the ALL was absent. Also different from the human cornea, the most anterior stromal lamellae were disposed in regular layers, without evident interweaving (Figure 4.3). Keratocytes were present predominantly between lamellae.

Two assembled montages from each of the eight corneas, one from the center and one from the periphery, were assessed for the overall corneal stromal thickness from the basement membrane of the epithelium to the posterior limiting lamina (PLL), the number of lamellae and individual lamellar and epithelial thickness was measured (Figure 4.2). The stroma had an average thickness of 115.9 ± 5.4 µm centrally compared to 72.9 ± 5.7 µm peripherally. The epithelium measured 44.6 ± 1.7 µm in the central cornea compared to 26.9 ± 2.2 µm in the periphery.

Utilizing LM for the axial, antero-posterior keratocyte count, the C57BL/6 mouse cornea had an average of 11.6 ± 0.2 keratocytes centrally compared to 8.0 ± 0.4 keratocytes peripherally (Figure 4.1). In contrast, by TEM, an average of 10.0 ± 0.6 keratocytes were found centrally compared to 8.5 ± 0.6 peripherally. A significant decrease in keratocyte numbers was found between central and peripheral cornea ($P < 0.005$) when keratocytes were counted under LM, but no significant difference ($P > 0.1$) was found between the central and peripheral cornea when keratocytes were counted by TEM (Table 4.1).

The C57BL/6 mouse cornea had an average of 49.8 ± 2.4 lamellae centrally (range 39-63), compared to an average of 35.5 ± 3.0 (range 26-53) lamellae peripherally (Figure 4.4A). The average individual lamellar thickness was measured as 2.10 ± 0.1 μm centrally and 1.86 ± 0.1 μm peripherally (Figure 4.4B). A significant decrease in both the average number and average thickness of the lamellae ($P < 0.01$) was found in the peripheral compared to the central cornea.

When comparing the central versus the peripheral lamellar counts, of the three, equal-sized stromal regions, the anterior and mid thirds of the central cornea had a greater number of lamellae compared to the posterior 1/3. In contrast, the peripheral cornea had an almost identical number of lamellae in the three regions (Table 4.1). The difference in number of lamellae between the central and peripheral cornea was found to be statistically significant for the anterior and mid regions ($P < 0.05$) but not for the posterior region ($P = 0.4$) of the cornea.

4.5 Discussion

The current study represents the first systematic attempt to provide anatomical basis for the central to peripheral thickness variation in mammalian cornea, using the mouse as a model. We employed a fixation protocol designed to maintain osmolality and pH at approximately physiological levels to minimize shrinkage artifacts [61]. The measurement technique utilized provides the observer with well-defined reference points for precise identification of intra-corneal interfaces. This is especially true with TEM, which permits lamellae to be clearly distinguished on the basis of fiber direction. Differentiation of lamellae is facilitated in the mouse by the lack of antero-posterior interweave between adjacent lamellae, which complicates measurement in the human cornea. The anterior lamellae in humans are often extremely thin and form a complex, interwoven pattern, while those of the mouse are more like those of the mid-stroma of human corneas.

There is some evidence that the lamellae in the mid and posterior regions of the human corneal stroma are of similar antero-posterior width to those of the mouse cornea. The average thickness of the central human cornea is 535 µm [2], which gives a stromal thickness of around 480 µm allowing 55 µm for the combined thickness of the epithelium, PLL and the endothelium. It follows, that the central, human, corneal stroma is 4 times thicker than that of the C57BL/6 mouse central corneal stroma. Recently, it was established that the human central corneal stroma is formed, on average, by 242 lamellae [4] while the number calculated in the mouse, in the present study was 50. This suggests that lamellar thickness is comparable between the two species and perhaps that

the basic building block of the stroma is of the same vertical dimension regardless of differences in corneal size.

One aim of the present study was to investigate whether counting keratocytes along an anterior-posterior axial band, 10 μm wide, using similar criteria for LM and TEM, could indicate lamellar width and the contribution of lamellae to total corneal thickness. This approach was based on the knowledge that keratocytes lie predominantly between the stromal lamellae in the primate [7 83 104 116], rabbit [7 31 83], mouse [62] and shark [115] cornea.

Using this approach it was found by LM, that 45% more keratocytes were intersected in the mouse central cornea than in the periphery, whereas by TEM, the number was only 18% greater (Table 4.1). The discrepancy between the two methods is most likely due to the difference in section thickness using the two techniques. The LM sections were approximately 10x thicker than the TEM sections and presumably increased the likelihood of cutting across individual keratocytes located between lamellae planes. Keratocyte counting by LM showed a smaller drop in lamellar count from center to periphery than that shown by the direct counting of lamellae under TEM, probably because of the scattered arrangement of the keratocytes within the inter-lamellar planes [116] so that keratocytes are not always encountered at each interface. We conclude that keratocyte counting under LM, which is a simple technique, may be of use as *rough* guide to lamellar numbers in wider comparative studies, but that it is not a substitute for direct lamellar counting under TEM.

A non-uniform antero-posterior distribution of stromal lamellae has been demonstrated in human central cornea, where around 50% more lamellae are present in

the anterior than in the posterior 100 µm of the stroma [4]. This emphasizes the value of counting all the lamellae across the stromal thickness, rather than extrapolating lamellar counts from regional samples. Using well-defined criteria, it is possible to achieve low inter-observer variation in measuring lamellar number across the thickness of the human cornea [4] and we used the same technique here, but with a single trained observer (JTH).

The central thickness of the corneal stroma reported in the present study is comparable to that reported in other studies, using various methods, in mice of different strains [13-15]. While the value of 116 µm found here, is approximately 20 µm thicker than that found in our earlier study [62], this is likely to be due to the normal thickness variation encountered in the strain studied. Age, is an unlikely explanation, since the mice were of similar age in both studies [62].

The mouse corneal stroma was found to be approximately 60% thicker centrally than peripherally (116 µm versus 73 µm). Part of this thickness variation was accounted for by a peripheral thinning of the lamellae and of the epithelium. Thus the average lamellar thickness was 2.1 µm in the central cornea compared to 1.9 µm in the periphery, a reduction of about 11%. Also, the peripheral epithelium was reduced in thickness by 40% (18 µm), compared to the center. However, the major contributor to the peripheral attenuation of corneal thickness was a significant fall in the average number of lamellae across the thickness of the cornea, from 50 in the center to 36 in the periphery.

The different lamellar counts reported here for the central and peripheral cornea of the mouse, and perhaps, to a lesser extent a minor reduction in lamellar thickness, explain the stromal contribution to corneal thickness variation. An important conclusion which may be drawn is that a proportion of lamellae in the center of the mouse cornea do

not extend to the limbus. This is implied by the decrease in lamellar number from center to periphery. The small decrease in lamellar thickness could also imply a decrease in collagen fiber number per lamella, although this apparent thinning could also be explained by a flattening of the lamellae in the plane of section.

This observation has a parallel in the human cornea, although operating in the opposite direction. In the human, corneal thickness is greater in the periphery than the centre and there appear to be more collagen lamellae in the periphery than in the central cornea [117]. One explanation put forward to explain this is the entry of collagen bundles of scleral origin to contribute to the limbal annulus [113]. Further, as noted, many lamellae presumed to originate from the limbus are inserted into the ALL. These insertions have been likened to the sutural fibers found in the dogfish shark [118] which prevent swelling in a cornea which possesses no endothelium [115]. Morishige *et al*. have referred to these lamellae as 'sutural lamellae' [118-119]. Additionally, as noted, anterior lamellae terminate in electron dense formations subjacent to the ALL [5].

A further structural finding in the present study was as follows: A comparison between lamellar counts from the anterior, mid and posterior stromal regions revealed that the posterior count did not show a statistically significant variation between central and peripheral cornea. However, the anterior and mid stromal regions showed a statistically significant lamellar drop out in the peripheral zone. This suggested that the posterior lamellae may indeed all cross the entire corneal width while a proportion of the more anterior ones do not. This conclusion is similar to that which has been drawn for the lamellae of the posterior two thirds of the human cornea [113].

In conclusion it may be summarized that the stroma of mouse cornea differs from that of the human cornea in several respects. The human cornea possesses an ALL, and an anterior stroma with a marked lamellar interweave. A proportion of its lamellae in the anterior third of the stroma either inserts directly into the ALL or terminate in electron-dense formations. It is evident that such lamellae do not cross from limbus to limbus and their peripheral origin may explain in part the greater thickness of the human cornea in the periphery. Their superficial insertion at the surface of the stroma probably contributes to its aspheric anterior contour. By contrast, the lamellae of the posterior two thirds of the human cornea lie in parallel bundles with more limited antero-posterior interweave. A high proportion of these lamellae are preferentially aligned in an orthogonal manner in the vertical/horizontal meridians and are considered to run from limbus to limbus. This arrangement contrasts with the situation in the mouse cornea which does not possess an ALL and whose lamellae are arranged in an array parallel to curvature of the cornea and do not end in electron-dense formations.

It is not known how this particular arrangement of the lamellae of the mouse cornea contributes to its anterior curvature and hence to its optical properties but it may be surmised to reflect an evolutionary response to biological forces. Various authors have suggested a relationship between the preferred, orthogonal orientation of collagen bundles in the posterior stroma of the human cornea and the disposition of forces imposed by the rectus muscles [120]. This implies either a postnatal role for extraocular muscle contraction in the adaptive modeling of the stromal lamellae or, more likely, the past influence of evolutionary pressures. In the mouse, corneal modeling, including completion of the limbal annulus, is not completed until the 28th postnatal day [121]. It may

be relevant that in animals which, like the primate, have frontally placed eyes, eye movements and thus activation of the extraocular muscles, play an important role in the location and tracking of visual targets whereas in animals with laterally placed eyes, such as the mouse, this function is subserved more by head movements. It is therefore of interest that the central region of the mouse cornea, unlike that of the human cornea, does not contain a significant amount of preferentially aligned, orthogonally disposed collagen [122]. It could be that the contribution to peripheral corneal thickness of arcing fibers of scleral origin, thought to exist in the human cornea [113] is lacking in those species in which eye movements in the horizontal plane are limited.

Importantly, as in the human cornea, the observations presented here indicate that all lamellae do not cross the cornea uninterrupted, from limbus to limbus. Given that, in the mouse, the central cornea contains more lamellae than the peripheral part, some central corneal lamellae must stop short of reaching the peripheral cornea. The terminating lamellae of the human cornea, termed electron dense formations [5], were not noted in the mouse. The anterior stroma in the human and the mouse are different structurally with the mouse lacking the interwoven, branching lamellar arrangement, characteristic in particular of the human anterior stroma. It is possible that the mouse utilizes an alternative biological solution to provide firm anchorage of the terminal end of lamellae.

In summary, the present study provided evidence that corneal thickness in the murine eye is modulated primarily by the number of lamellae present in the anterior 2/3 of the stroma. This intracorneal axial lamellar count variation suggested that not all stromal lamellae bridge from limbus to limbus. These principals of stromal architecture

may also apply to the human cornea, although its thickness variation is the reverse of that in the mouse.

4.6 Figures and Tables

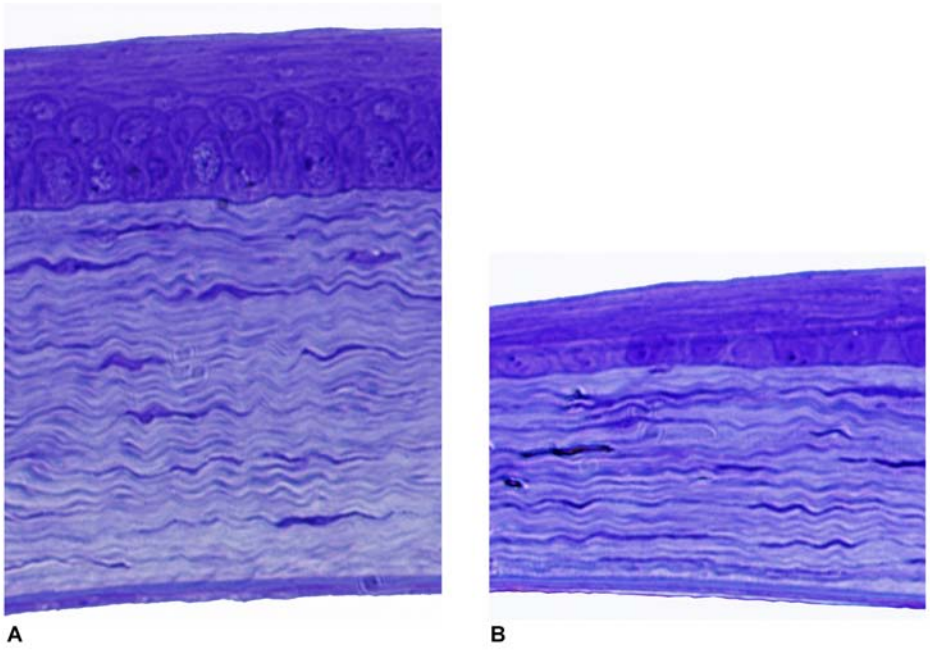

Figure 4.1 Light micrograph of central and peripheral murine cornea

Light micrograph of central (A) and peripheral (B) cornea of the same eye. Towards the peripheral cornea the thinning of the stroma is greater than the attenuation of the epithelium. Magnification: X400

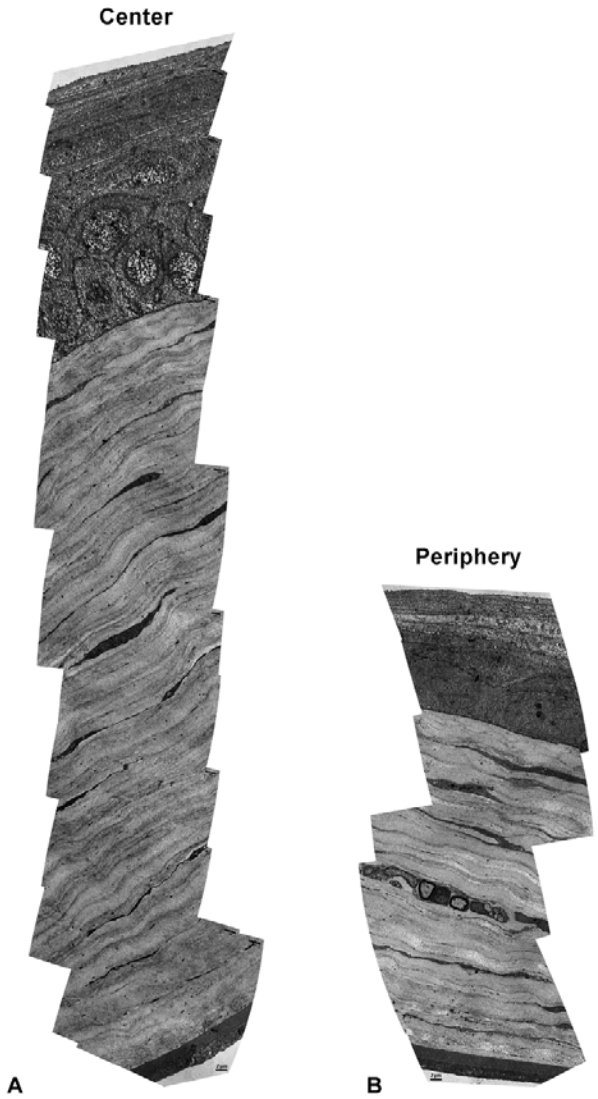

Figure 4.2 Transmission electron micrograph of montages

Transmission electron micrograph montages illustrating transverse section of central (A) and peripheral (B) cornea in the same eye. The reduced number of lamellae in the peripheral cornea compared to the central cornea is clearly demonstrated.

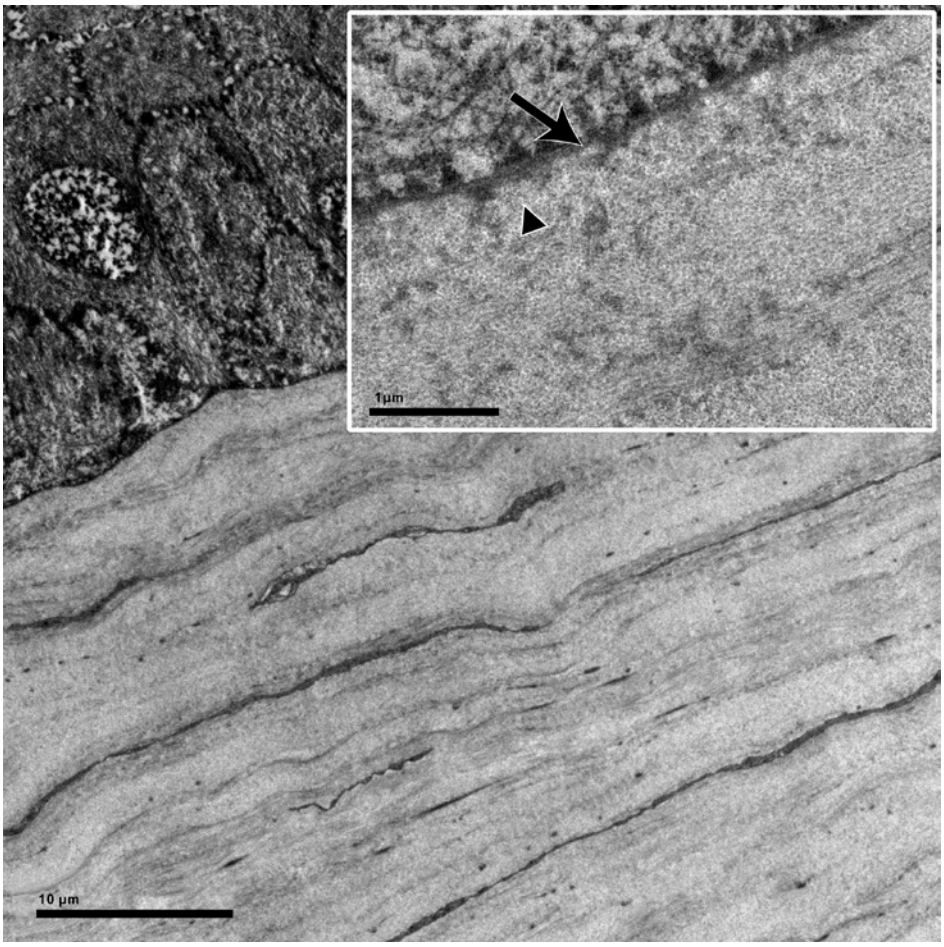

Figure 4.3 Ultrastructural detail of epithelial- stroma interface

Ultrastructural detail of anterior stroma and its interface with the epithelium. Lamellae of the anterior stroma are laid down over each other in a uniform manner and the interwoven and thin lamellae of the primate anterior stroma are absent. **Inset:** High magnification: The epithelial basement membrane (arrow) is lined by collagen fibers (triangle) of parallel orientation. Note that the anterior limiting lamina with its randomly oriented fibrils is not present.

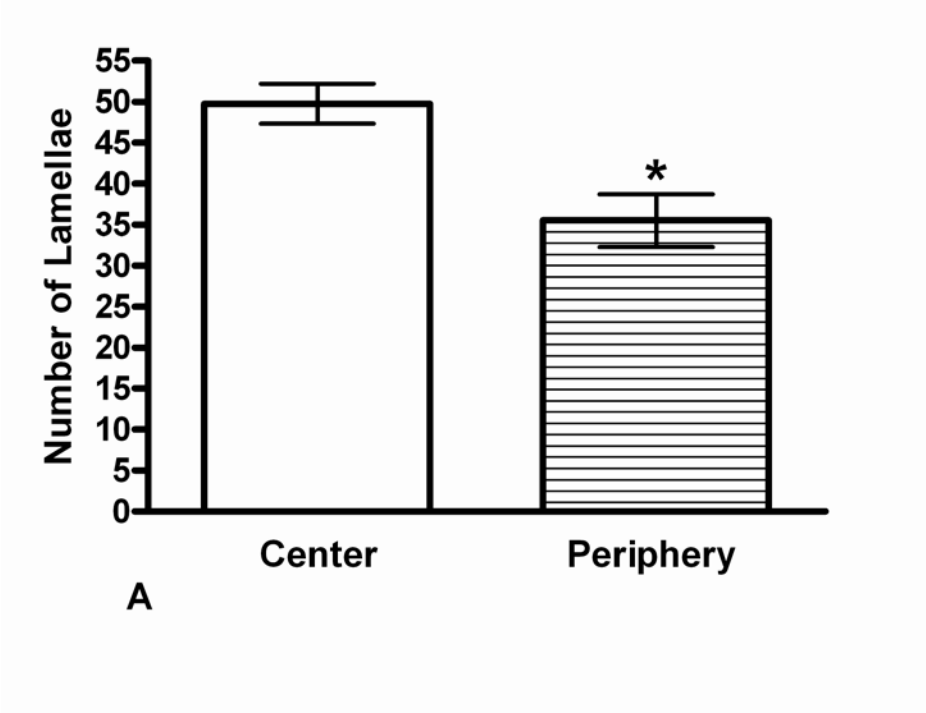
Number of Lamellae
55
50
45
40
35
30
25
20
15
10
5
0
*
Center
Periphery
A

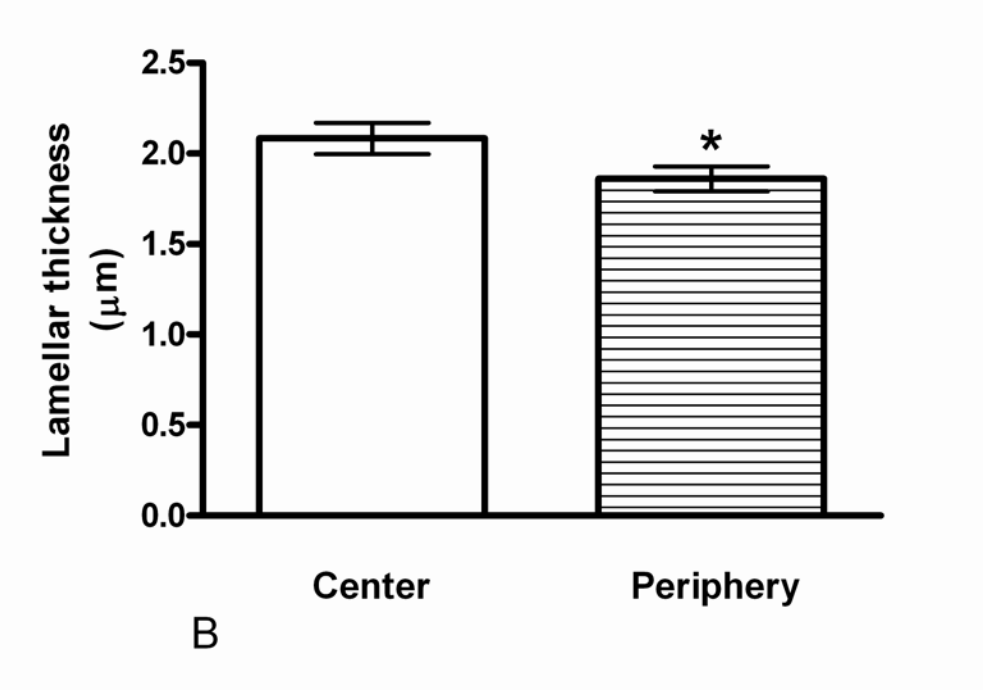
Lamellar thickness (μm)
2.5
2.0
1.5
1.0
0.5
0.0
*
Center
Periphery
B

Figure 4.4 Number and thickness of lamellae

Average number (A) and thickness (B) of lamellae present centrally and peripherally. A match paired t-test was utilized to compare number of lamellae and lamellar thickness between the central and peripheral cornea. Data are presented as mean ± SEM. Asterisk = ($P < 0.01$).

	Central (C)	Peripheral (P)	P-value C vs P
Keratocyte Counts			
Light microscopy	11.6 ± 0.2	8.0 ± 0.4	0.005
Transmission Electron Microscope	10.0 ± 0.6	8.5 ± 0.6	0.1
Number of Lamellae			
Anterior 1/3	18.5 ± 1.0	10.6 ± 1.2	0.05
Mid 1/3	17.9 ± 1.6	13.0 ± 1.3	0.05
Posterior 1/3	13.4 ± 0.9	11.9 ± 1.4	0.4

Table 4.1 Number of lamellae and keratocytes

Average number of keratocytes present within a 10 µm wide anterior-posterior vertical band and average number of lamellae present in three stromal regions. A paired t-test was used to compare between the central and peripheral cornea. Data are presented as mean ± SEM.

Chapter 5 - Morphological Alterations of the Palpebral Conjunctival Epithelium in a Dry Eye Model

Johanna Tukler Henriksson[a], Cintia S. De Paiva[b], William Farley[b], Stephen C. Pflugfelder[b], Alan R. Burns[a], Jan P.G. Bergmanson[a]

[a]Texas Eye Research and Technology Center, University of Houston College of Optometry, Houston, Texas; [b]Ocular Surface Center, Cullen Eye Institute, Department of Ophthalmology, Baylor College of Medicine, Houston, Texas.

Manuscript in preparation for publication

5.1 Abstract

Purpose: To utilize a histologic and morphometric approach to provide needed normative data on the normal palpebral conjunctiva and goblet cells in C57BL/6 mice, and to investigating structural changes occurring in an established dry eye mouse model.

Methods: 24 C57BL/6 mice, 8 untreated (UT) and 16 exposed to experimental ocular surface desiccating stress (DS). Ocular dryness was induced by administration of scopolamine hydrobromide (0.5 mg/0.2 ml) QID for 5 (DS5) or 10 (DS10) days. The eyes with surrounding lids were fixed in either 2% glutaraldehyde and processed according to an established protocol for light- (LM) and transmission (TEM) electron microscopy or in 10% formalin and embedded in paraffin. Stereology was utilized to evaluate surface density and volume fraction of goblet cells and granules. All counts and measurements were obtained using well established reference points and goblet cell density was investigated with a variety of stains.

Results: Near the junction between the lid margin and the normal palpebral conjunctiva the epithelium had an average thickness of 45.6 ± 10.5 μm and 8.8 ± 2.0 cell layers, versus 41.8 ± 6.5 μm and 8.0 ± 0.9 layers in the DS5 ($P > 0.05$) and 37.7 ± 5.6 μm and 7.4 ± 1.3 layers in the DS10 ($P < 0.05$). In the goblet cell populated palpebral region the normal conjunctival epithelium averaged 23.5 ± 4.0 μm and was significantly ($P<0.05$) thicker than in the DS5 (18.2 ± 2.8 μm) and the DS10 (19.0 ± 3.1 μm). In the control 43% of the goblet cells had an epithelial coverage, compared to 58% for the DS5 and 63% for the DS10 ($P < 0.05$). No difference was found in surface density of goblet

cells or volume fraction (approximately 43%) between the three groups. Some stains indicated a decreased number of goblet cells in the dry eye (PAS and Alcian blue), while (MUC5AC, histology) did not.

Conclusions: The mouse palpebral conjunctival epithelium had a structure similar to the human. In the dry eye, the palpebral conjunctival epithelium decreased in thickness and this was associated with a decreased layer of epithelial cells at the junction of the lid margin and the conjunctiva. After DS goblet cell access to the surface appears to be inhibited by surrounding epithelial cells, which potentially may slow down their migration to the surface. Goblet cell density differed depending on stain used for evaluation of mucous secreting cells, suggesting that there may be different subtypes of goblet cells on the ocular surface or may be PAS and Alcian blue are mucin specific and not goblet cell specific. The mouse conjunctival epithelium has a structure similar to the human and appears to be viable model for conjunctival and dry eye research.

5.2 Introduction

'Dry eye is defined as a multifactorial disease of the tears and ocular surface that results in symptoms of discomfort, visual disturbance and tear film instability with potential damage to the ocular surface. It is accompanied by increased osmolarity of the tear film and inflammation of the ocular surface' [39]. Almost 5 million Americans, 50 years or older - 3.23 million women and 1.68 million men – have dry eyes [40-41]. However, the Dry Eye Workshop (DEWS) report suggests tens of millions more have less severe symptoms, which may become manifest only during stressful conditions for the ocular surface e.g., during contact lens wear, airline travel and drafty environmental conditions [42].

Evaluating the pathological changes in the conjunctival epithelium in human dry eye patients requires biopsying one or more sites and is not feasible due to ethical considerations. As a consequence, studies concerning the pathology of the dry eye require an animal model. The dry eye mouse has proved useful in assessing the effects of dryness on the ocular surface epithelial and immune/inflammatory cells [45]. Although, the mouse is widely used for ocular surface studies, literature has, surprisingly, only limited structural information to offer on the normal conjunctiva in both humans and mice [9 48].

Morphological and dimensional alterations occurring in the dry eye palpebral conjunctival epithelium are yet to be investigated. Therefore, ultrastructural studies evaluating the normal and the dry eye palpebral conjunctival epithelium are needed and will enhance our understanding of the dry eye. An increased understanding of the dry eye palpebral conjunctival epithelium may help direct clinicians toward an improved diagnosis and management of dry eye sufferers and can potentially also be beneficial in

the future when designing pharmacological agents intended to cure or relieve patient's symptoms.

The purpose of the present study was to utilize a histologic and morphometric approach to provide needed normative data on the normal palpebral conjunctiva and goblet cells in C57BL/6 mice, while also investigating structural changes occurring in an established dry eye mouse model.

5.3 Materials and Methods

All experiments were conducted in accordance with the ARVO Statement for the Use of Animals in Ophthalmic and Vision Research. A total of 24 mice of both genders, 6-8 weeks of age were utilized for this experiment. Eight untreated (UT) C57BL/6 mice (control) were used for morphometric assessment and description of the normal palpebral conjunctiva. The data obtained from the untreated mice were compared to data obtained from the palpebral conjunctiva of 16 mice, 8 per group who were exposed to experimental ocular surface desiccating stress (DS) for 5 or 10 days (DS5 and DS10). DS was created by injection of scopolamine hydrobromide (0.5mg/0.2ml) QID, alternating between the left and right flanks [43]. Mice (up to 5 per cage) were exposed to a constant air draft for 16hr/day from a fan placed 6" away from a side of their cage. Room humidity was maintained at 35-40% and temperature at 80°F. Aqueous tear production/volume was assessed using cotton thread (Quick Zone Thread; Oasis) [63]. Following euthanization, eyes with surrounding eyelids were dissected, the right eyes processed for histology and the left eyes for immunohistochemistry.

Histochemistry

The eyes with surrounding eyelids were fixed in 10% buffered formalin over night and embedded in paraffin. 5 µm thick serial sections from each sample were cut with a microtome (Microm HM 340E). The sections were deparaffinized and stained with 0.5% periodic acid-schiff (PAS) stain, Alcian blue (pH 2.5) or with MUC5AC antibody (SC-20118 Santa Cruz) for identification of goblet cells. Digital images of four sections, (eight eye lids), from 3 animals per group were captured (DXM, 1200; Nikon) and

evaluated (NIS Elements, Nikon). The number of positively stained goblet cells was counted and the length of the basement membrane between the first and last goblet cell measured. In addition, the MUC5AC positive area was also measured. The data are presented as the average number of goblet cells and total goblet cells/mm per eye lid.

MUC5AC Immunohistochemical staining

After deparaffinization, heat induced antigen retrieval was performed for 20 minutes in sodium citrate buffer (10mM sodium citrate, 0.05% Tween 20, pH 6.0). Subsequently, the sections were treated with 0.3% H_2O_2 in PBS to quench the endogenous peroxidase activity and then incubated with an avidin-biotin block (Vector Laboratories) for 10 minutes each. After blocking with 20% normal goat serum in PBS for 30 minutes, the rabbit polyclonal primary antibody, SC-20118 Santa Cruz (1:200) diluted in 5% goat serum was applied and incubated for 60 minutes at room temperature. Next, the secondary antibody (rabbit polyclonal BD Pharmingen CN 550338, 1:50) in 5% goat serum was applied for 30 minutes also at room temperature. The tissue was then incubated in an ABC solution (Vectastain Elite ABC Kit, Vector Laboratories), an immunoperoxidase procedure where the antibody is visualized through a peroxidase-catalyzed reaction, and stained with a diaminobenzidine (DAB) solution (NovaRed substate kit, Vector, CN-4800, red stain) for 2 minutes. The reaction was terminated in distilled water, the sections counterstained with Mayer's Hematoxylin, rinsed in tap water, dehydrated, cleared and mounted with 1-2 drops of Permount (SP15-100, Fisher Chemicals). Normal rabbit serum concentration (1:200) was substituted for the primary antibody as an irrelevant control.

Light (LM) and Transmission Electron Microscopy (TEM)

A few drops of 2% glutaraldehyde in 80mM sodium cacodylate buffered, 330mOsm/kg fixative [61] was immediately applied to the right cornea and eyelids after euthanization of the animals. Subsequently, the eyes with attached lids were carefully removed and immersed in fixative for 4-6 hours to ensure proper cross linking and preservation of the tissue. After fixation, transverse pieces (1x 1.5mm) were cut from both the superior and inferior eyelids. Next, the tissue pieces were washed three times in sodium cacodylate buffer (pH 7.4) at room temperature for 10 minutes per wash. The samples were then immersed in a freshly prepared 1% solution of osmium tetroxide in100mM sodium cacodylate buffer for 1 hour under dim light. After osmofication the samples were washed several times in sodium cacodylate buffer, and at 10 minutes per wash. A Leica EM TP tissue processor (Bannockburn, IL) was used for dehydration, transition, infiltration and embedding. The tissue samples were dehydrated through a graded alcohol series (30% - 100% in 6 steps) at room temperature and infiltrated with propylene oxide. Embedding with agitation was achieved through an initial 2:1 mixture of propylene oxide and Araldite resin for 3 hours followed by overnight immersion in a 1:1 mixture of propylene oxide and Araldite resin. Thereafter, the tissue samples were immersed in a propylene oxide and Araldite resin (SPI, Westchester, PA) 1:3 mixture for 4-8 hours before being transferred to 100% Araldite resin overnight. The tissue samples were then oriented in embedding molds and left 12 hours for polymerization in an oven at 60 °C. An ultramicrotome (Research Manufacturing Co. Inc MT-7000, Tucson, AZ) was used to cut thick (0.5 – 1 µm) and ultrathin transverse sections (60-100 nm). The thick sections were stained with 1 % toluidine blue for examination with an Olympus BX51

(Center Valley, PA) light microscope (LM). Slightly overlapping digital images were captured at 100X, montages assembled using PanaVue ImageAssembler 3 (Sharelt Inc, USA) and printed (Roland FJ-52). First, the thickness of the conjunctival palpebral epithelium was measured in triplicate using NIH Image Software and the number of cell layers counted in the marginal, central and peripheral palpebral conjunctiva. Second, the number of goblet cells was counted based on histological criteria. Cells meeting one or more of the following criteria, a triangular shaped nucleus, cytoplasm packed with secretory granules or a bloated or ballooning cell body, were classified and counted as goblet cells. Their location within the epithelium (basal or superficial) was also determined.

For morphological analysis ultrathin sections were mounted on oval slot (2x1 mm) formvar/carbon coated copper grids (FCF2010-Cu, Electron Microscopy Sciences, Hatfield, PA). These sections were double stained, first, in 3.5% uranyl acetate for 20 minutes, followed by Reynold's lead citrate for 10 minutes at room temperature. The stained grids were examined in a Tecnai G2 Bio Twin Spirit (FEI Company, Hillsboro, OR) Transmission Electron Microscope (TEM). TEM micrographs of goblet cells were captured digitally at a magnification of 890X.

Morphometry

Stereology is a widely used biological technique utilized to obtain three dimensional data from sampling in two dimensions (e.g from tissue sections) [64]. Statistical analysis was used to determine that 10 goblet cells from each sample were sufficient for accurate morphometric analysis; a random number generator and systematic

random uniform sampling (SURS) were used for unbiased selection of 10 goblet cells from each sample to include in the data analysis.

To determine surface density (Sv) of the goblet cell and volume fraction (Vv) of granules per goblet cell, the point counting method was used, by randomly placing a cycloid grid oriented perpendicular over the goblet cell of interest [65-66]. Surface density (Sv) was calculated by the formula, $Sv = (2*\Sigma I)/ (l/p *\Sigma P)$ where I = the number cycloid intersects with the goblet cell plasma membrane or granule plasma membrane, P = points falling on the entire goblet cell or on granules and l/p equals a constant corrected for linear magnification [64 67]. The volume fraction (Vv) was calculated by counting all dots falling on granules and dividing by all dots falling on the goblet cell. To investigate the volume fraction (Vv) of goblet cells in the entire palpebral conjunctival epithelial goblet cell region a point counting grid was used. (Vv) was computed by counting all dots falling on goblet cells and dividing by the total number of dots falling on the palpebral conjunctival epithelium. The average area per goblet cell in each of the three conditions was also measured.

Statistical Analysis

One way analysis of variance (ANOVA) with Dunnett post hoc testing was performed to compare morphometry, palpebral conjunctival epithelial thickness measurements and counts between the three conditions (UT, DS5 and DS10). Statistical significance was set to ($P < 0.05$). Data are presented as mean ± SD. Prism 4.0 software (GraphPad Software Inc., San Diego CA) was utilized for the statistical analysis.

5.4 Results

The first part of this study utilized light microscopy and investigated whether morphological differences existed between the normal superior and inferior palpebral conjunctival epithelium. The only difference noticed between the two lids was at the lid margin, where the superior conjunctival epithelium was approximately 14 μm and 3 cell layers thicker than the inferior. Since no other differences were found between the two lids, the data are reported as the combined averages ± SD from the superior and inferior lids.

At the junction of the lid margin and palpebral conjunctiva the epithelium can be described as a stratified multi-layered epithelium devoid of goblet cells. In this region the epithelium was composed of 8.8 ± 2.0 cell layers with average thickness of 45.6 ± 10.5 μm. Going in a peripheral direction over the next 372.1 ± 79.3 μm the epithelium tapered down to 3-4 layers of cells but lacked goblet cells. However, goblet cells were present over the next 1356.3 ± 154.9 μm where the epithelium maintained an approximately uniform thickness (Figure 5.1).

In the goblet cell-rich region the thickness of the normal conjunctival epithelium averaged 23.5 ± 4.0 μm and was significantly ($P < 0.05$) thicker than the DS5 (18.2 ± 2.8μm) and the DS10 (19.0 ± 3.1μm). When comparing regional epithelial thickness variations all three palpebral conjunctival regions (marginal, central and peripheral) showed a statistical significant difference in thickness between the DS5 and DS10 compared to the control (UT) (Figure 5.1, Table 5.1). A decreased thickness and a loss of epithelial cells were also noticed at the junctional lid margin in the DS10 compared to the normal (Table 5.1). There was no statistically significant difference ($P >$

0.05) in the number of goblet cells between the superior and inferior lids or between the different treatment groups (Figure 5.2). However, in normal eyes, 43% of the goblet cells were covered by epithelial cells, compared to 58% for the DS5 and 63% for the DS10 ($P < 0.05$) (Figure 5.3 and Figure 5.4 A,B).

Since no difference in number of goblet cells was found between the normal and the two dry eye groups, morphological analysis was utilized to investigate whether the volume fraction of goblet cells per area of epithelium changed in the dry eye. No statistical differences were found between treatments when evaluating volume fractions of goblet cells, volume fractions of granules per goblet cell or the surface densities of goblet cell and granule membranes (Table 5.2).

Finally, this study investigated whether experimental dryness would decrease the number of goblet cells stained with mucous specific stains. This experiment showed a statistically significant decrease of PAS and Alcian blue positive goblet cells in DS5 and DS10 compared to the UT, however, no difference was found when the MUC5AC positive cells were counted. Nor was any difference noticed between the three conditions when the MUC5AC positive area was measured. However, in the UT there was a statistically significant lower number of MUC5AC cells than cells stained by PAS or Alcian blue (Figure 5.5, Table 5.3). This is in agreement with the observation that some of the mucous filled goblet cells stained only with PAS, while others only stained with Alcian blue or MUC5AC (Figure 5.6).

5.5 Discussion

This study represents the first attempt to utilize a systematic, histologic approach to morphometrically and dimensionally assess the normal palpebral conjunctival epithelium, while also investigating structural changes occurring in the dry eye. To ensure proper cross-linking and preservation of the tissue, a fixation protocol that approximates physiological osmolality and pH values and, as a result, produce minimal tissue shrinkage and distortion was employed [61]. The histological approach chosen allowed the observer to conduct accurate intra-conjunctival measurements by utilizing well defined specific reference points. In addition to counts and measurements, a stereological approach was used to conduct morphometric analysis. Design-based stereology became the method of choice since it allows the observer to sample in two dimensions (e.g. from microscope slide), and relate the interpretations to three dimensional space [67].

Our data showed that similar to the human, the mouse palpebral conjunctival epithelium can be described as a stratified multi-layered epithelium rich in goblet cells with surface cells that feature a glycocalyx. The superior human palpebral conjunctiva is stated to have only two layers of cells with a third layer appearing close to fornix, while the inferior palpebral conjunctiva has on average 3-4 layers of cells [48]. Both the superior and inferior C57BL/6 mouse palpebral conjunctiva had an average of 3 cell layers, and agrees with what has been documented for the human [48], rabbit [123-124], gerbil [125] and guinea pig [126] but contrasts with the 5-8 layers of cells reported for the Sprague-Dawley rat [127-128].

The present study is unique in providing epithelial thickness values for the different regions, and, in addition, morphometrically defining the portion of the lid containing goblet cells in the normal and dry eye palpebral conjunctiva. The latter is particularly applicable to the mouse conjunctiva where the goblet cells may only be visualized in a limited region. Nor has a decreased epithelial thickness and reduction of epithelial cells at the lid margin in the dry eye previously been reported. Increased friction from desiccation of the tissue, an increased frequency of blinking or a combination of both can be potential causes for the decreased epithelial thickness and loss of cells at the lid margin in the dry eye. The lid wiper is defined as the portion of the marginal conjunctiva of the upper lid that spread the tear film over the ocular surface [129]. Clinically, this area has shown positive (rose bengal, lissamine green and/or flourescein) staining in patients with dry eye symptoms [129-130]. The conjunctival epithelial thinning and reduction of epithelial cells at the junction of the lid margin and the conjunctiva may be a potential explanation behind the staining caused by this condition.

In the palpebral conjunctiva the goblet cells were noted as isolated cells or were arranged in clusters. This configuration is in agreement with what has been reported for the mouse bulbar conjunctiva [131], the mongolian gerbil [125], human [132] and rabbit [124] but contrary to the guinea pig where goblet cells have been reported to be arranged singly [126] and to the Sprague-Dawley rat, where goblet cells are found only in clusters [128].

Goblet cells, their granules and secretion have been investigated ultrastructurally in other organs e.g. lung and airway epithelium [133-134] and intestines [135-136]. A few studies are available providing ultrastructural information on conjunctival goblet cells in different species e.g. the human [132 137-138], rabbit [123-124], rat [125 127 138-140] and

guinea pig [126 141-142].The goblet cells were reported to be on average 11-15 µm (rabbit)[123-124] and 15-20 µm (human)[143] in height and rich in secretory granules. These membrane bound granules were spheroid or ovoid in shape and between 0.3-1 µm in diameter [124 132 137-138]. They had heterogeneous or homogenous electron density and their shades varied from light gray to very dark [123-124 132 137].

Only two studies were found that incorporated ultrastructural analysis of the normal mouse conjunctiva. While these studies provided valuable information on goblet cells and their granules, they do not address conjunctival and goblet cell morphology in the dry eye. The study by Aargona *et al.* [131] used the superior bulbar conjunctiva and investigated the effects of tear substitutes on the conjunctival epithelium in 3 month old CD1 mice. Paz *et al.* [144] studied the role of calcium in mucin packaging within goblet cells, in C57/129/sv hybrids but did not identify the conjunctival region examined nor were the ages of the mice reported. None of these studies provided thickness measurements of the conjunctival epithelium or studied the same region of the conjunctiva (palpebral) as reported in the current study.

Ultrastructurally goblet cell granules were found to be homogenous with different shades of gray to black. A variety of granule shades was observed both within and between goblet cells. There was no difference in granule appearance between the unstressed and dry conditions and thus, all shades were seen in all conditions. Aragona *et al.* [131] reported a homogenous light gray granule appearance while Paz *et al.* [144] reported goblet cells with mostly dark granules in normal mice and a mixture of electron-dense granules in a group treated with sodium hyaluronate. Because all these varieties of granules were seen in our samples, this study agrees with both of these previous reports.

The majority of previously reported studies investigating goblet cell density light microscopically, counted either PAS or Alcian blue positive goblet cells. The present study detected a decreased number of goblet cells in the dry eye when either of these stains were used, and this finding is in agreement with previous reports [43 46 50]. As shown in Table 5.3, fewer goblet cells were detected by MUC5AC staining in control eyes (56.7 ± 11.8) compared to immunohistochemistry (73.8 ± 16.5 PAS), (68.9 ± 13.3 Alcian blue). The total number of goblet cells detected by PAS, Alcian blue or MUC5AC immunostaining was similar after 5 and 10 days of dry eye. Comparison of the number of cells detected by histochemistry and immunohistochemistry in the present study suggests that there is more than one type of goblet cell (Figure 5.5, Figure 5.6). A change in histochemical characteristics of the goblet cells have previously been reported as a consequence of treatments with different tear substitutes [131], but it is a novel finding that the percentage of goblet cells staining with either PAS or Alcian blue but not with MUC5AC decreases in dry eye.

One possible explanation is that different subtypes of goblet cells present at the ocular surface are programmed to produce mucin of different biochemical and histochemical characteristics. If so, it appears that the goblet cells producing neutral mucin (stained by PAS) or acidic mucin (stained by Alcian blue) are more likely to be affected by a dry eye condition than those producing MUC5AC. MUC2, another mucin secreted by goblet cells has been detected in human conjunctiva and tears [145-146]. It is possible that some of the PAS or Alcian blue positive cells that don't stain for MUC5AC secrete MUC2.

Goblet cell counts carried out histologically showed a smaller number and no difference was detected between groups. The discrepancy in counts between goblet cells counted in semi-thin plastic sections and goblet cells counted in paraffin sections is explained by the difference in thickness between the 0.5µm thick resin embedded sections versus the 5 µm thick paraffin embedded sections.

A morphometric approach was utilized to enhance our understanding of how the goblet cells are affected by the dry eye. Volume fraction of goblet cells within the epithelium did not show a difference between the groups. Before drawing conclusions from this experiment it is important to factor in the shrinkage of the reference space (epithelium) in the dry eye [147]. In the dry eye there was a 29% (5D) and 24% (10D) decrease in epithelial volume while the volume fraction and shape (Sv) of the goblet cells remained constant (Table 5.2). Taking this epithelial change into account we would like to propose that the goblet cells size decreases in the dry eye and this reduction in size was proportional to the decreased thickness of the epithelium. Although the goblet cell size decreased in the dry eye, the volume fraction (approximately 43%) and surface density (Sv) of granules remained unchanged between the three conditions. The same surface density and volume fraction of granules could be explained either by the granules having the same size or by the granules being smaller and more numerous in the dry eye. However, if the size or the numbers of granules are altered in the dry eye it does not appear to have an effect on mucin production, since the present study showed the same number of MUC5AC positive cells and the same area of MUC5AC staining in the three conditions (Table 5.3).

Earlier studies have proposed that parasympathetic innervation regulates goblet cell secretion [148]. In the current study experimental ocular surface desiccating stress was induced by scopolamine injections, which generate dry eye by pharmacologically blocking cholinergic receptors. If the administered scopolamine injections had an effect on goblet cell secretion, a larger volume fraction of goblet cells and an increased area of mucin in the dry eye epithelium would be expected as a result of the blocked secretion. However, this was not seen and therefore, we would like to conclude that the results shown in this study were not a side effect of the administered injections.

An increased epithelial coverage was detected in the dry eye (Figure 5.3). One possibility is, therefore, that the dry eye has the same number of MUC5AC positive goblet cells and produces the same amount of this mucin, as illustrated by the number of MUC5AC stained goblet cells and the total area of mucin detected. However, the goblet cell access to the ocular surface is blocked by the surrounding epithelial cells. This epithelial coverage could potentially lead to a slowing of the progress of the goblet cells to the ocular surface and as a result there is a decreased release of mucin is in the tears in dry eye [49].

In conclusion, this study explained a decreased epithelial thickness, with a loss of cell layers at the junctional lid margin in the dry eye. The ability to detect a decrease of goblet cells in the dry eye by histochemical stains but not MUC5AC staining, indicates that not all goblet cells produce mucin of the same histochemical characteristics. Goblet cells secreting more neutral or acidic mucin seemed more likely to be susceptible to the dry eye environment. Due to a greater epithelial coverage, the migration of the goblet

cells towards the surface appeared to be prevented by the surrounding epithelial cells in the dry eye.

The mouse appears to be an applicable model for the palpebral conjunctiva and dry eye research.

5.6 Figures and Tables

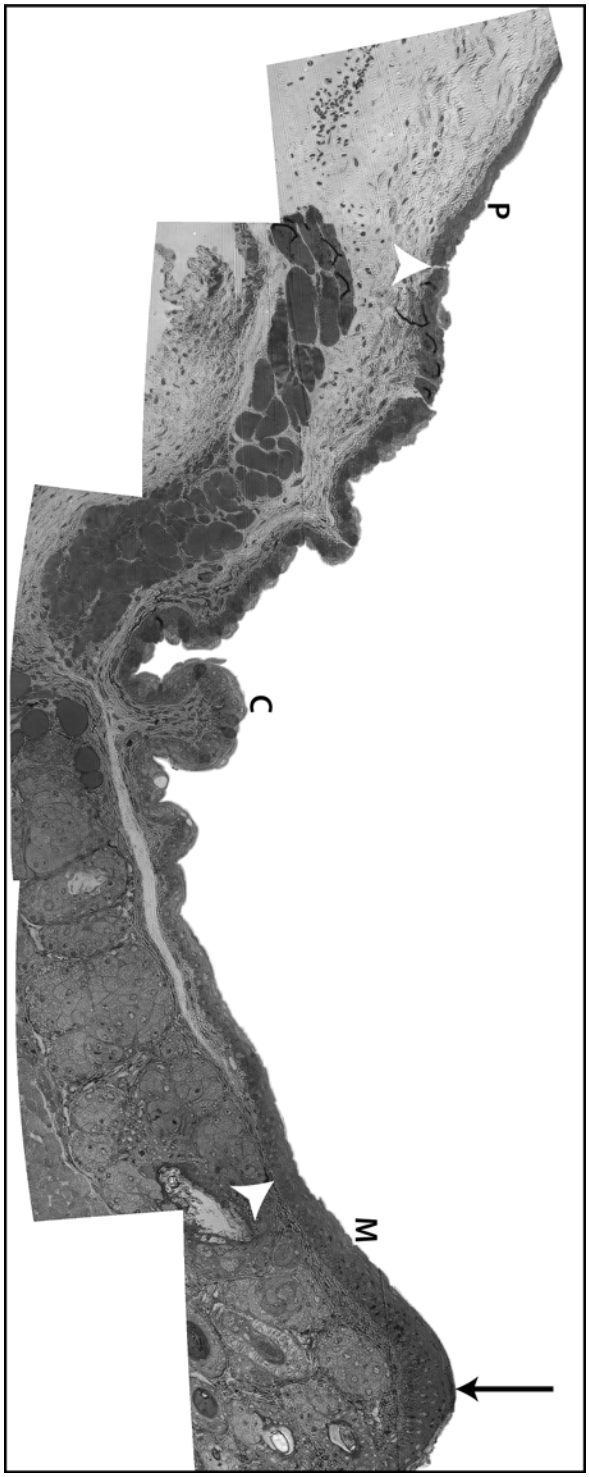

Figure 5.1 Normal palpebral conjunctiva

Normal palpebral conjunctiva illustrating its three regions. M=Marginal, C=Central and P=Peripheral. Close to the lid margin (arrow) is the stratified multi-layered epithelium thickest and devoid of goblet cells. The region where goblet cells are present is indicated between the two white arrow heads (triangles). (Magnification 100X).

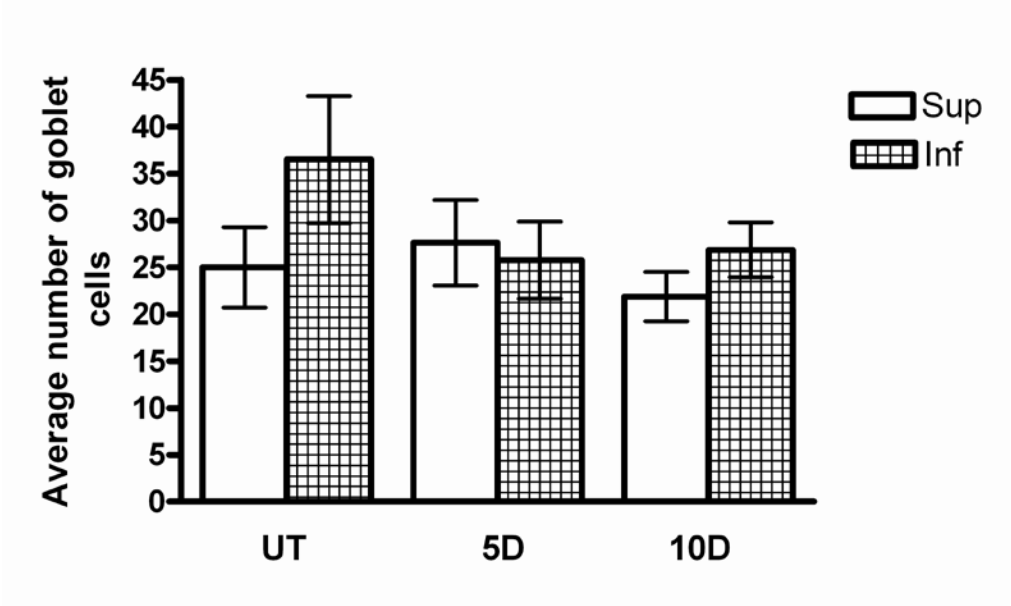

Figure 5.2 Average number of goblet cells

No statistical difference was found between the number of goblet cells between the superior and inferior lids or between the three conditions ($P > 0.05$). Error bars show SD.

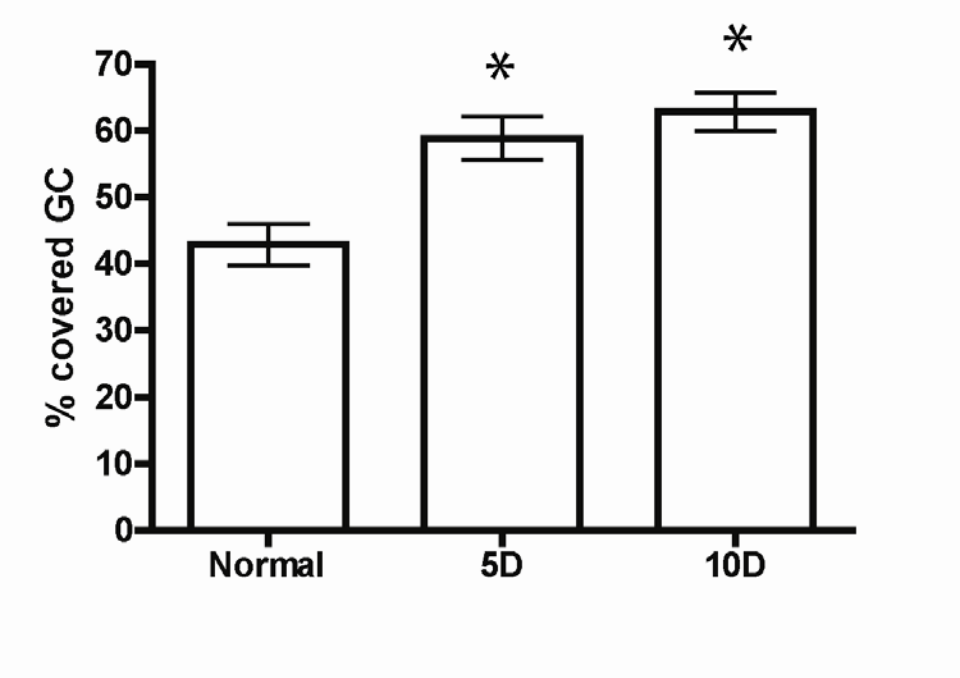

Figure 5.3 Percent covered goblet cells

Data showed a statistically significant difference in percent covered goblet cells between the 5 and 10 day dry eye compared to the normal. Asterisk = ($P < 0.001$). Error bars show SD.

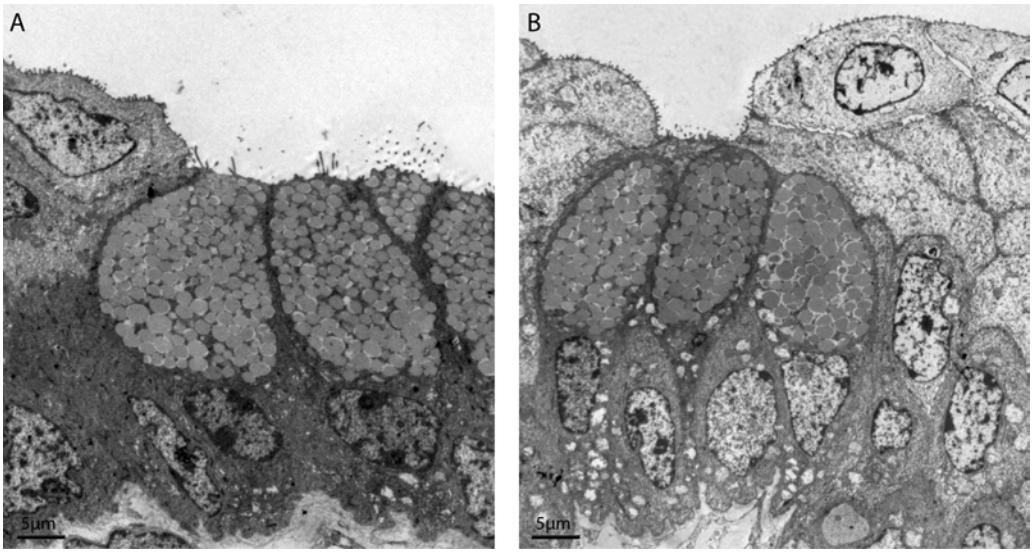

Figure 5.4 Goblet cells

Micrographs illustrating goblet cells at the surface (A) or covered by epithelial cells (B).

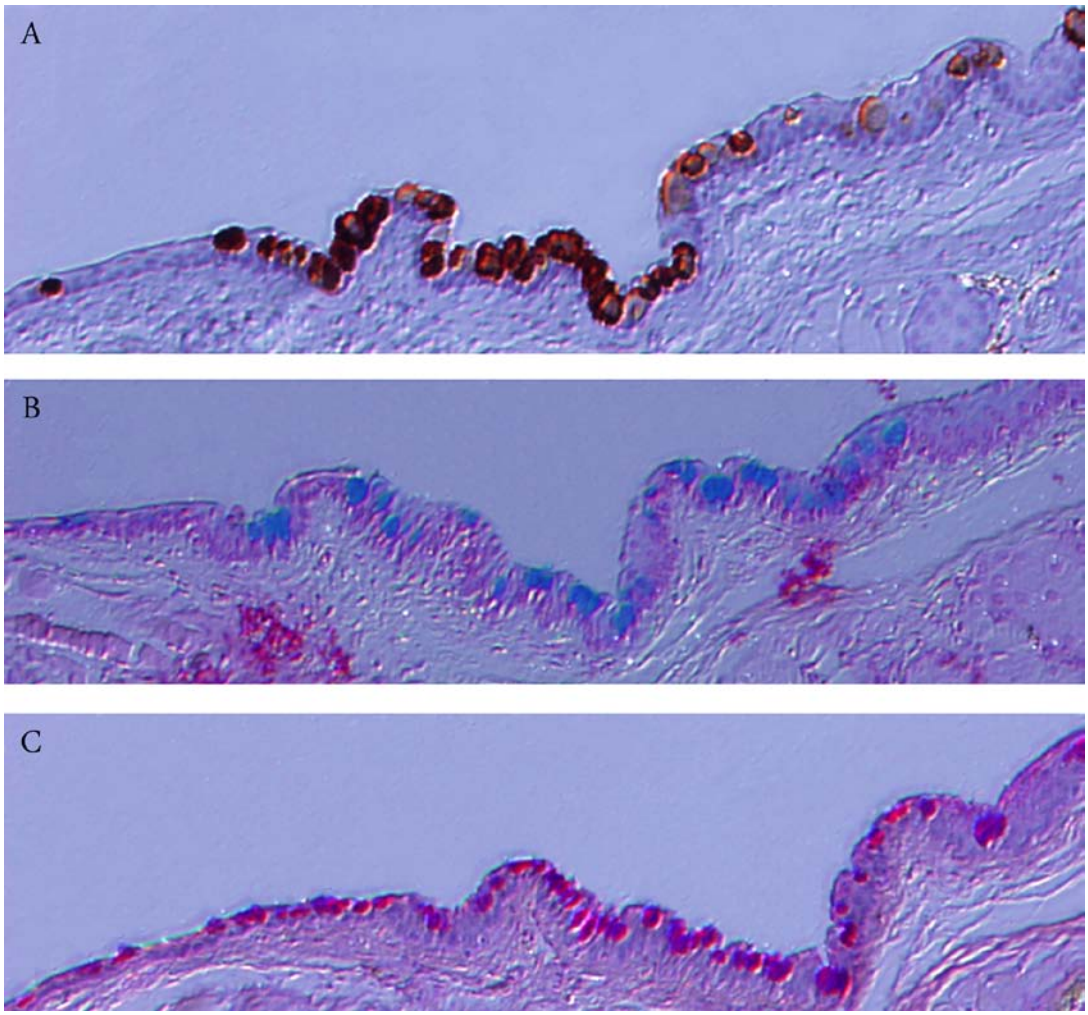

Figure 5.5 Conjunctiva stained with MUC5AC, PAS and Alcian blue

The same region of the conjunctiva stained with three different stains. These images illustrate that the goblet cell count obtained will differ depending on stain used. A = MUC5AC, B = Alcian blue and C = PAS. (Magnification 100X).

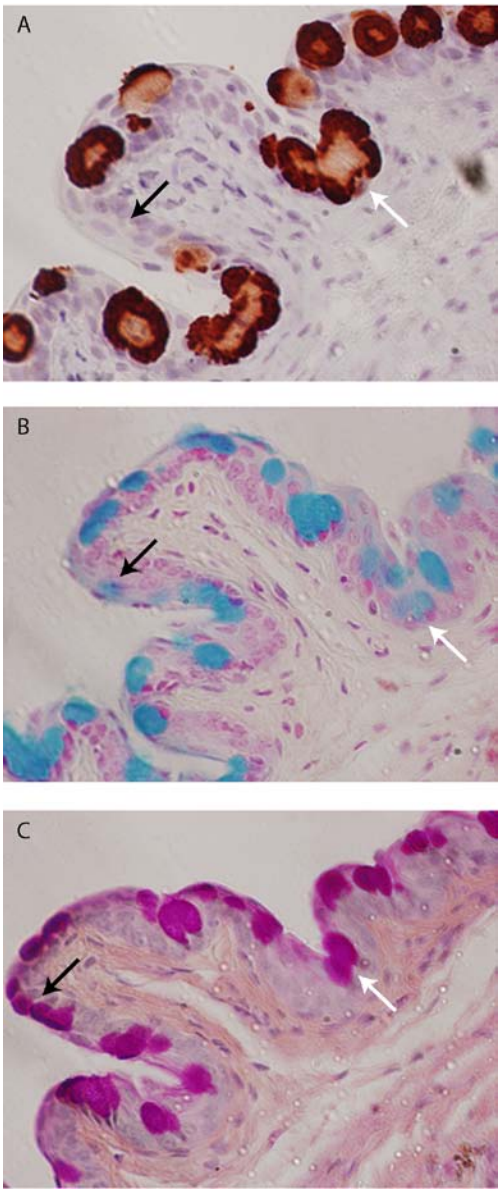

Figure 5.6 Goblet cells stain differently depending on stain

Images illustrating that not the same goblet cell is stained with all three stains. A = MUC5AC, B= Alcian Blue and C= PAS. Arrows indicate two apparent examples. Black arrows = Example 1 and White arrows = Example 2. (Magnification 400X).

	Normal (UT)		5D		10D	
	Thickness (µm)	**Cell layers**	**Thickness (µm)**	**Cell layers**	**Thickness (µm)**	**Cell layers**
Marginal	22.8 ± 2.5	3.5 ± 0.6	18.0 ± 3.3*	3.2 ± 0.8	18.4 ± 2.8*	2.8 ±0.7
Central	26.3 ± 3.0	3.3 ± 0.6	18.5 ± 3.1*	3.4 ± 0.5	19.7 ± 4.4*	2.6 ± 0.6
Peripheral	21.4 ± 2.1	3.3 ± 0.4	18.1 ± 2.6*	3.0 ± 0.5	18.8 ± 2.1*	2.7 ± 0.6
Junctional lid margin	45.6 ± 10.5	8.8 ± 2.0	41.8 ± 6.5	8.0 ± 0.9	37.7 ± 5.5*	7.4 ± 1.3*

Table 5.1 Regional conjunctival thickness variations

Regional conjunctival epithelial thickness variations. Junctional region is where the palpebral conjunctival epithelium meets the epithelium of the lid margin. Data are presented as mean ± SD. Asterisk = ($P < 0.05$).

	Normal (UT)	5D	10D
(Vv) of goblet cells in the histologically defined goblet cell region (%):	12.5 ± 3.7	15.5 ± 3.2	14.0 ± 5.0
(Vv) of granules per goblet cell (%):	43.6 ± 6.7	42.6 ± 3.1	43.2 ± 2.9
(Sv) of goblet cells (μm^{-1}):	1.3 ± 0.2	1.2 ± 0.1	1.3 ± 0.1
(Sv) of granules (μm^{-1}):	11.7 ± 0.6	11.3 ± 0.9	10.2 ± 0.2

Table 5.2 Volume fraction (Vv) or Surface density (Sv) of goblet cells

Volume fraction (Vv) and surface density (Sv) of granules or goblet cells. Data are presented as average ± SD.

	Normal (UT)	5D	10D
Alcian blue			
Number of goblet cells	68.9 ± 13.3	50.2 ± 11.6*	55.0 ± 9.1*
Goblet cells/mm	46.0 ± 10.9	38.8 ± 7.4*	37.1 ± 11.7*
PAS			
Number of goblet cells	73.8 ± 16.5	55.3 ± 13.1*	52.6 ± 9.8*
Goblet cells/mm	54.4 ± 7.8	48.0 ± 8.3*	41.3 ± 9.5*
MUC5AC			
Number of goblet cells	56.7 ± 11.8**	54.2 ± 9.2	57.0 ± 14.8
Goblet cells/mm	44.8 ± 7.1	46.4 ± 5.0	45.1 ± 5.9
Mucous area (μm^2)	247.2 ± 57.4	231.7 ± 56.1	283.7 ± 75.8

Table 5.3 Goblet cells counts with 3 different stains

Counts of goblet cells stained with mucin specific stains. The data show the average number of goblet cells or the number of goblet cells/mm for Alcian blue, PAS and MUC5AC. For MUC5AC the total mucous area (μm^2) was also investigated. UT = Untreated. Data are presented as average ± SD. Asterisk = ($P < 0.05$), UT vs 5D and 10D within groups. Double asterisk = ($P < 0.05$), comparison between UT groups.

Chapter 6 - Ultraviolet Radiation Transmittance of the Mouse Eye and its Individual Media Components

Johanna Tukler Henriksson[a], Jan P.G Bergmanson[a], and James E. Walsh[b]

[a]Texas Eye Research and Technology Center, University of Houston College of Optometry. 4901 Calhoun Rd,. 505 J. Davis Armistead Bldg. Houston, TX, 770204-2020, USA [b]School of Physics, Dublin Institute of Technology, DIT Kevin Street, Dublin 8, Ireland

As published in: Experimental Eye Research 2010: 90(382-387)

6.1 Abstract

Recently, the mouse has become the preferred animal model in ophthalmic research. Therefore, there is a need for enhanced understanding of the mouse eye to validate its use in different experimental setting. The purpose of this study was to determine the ocular transmittance of the whole mouse eye, the cornea and the crystalline lens, particularly in the ultraviolet radiation (UVR) wavebands. This was carried out using a non-cuvette based fiber optic spectrometer system and the resulting transmittance curves were compared with published cone spectral response curves and mouse ocular transmittance data.

First, transmittance curves of the whole mouse eye were measured by removing a small disc of sclera from the posterior pole to provide an anterior to posterior optical path. No statistical difference was found between left and right eye in each of the four mice sampled, therefore, all eight eyes were included in the final statistical analysis. The average of five test measurements from each left and right eye for the four test mice showed a transmittance cut off at approximately 310 nm. Secondly, the cornea with a scleral rim was excised and transmittance curves obtained for all eight eyes. This data showed an average transmittance cut off at 280 nm for the cornea. Similarly measured data for the excised crystalline lens showed UVR transmittance down to 310 nm.

The good correlation between total ocular UVR transmittance and the sum of the individually measured components (i.e. the cornea and the crystalline lens) supported the validity of our method and its findings. This experiment demonstrated that the mouse cornea transmits more UV-B (280-315 nm) than the rabbit and the human corneal transmittance. The mouse crystalline lens on the other hand showed a cut off in the UV-B

at 310 nm, which is at a much lower UV-B wavelength than the approximate UV-A (315-400 nm) cut off for the human crystalline lens at around 390 nm. The increased transmittance of UVR in the mouse eye serves its vision, since the mouse has a cone photopigment peaking at approximately 350 nm. Due to the above stated differences between the mouse and the human it is concluded that the mouse is not an ideal model for the human eye in experiments involving UVR.

6.2 Introduction

An important role of the cornea and the crystalline lens is to protect the retina from toxic solar and artificial ultraviolet radiation (UVR), with solar radiation being the primary source for humans and animals. UVR is generally divided into three wavebands defined by the Commission Internationale d'Eclairage (CIE) as UV-A extending from the visible blue/violet at 400 nm down to 315 nm, UV-B from 315 nm down to 280 nm and UV-C from 280 nm to 100 nm [149 150]. These wavebands have increasing toxicity with decreasing wavelength but when the ozone layer is intact the short waveband solar UV-C will be filtered out by the atmosphere. Therefore it is UV-B that is the major concern when investigating ocular damage caused by UVR with UV-A also exhibiting toxicity at high dosages [151].

The level of UVR irradiance at various points in the eye depends on the ocular media anterior to a particular point and the species investigated. In most species that see primarily visible light, such as humans and rabbits, the cornea and the crystalline lens accomplish almost all of the absorption and have spectral absorbance/transmittance curves that block the majority of UV-B and UV-A respectively. In contrast, both the aqueous and the vitreous are relatively transparent to the entire solar UVR waveband [51-52]. However, animals such as dogs, cats, horses, cows and the guinea pig, as well as the mouse transmit UVR, due to the lack of a UVR filter in the lens, but many of these species do not have UVR receptors like the mouse [54-55]. In addition, the UVR filter in some species appear to develop at or near birth and may continue postnatally in mice [56 152].

Literature has provided a great deal of experimental and epidemiological evidence that UVR causes ocular defects. Excessive amounts of UVR exposure can cause acute damage such as photokeratitis [153-157] or be a contributing factor in regards to chronic ocular damage in the form of cataract [156 158-160] or pterygium formation [161-163].

Animal eyes are frequently serving as a model for the human eye in ophthalmic research. It is therefore, important to precisely determine the contribution of each ocular component in the overall ocular UVR filter for a particular test species so that the effects of UVR exposure can be predicted and related to the spectral sensitivity of the retina for the species in question.

Lately, the mouse has become an increasingly popular model in ophthalmic research due to its sequenced genome, which makes developments of knockout and transgenic strains possible [9 164]. Additional advantages when using mouse models are that it is easy to breed, grows rapidly and is cost effective [9-10 12].There is, therefore, a requirement to enhance our understanding of the mouse eye, particularly the young adult mouse (e.g. 6-8 weeks), and to validate its use in different experimental settings [56].

There are a number of studies that quantify the spectral transmittance of the rabbit eye [52 57-58] but there appears to be relatively few publications on the transmittance of the mouse eye and its individual components. For example, by using a cuvette based fiber optic spectrometer system Dillon *et al.* [60] reported that the mouse corneal spectral transmittance starts at 285 nm and that the crystalline lens starts to transmit most of the UVR above 300 nm. Lei *et al.* [59] used a cuvette based fiber optic spectrometer system in conjunction with a halogen lamp to obtain their measurements and concluded that the mouse lens had a significant transmittance at 360 nm. Studies performed on the rat

showed similar transmittance [60 165]. Compare these to the same ocular components in rabbits and humans where the cornea cuts off at around 300 nm in the UV-B and the crystalline lens cuts off around 390 nm eliminating the UV-B and most of the UV-A. Some species of fish also show partial transparency in the UVA range [166]. The probable reason for the lower wavelength cut offs in mice is due to the fact that the mouse has UVR sensitive cones that can detect down to 300 nm [167-168]. Recent literature suggested that mice are using UVR for increased light and contrast detection while their short lifespan minimizes the UVR dose at the retina [169].

Non-cuvette based fiber optic spectrometer systems have previously been shown to have advantages over conventional cuvette-based systems when measuring ocular transmittance immediately post-mortem [51 166]. These include short pathlength, rapid spectral acquisition and minimum tissue handling [51]. To our knowledge the transmittance of the whole mouse eye and its individual components has not been investigated with these recent technological developments.

The purpose of this study was to utilize this improved technology to determine the transmittance of the whole mouse eye, the cornea and the lens, and to compare the measured transmittance curves with published mouse ocular transmittance data and cone spectral response curves.

6.3 Materials and Methods

All experiments were conducted in accordance with the ARVO statement for the Use of Animals in Ophthalmic and Vision Research. Four adult C57BL/6 mice were euthanized and the intact eyes were carefully enucleated. To determine the spectral transmittance of the whole mouse eye a small disc of sclera was removed from the posterior pole to provide an anterior to posterior ocular optical path. The cornea with a scleral rim and the crystalline lens were subsequently removed by dissection and measured independently. Before the corneal transmittance measurements were taken, the effects of post mortem optical deterioration of the tissue were monitored, to determine the time frame that corneal clarity could be maintained. Earlier work reported by the present authors showed that the rabbit cornea becomes more scattering with time and there was a 20 minute period immediately post mortem during which the cornea remained clear [51]. This immediately post mortem period is essentially when an in vivo approximation of spectral transmittance should be made. Corneal clarity can be prolonged with careful handling during dissection and mounting and by irrigating with Alcon BSS (Alcon, Fort Worth Texas). The crystalline lens is an isolated organ completely enclosed and protected by its own basement membrane and more resistant to changes in its environment. Therefore, the transparency of this tissue is maintained for a long period of time after removal from the whole eye allowing measurements to be obtained without concerns for a change in light scatter produced by its components.

To test this period of corneal clarity in mice a series of spectra were recorded over a 90 minute period on one additional typical mouse cornea, starting as soon as possible post mortem. The time it took to enucleate the mouse eye, dissect out the cornea and

mount in the spectrometer was around 10 minutes. Spectra were initially recorded as rapidly as possible and periodically thereafter over a period of 90 minutes. During the experiment the excised tissue was kept artificially hydrated by Alcon BSS (Alcon, Fort Worth, Texas) to prevent dehydration and distortion of the tissue. For the remainder of the data the whole eye and component media were tested immediately post mortem to minimize any optical deterioration. To ensure repeatability, transmittance spectra were rapidly recorded at five test points near the center of each whole mouse eye, cornea and crystalline lens. To minimize the decay in optical clarity post mortem, the enucleated whole mouse eye, dissected cornea and dissected crystalline lens were sampled within 10, 15 and 20 minutes respectively. In addition, left and right eyes were measured to give intra-mouse consistency and inter-mouse variations were determined by sampling four mice in total, giving a total final value of n = 8 for each ocular component tested.

Spectral transmittance of the samples was measured using a non-cuvette based fiber Ocean Optics USB4000 optic spectrometer system (Ocean Optics, Dunedin FA), with a spectral range of 200-800 nm. Samples were illuminated by an Ocean Optics DT-Mini-2-GS deuterium-halogen light source, with a 200-2000 nm output spectral range. All media were illuminated from the front with a collimated beam from a 400 μm diameter fiber optic fitted with 10 mm focal length collimating lens that was coupled to the light source. The bare front end of the 200 μm diameter detecting fiber was placed immediately behind the test medium, with the other end coupled to the 5 μm input slit of the spectrometer that provides a spectral resolution of less than 3 nm [51]. The overall set-up is shown schematically and pictorially in Figure 6.1 and the basic principles of the

system have previously been calibrated, tested and proven on contact lenses of known transmittance [68-69] as well as on rabbit corneas [51].

After the spectrometer dark current and the reference spectra have been established transmittance spectra can be computed and recorded in a few milliseconds. The rapid data collection from the spectrometer CCD detector and the small aperture on the illuminating and detecting fiber optics allow for transmittance of small tissue samples such as the whole mouse eye, its cornea and crystalline lens to be recorded. The reference spectrum was simply the spectrometer observing the lamp through the empty sample holder, which is effectively the 100% transmittance baseline. The tissue transmittance is observed when a specific sample is carefully placed normal to the light beam. Transmittance data was saved by the Ocean Optics software and analyzed using Matlab.

Intra-mouse, left versus right eye, as well as inter-mouse transmittance curves were recorded to test homogeneity and variation throughout our sample eyes. Due to their minute size it was not always possible to place each mouse eye in the test beam in exactly the same manner, causing variations in the overall transmittance levels from sample to sample. Placement variations were greatly reduced by normalizing all spectra in the visible at 600 nm where the test media have high transmittance and no absorption feature of note [51 68]. The whole eye spectra were normalized to 65% and the cornea and crystalline lens spectra to 80%, these values were based on the mean of the five spectra taken on each of the eight test eyes and incorporated the relative thickness of each test medium and the amount of surface or Fresnel reflection encountered. Subsequent comparison of the absorption spectra of the whole eye and the cornea and crystalline lens combined, shown in the results below, validated the normalization values at 600 nm for

each test medium. In addition the spectral transmittance of a drop of Alcon BSS was determined to ensure that it did not absorb any UVR in the region of interest. After testing whole eyes the individual corneas and crystalline lenses were carefully excised and placed in the test beam for measurements, with less placement error than the whole eyes due to their relative optical simplicity.

6.4 Results

First, transmittance curves for the whole mouse eyes were determined and the average of these curves from the left and right eyes of the four test mice showed a transmittance cut off at approximately 310 nm and transmittance increasing from the UV-A to the visible wavebands (Figure 6.2). Subsequently the, transmittance spectra of the cornea and crystalline lens were assessed. Due to the quicker degradation of the cornea compared to the crystalline lens, corneal transmittance was measured first of the two ocular media. The average of the corneal transmittance curves showed a cut off at 280 nm and higher overall transmittance than the whole eye (Figure 6.3). The data for the mouse crystalline lens showed a UVR transmittance down to approximately 310 nm, again with higher overall transmittance than the whole eye (Figure 6.4). The significance of the cut off wavelengths for the cornea and crystalline lens is highlighted in figures 6.2 to 6.4 by superimposing the mouse cone receptor sensitivity curve on each graph [168].

The error bars shown in figures 6.2 to 6.4 indicate the standard deviation about the mean of the eight sampled eyes, as no statistical difference between left and right eye was evident for each mouse. There is good consistency across the eight samples for the whole eye and crystalline lens with slightly larger error bars on the corneal data, possibly due to the corneal delicacy and the extra handling required in its excision.

Next, the decay in corneal transparency over 100 minute timeframe was assessed by repeatedly measuring transmittance spectra on one cornea. The cornea was left in the optical test set-up and hydrated using Alcon BSS during this test segment. The graph generated in this experiment showed a decrease in transmittance due to an increase in scatter with time. The decreased transmittance was mainly observed at 350 nm (Figure

6.5). By plotting the transmittance at 350 nm against time, the period, over which valid transmittance measurements may be acquired, can be determined and shows a 5% drop within 20 min after euthanization of the animals (Figure 6.6).

From the transmittance data in figures 6.2 to 6.4 absorption spectra of the mouse whole eye can be computed and compared to the sum of the corneal and crystalline lens absorption. This showed that the cornea and the crystalline lens are the two dominant absorbers in the mouse eye (Figure 6.7). The slightly higher absorption due to the sum of the cornea and crystalline lens, being due to factors such as increased Fresnel reflection from the individual media and optical decay due to the extra handling involved.

6.5 Discussion

The in vitro non-cuvette based fiber optic spectrometer system used for this experiment produced consistent results as has been shown previously [51]. The close correlation found between total ocular UVR transmittance and the sum of the individually measured cornea and crystalline lens supported the validity of our findings. Optimal readings were obtained due to a short post-mortem interval (less than 30 minutes), which allowed the maintenance of good transparency and consistent transmittance. The rapid data collection was made possible by the simplicity of the equipment design and set up. Measurements taken postmortem after the optimal period, showed a significant decline in transparency due to increased scattering over time. The decreased transmittance is a result of handling and natural postmortem changes. Comparisons made in this study, between optimal readings from whole eyes, crystalline lenses and corneas from four different animals (8 eyes), showed little variation and suggested that the methodology used in this experiment was accurate even for a small eye. The low broadband transmittance in the UV-A and blue light wavebands may also protect the mouse retina from excessive toxic exposure while allowing sufficient light through to permit UVR vision with minimal glare, in the same way that humans use sunglasses in the visible with a UV-A cutoff.

The few transmittance studies available on the mouse crystalline lens have all shown variable outcomes. Both Dilllon *et al.* [60] and Lei *et al.* [59] used an Ocean Optics cuvette based system to obtain their data. Dillon *et al.* [60] showed high absorbance up to about 320 nm and Lei *et al.* [59] showed 80% lens transmittance at 360 nm. In accordance with Dillon *et al.* [60] our study revealed a transmittance cut- off at 310 nm for the mouse

crystalline lens, however, Dillon *et al*. [60] showed a higher transmission, 70% for the cornea and 80% for the crystalline lens in the UVR region compared to our data. This discrepancy is likely due to that Dillon *et al.* [60] first normalized the transmission spectra to 90% and subsequently subtracted for Rayleigh and Tyndall scatter, caused by the long pathlength present in a cuvette based system. This dilemma was eliminated in our study by using a short pathlength by placing the detecting fiber optic immediately adjacent the test lens or cornea to decrease scattering. Another possible explanation for the discrepancy found could be due to the different strains and ages of the mice used in the two studies. Dillon *et al.* [60] used a BALB/c mouse, an albino mouse, and in our study a C57BL/6 mouse, a highly pigmented mouse was used. A study by Gouras *et al*. [170] comparing UVR sensitivity between albino Fisher-344 rats and pigmented Brown Norway rats showed that the albino rats where more sensitive to UVR. Yet, another possibility is that there is a genetically inherited difference in UVR sensitivity between the two strains of mice (the C57BL/6 and the BALB/c) independent of eye pigment. Also worth noting is that the spectrometer used by Lei *et al.* [59] only obtained transmittance spectra above 350 nm, 40 nm above the cut off found in our study for the mouse crystalline lens. The spectrometer system used in the present study was sensitive over a greater range, and this may also be a factor in the discrepancy between the two studies. Our system also has advantages over a cuvette based system by minimizing handling of the tissue, allowing prompt measurements post mortem, minimizing beam pathlength to reduce the effects of scatter and avoiding reflection and unwanted refraction from optical interfaces and cuvette media.

Discrepancies found when comparing literature on mouse crystalline lens transmittance, were evident also in transmittance studies involving the human eye. As pointed out by several authors [53 171-172] multiple factors affect the validity of the findings, including the condition and age of the eyes, time between enucleation and measurements, and the accuracy of the instruments and measuring techniques used. Therefore, there is a need for a standardized, accurate fast recording system that can be used measuring transmittance of contact lenses and on different species such as the human, rabbit and mouse eyes. The current instrument design appears ideal for such a purpose and variants of this equipment set up has been successfully utilized on small fish [166].

Only one previous study, Dillon *et al.* [60], was found in regards to mouse corneal transmittance. They recorded a corneal transmittance starting at 285 nm, which is in agreement with the transmittance data in this study, but higher overall transmittance possibly the same for reasons highlighted above. Another factor that may also be important is the age of the test mouse [173]. It has been reported in the literature that the ocular structures of the immature mouse are still developing and this may affect the relative clarity of the media [174].

An interesting observation was made when comparing the mouse transmittance cut offs to other species such as the rat, rabbit and human. The mouse cornea had a cut off at 280 nm which is further into the UV-B than corneal cut offs recorded for some other species such as the rat 285 nm [60], the rabbit 290 nm [51] and the human 290 nm [52 175]. Therefore, this experiment demonstrated that the mouse cornea transmits more UV-B than the rat, rabbit and the human corneal transmittance. The mouse crystalline lens, on the other hand showed a cut off in the UV-B at 310 nm which is slightly lower than the

cut-off in Dillon *et al.* [60] and similar to the rat 310 nm [165] and at a much lower UV-B wavelength than the approximate UV-A cut off for the rabbit 360 nm [176] and human 390 nm [52 177] crystalline lens.

As stated above the mouse crystalline lens is transparent to the majority of the UVA-B spectral waveband which in contrast differs to the human crystalline lens. Why would the mouse lens need the ability to transmit UVR radiation? The mouse retina has a cone photopigment sensitive to UVR with peak sensitivity at 350 nm [167-168] and, according to the present study, the mouse cornea and crystalline lens have approximately 50% transmittance in this region. However, this apparently reduced transmittance may still allow sufficient light in the related waveband to stimulate receptor cells containing the UVR photopigment. When and how an animal, such as the mouse, that operates in a twilight environment would utilize and benefit from this UVR perception is not yet clearly understood. In agreement with Gouras and Ekesten (2004)[169] we believe that the UVR sensing cones allow the mouse enhanced electromagnetic radiation detection and added contrast, which may help when searching for food, mates or escaping from predators. Alternatively in its natural light starved environment the nocturnal mouse may need to utilize any available electromagnetic wavelength available for its survival.

Due to the above stated significant differences that exist between the mouse and the human it is concluded that the mouse is not an ideal model for the human eye in experiments where UVR is a factor.

6.6 Figures and Tables

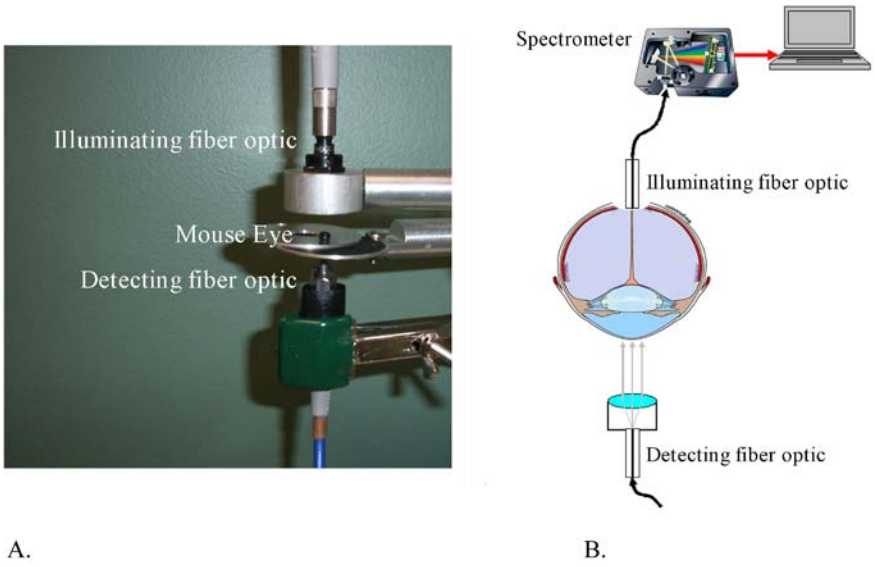

Figure 6.1 Spectrometer set up

Photograph of instrumentation set up (A) explained by schematic diagram (B).

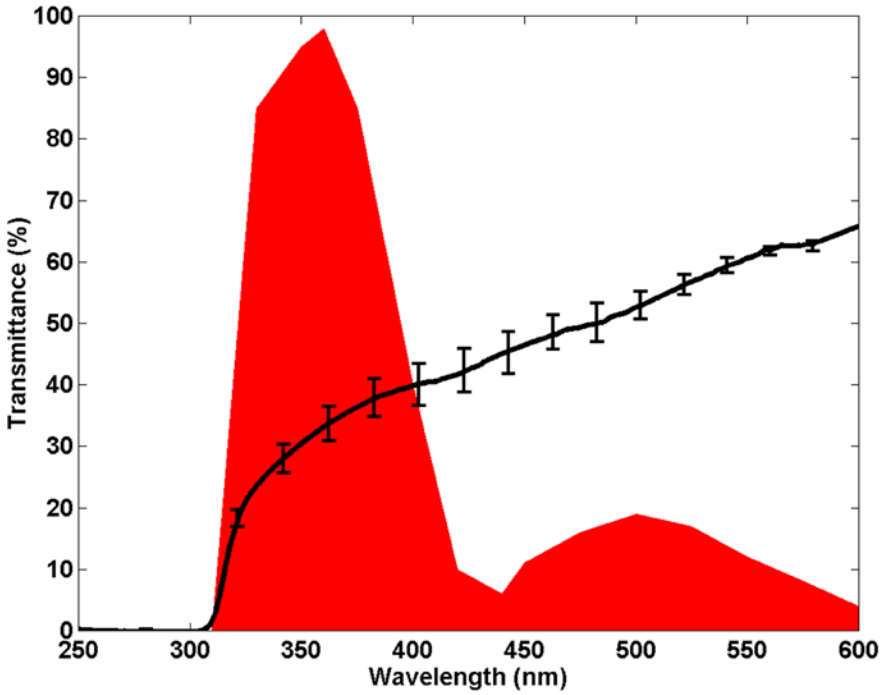

Figure 6.2 Mouse whole eye transmittance

Mouse whole eye transmittance with the mouse cone receptor sensitivity curve superimposed to show that the transmittance needs to extend down to the UVB (after Lyubarsky et al. 1999).

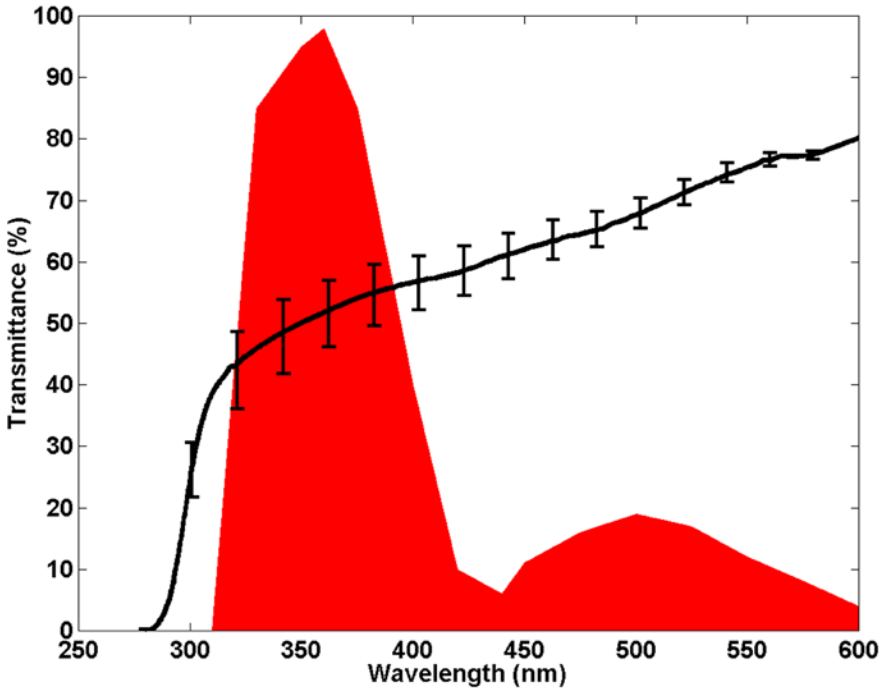

Figure 6.3 Mouse corneal transmittance

Mouse corneal transmittance with the mouse cone receptor sensitivity curve superimposed (after Lyubarsky et al. 1999).

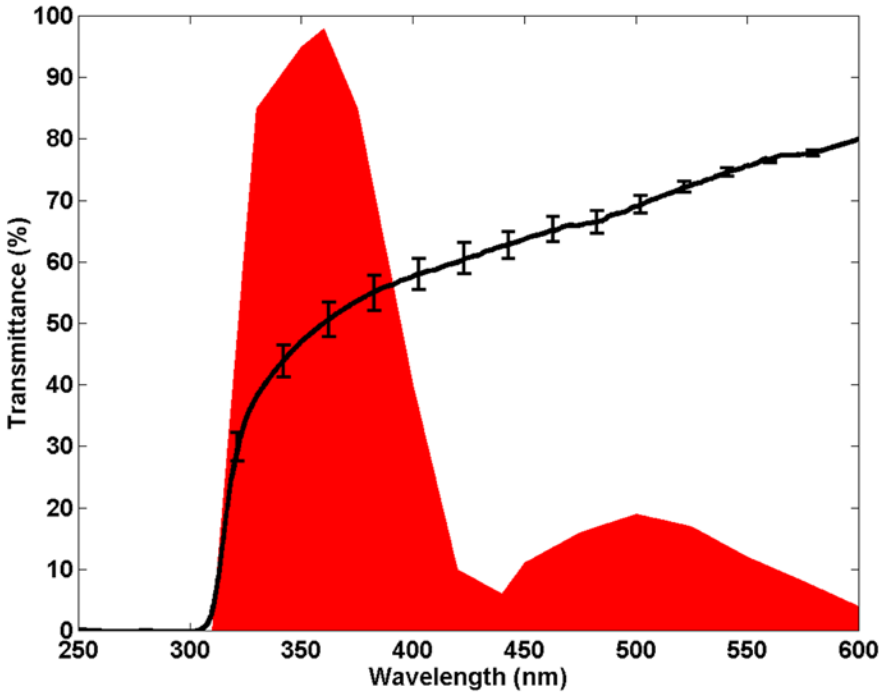

Figure 6.4 Mouse crystalline lens transmittance

Mouse crystalline lens transmittance with the mouse cone receptor sensitivity curve superimposed (after Lyubarsky et al. 1999).

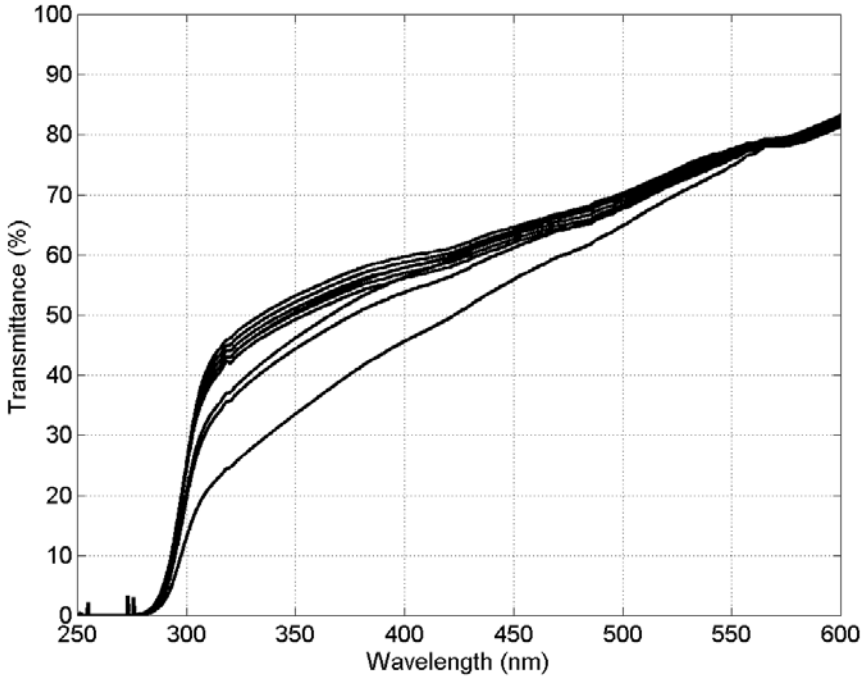

Figure 6.5 Mouse corneal transmittance over time

Mouse corneal transmittance decreasing over time showing the increase in scatter over a 90 minute hour period.

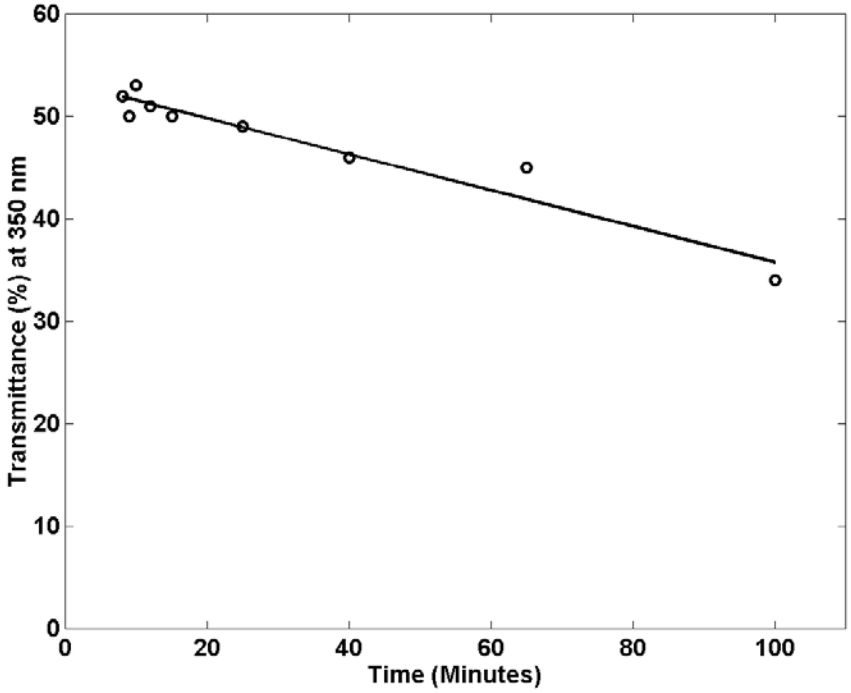

Figure 6.6 Decreased corneal transmittance due to scatter

Decrease in corneal transmittance at 350 nm due to the increase in scatter over a 90 minute period, taken from figure 6.5.

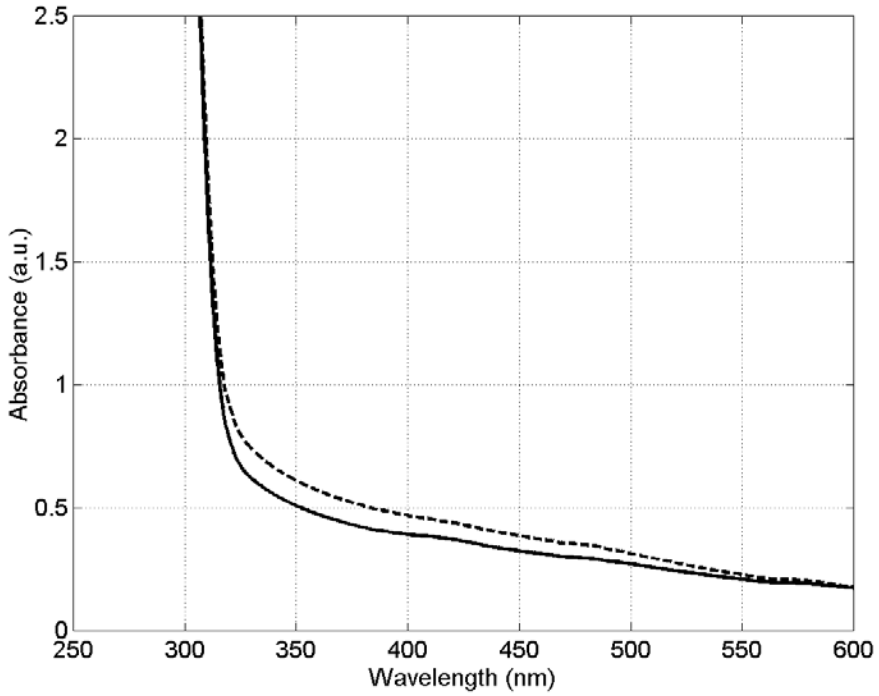

Figure 6.7 Absorbance curve

Mouse whole eye absorbance (——) compared to the sum of the corneal and crystalline lens curves (----) that shows that these two ocular structures are the dominant absorbers in the mouse eye.

Chapter 7 - General Discussion

General Discussion

The young adult mouse has recently become an increasingly popular model in corneal and anterior segment research e.g. dry eye mouse models have proven to be useful when investigating tear functions [43 45-47] and its genome has been sequenced, which allows for development of knockout and transgenic strains [9 164]. Although the mouse is commonly used in ophthalmic research, current literature provides limited information on the normal mouse anterior segment and its similarities or differences to the human.

The first experiments in this dissertation were therefore, designed to characterize and to assess the applicability of the normal mouse cornea and conjunctiva to the human and subsequently to enhance our understanding of morphological changes occurring in the dry eye. These studies represented the first attempts to investigate the mouse cornea, the normal and dry eye palpebral conjunctiva by utilizing a systematic, histologic approach using well defined reference points allowing the observer to conduct accurate intra-corneal or intra-conjunctival morphometric assessments.

Since the mouse eye is commonly used in many different areas of ophthalmic research, there was a need to enhance our understanding of this small eye in a variety of experimental settings. An additional experiment was, therefore, designed to investigate the applicability of this small eye to the human in regards to UVR transmittance.

As is illustrated above, this research investigated the relevance of the mouse eye as a model for the human eye in various tissues and experimental settings. For clarity the outcomes from these studies and the similarities or differences found between the mouse and the human are discussed for each tissue or experiment below.

7.1 Mouse Cornea

Dimensions

The histological evaluation of the mouse cornea in the three most commonly used stains of mice (129/SVJ, C57BL/6, BALB/c) demonstrated an average diameter of (2.3-2.6 mm depending on strain), which was much smaller than the human cornea that has an average diameter of (11.7 x 10.6 mm)[7]. The measurements obtained in the current study were substantially smaller than the 3.5 mm BALB/c corneal diameter reported by Zhang *et al.* [12]. This discrepancy may be explained by the difference in age between the mice 6 to 8 weeks versus 6 months [12 62].

In contrast to the human, the mouse cornea was thickest centrally (123-137 µm) and thinned by 55-66% towards the periphery where it measured (68-90 µm). This thickness difference was explained by both a decreased thickness of the epithelium and the stroma towards the periphery, but primarily due to a reduction in stromal thickness.

The nocturnal mouse has a relatively large eye and wide palpebral aperture for its size. Together with a large almost spherical crystalline lens and a strongly curved cornea this supplies the mouse eye an eminent light gathering ability needed for survival in its natural habitat [178]. One possibility is therefore, that the mouse corneal shape has evolved to benefit this nocturnal animal optically. Another source stated a crystalline lens anterior radius of curvature for a 12 week old C57BL/6 mouse of 1.13 [179] and thus maybe the corneal shape has evolved to be able to provide room for this relatively large steep crystalline lens.

Contrary to the human, where the epithelium and the stroma contribute 10% and 90% respectively [7] to the corneal thickness, the mouse corneal epithelium contributed

approximately 30% and the stroma approximately 70% to the total thickness. This finding was in agreement with proportional contributions of the epithelium and stroma to the total cornea thickness previously reported on the BALB/c mouse [12].

Epithelium

The ultrastructural investigation of the mouse corneal epithelium demonstrated stratified epithelium similar to what has been described for the human [28 180]. An important difference between the human and the mouse was the number of epithelial cell layers. In contrast, to the average of 5-7 layers of cells reported in the human, [180] the mouse cornea in all three strains of mice had an average of 13 layers centrally compared to an average of 10 cell layers peripherally. This decrease of cell layers amounted to a thinning of the epithelium by 40% (18 µm) in the periphery. The difference in cell layers between the two species was explained by an increased number of squamous cell layers in the mouse cornea. In its natural habitat the relatively protruding mouse cornea is likely to be exposed to dangers from the surrounding vegetation and it is, therefore, possible that the additional cell layers serve as enhanced corneal protection. The greater relative contribution of the epithelium to the overall corneal thickness and the increased number of epithelial cells in the mouse cornea are significant differences that may have an impact when relating, for instance, wound healing studies on the mouse to the human.

ALL

In the human, the ALL may be described as a well defined 8-10µm thick layer located between the epithelium and the stroma. The mouse cornea did not possess such a

layer and I therefore, confirmed Rehbinder's observation [17] who reported that the mouse cornea lacked this corneal layer. The ALL is present in some species and not in others. The need to develop an ALL, or, indeed its functions have not been explained. Therefore, it is not clear why the mouse does not possess one. It has been proposed, that the ALL may have evolved for optical or structural reasons or may be a combination. Future research may be able to provide an answer to this question.

Stroma

Similarly to what has been reported for the human, the mouse corneal stroma was composed of collagen fibers, organized into lamellae, with keratocytes present mainly between the lamellae [31 31-33 62 83 104 115 180-181]. The number of keratocytes present along a vertical line in a thick (0.5-1 µm) transverse section can give an approximate estimate of the number of lamellae present at a specific corneal location.

The mouse corneal lamellae were arranged as flattened sheets oriented parallel to the epithelium and resembled the architecture of what has been reported for the human middle and posterior stroma [4]. The complex interweaving of the anterior lamellae [4-5 180] and the presence of electron dense formations indicating mid-corneal stromal terminations [5] found in the human were absent in the mouse, but, EDF may have been present peripheral to central cornea. As mentioned previously the mouse corneal stroma decreased in thickness towards the periphery, and hence has a shape opposite to what has been reported for the human [18-19 21-23 101]. In the mouse, the central to peripheral thickness variation was explained by both a significant decrease in number (50 versus 36) and thickness (2.1 µm versus 1.9 µm) of lamellae. The decrease in number of lamellae

towards the periphery was mainly due to a lamellar drop out in the anterior 2/3 of the stroma. In contrast to previous reports, [25-26 78 103-104] these lamellar counts suggested that not all stromal lamellae cross the cornea from limbus to limbus. Although, the human cornea has the opposite shape of the mouse cornea, this observation might have a parallel in the human, since there appear to be more lamellae in the peripheral human cornea [117] compared to the center [4]. Intra-corneal counts, (central and peripheral lamellar counts within the same cornea), have yet to be performed in the human cornea to confirm this statement.

Another interesting difference between the human and the mouse was the distribution of corneal nerves. In contrast to the primate, where corneal nerve fibers primary function are defense and they only are present within 50 μm of the epithelium, [84 180] corneal nerves were located throughout the entire corneal stromal thickness in the mouse. Since the mouse cornea is significantly thinner than the human cornea it is proposed that the more posterior nerve fibers still mainly respond to anterior stimuli.

PLL

In the human the PLL terminates at the trabeculum and it consists of a fetal (banded) and post-natal (more uniform) portion and function as a basement membrane to the endothelium [1 9 180]. The mouse PLL had a similar organization but in contrast to the normal human, the mouse PLL has striated bodies located in the post-natal portion. These striated bodies are shown in images from the mouse cornea but have not been discussed in the text [9 17]. Similar striated bodies have been imaged and described in the posterior collagenous layer in the pathological human cornea as a result of Fuchs' endothelial

dystrophy [82]. These striated bodies are part of the abnormal basement membrane laid down by the diseased endothelium. It appears that in the mouse the endothelial basement membrane production is not a perfect secretion, however due to the short lifespan of the mouse it does not seem to have an effect on corneal or endothelial health.

Endothelium

The structure of the mouse corneal endothelium corresponded to what has been described ultrastructurally for the human [1 180]. In a transverse section the mouse endothelium measured 2.1 µm in thickness, and was thinner than the 5 µm that has been reported for the human [83].

As stated above, significant dimensional and some noticeable ultrastructural differences existed between the mouse cornea and the human. It is therefore of importance to take these differences into consideration when applying research from the mouse to the human.

7.2 Mouse Conjunctiva

Epithelium

Analogous with the human, the mouse palpebral conjunctival epithelium can be described morphologically as a stratified multi-layered epithelium rich in goblet cells with surface cells that feature a glycocalyx. The human superior palpebral conjunctiva has an average of 2 and the inferior an average of 3-4 layers of cells [48]. Both the superior and inferior C57BL/6 mouse palpebral conjunctiva had an average of 3 cell layers, thus structurally the palpebral conjunctival epithelium of the mouse was similar to what has been documented for the human.

A decreased epithelial thickness was detected in the dry eye; this was accompanied by a loss of cell layers at the junctional region, where the palpebral conjunctival epithelium meets the epithelium of the lid margin. Increased friction from desiccation of the tissue, an increased frequency of blinking or a combination of both are likely causes for the decreased thickness and loss of cells in this region.

The lid wiper is defined as the portion of the marginal conjunctiva of the upper lid that spread the tear film over the ocular surface [129]. Clinically, this area has shown positive (rose bengal, lissamine green and/or flourescein) staining in patients with dry eye symptoms. This condition is named lid wiper epitheliopathy (LWE) [129-130]. The conjunctival epithelial thinning and loss of epithelial cells at the junction of the lid margin and the conjunctiva reported by this research may be a potential explanation behind the staining caused by this condition.

Goblet cells

In the mouse palpebral conjunctiva the goblet cells were found either singly or in clusters and this arrangement was similar to what has previously been reported for the human [132 138]. A feature of the mouse palpebral conjunctiva was that the goblet cells may only be visualized in a restricted region.

Goblet cells were counted utilizing different techniques to investigate whether goblet cell density would change in dry eye. These counts differed depending on technique used. In agreement with previous studies, this study also detected a decreased number of goblet cells when PAS and Alcian blue stains were used [43 46 50]. However, this decrease was not detected when MUC5AC positive goblet cells or goblet cells were counted based on histological criteria. One possible explanation was that different subtypes of goblet cells are present at the ocular surface programmed to produce mucin of different histochemical characteristics, and thus, different numbers of goblet cells were visualized when different stains were used. If so, it appears that the goblet cells producing neutral mucin (stained by PAS) or acidic mucin (stained by Alcian blue) are more likely to be affected by the dry eye condition. It is possible that some of the PAS or Alcian blue positive cells that don't stain for MUC5AC secrete MUC2.

A thicker section is more likely to contain goblet cells. Yet, another potential explanation for the discrepancy in counts between goblet cells counted histologically and goblet cells stained with mucin specific stains may be the difference in thickness between the 0.5µm thick resin embedded versus the 5 µm thick paraffin embedded sections.

The goblet cell size reduction in the dry eye was proportional to the decreased thickness of the epithelium. However, there was no change in volume fraction

(approximately 43%) and surface density of the granules between the three conditions, thus indicating, the same amount of mucin production in the normal and the dry eye. This finding was in agreement with the area of MUC5AC staining found in the epithelium.

Another factor affecting the goblet cells in the dry eye was a greater coverage of epithelial cells. Perhaps it is not a decreased number of goblet cells or decreased mucin production (as illustrated by our MUC5AC staining and histological counts) but instead the slower or inhibited migration of goblet cells from the basement membrane to the surface that resulted in a lower amount of MUC5AC in the tear film in the dry eye [49].

The mouse superior and inferior palpebral conjunctiva has a structure similar to the human and I would therefore, like to conclude that the mouse palpebral conjunctiva is an applicable model for conjunctival and dry eye research.

7.3 Mouse Eye and UVR Transmittance

These experiments utilized a non-cuvette based fiber optic spectrometer system and demonstrated a transmittance cut off at approximately 280 nm for the cornea and 310 nm for the crystalline lens. These results were in agreement with previous reports by Dillon *et al.* [60] In contrast to our study, Dillon *et al.* [60] reported a higher transmission in the UVR, 70% for the cornea and 80% for the crystalline lens. These discrepancies were likely due to the fact that Dillon *et al.* [60] corrected their transmission spectra for Rayleigh and Tyndall scatter, caused by the longer pathlength present in their system. The difference in strains and ages of mice could be another explanation for the variability in transmittance between the two studies [60 182].

In contrast to the mouse, the human cornea and crystalline lens have transmittance cut offs at 290 nm [52 175] and 390 nm [52 156] respectively. Transmission at lower wavelengths allows the majority of the UVA-B spectral waveband to reach the mouse retina. These wavelengths are for safety reasons blocked out in the human mainly by the cornea and the crystalline lens.

The mouse has a cone photopigment sensitive to UVR, peaking at 350 nm [167] but, how this UVR perception benefits a nocturnal animal, such as the mouse, is not clearly understood. One possibility is that the UVR sensing cones allow the mouse enhanced electromagnetic radiation detection and added contrast, which may help when searching for food, mates or escaping from predators [169]. Mouse urine has shown to be highly UVR reflectant [183]. The mouse uses its urine to mark its territory or trails to common wallowing places, [184] suggesting that the UVR sensitivity of the mouse eye is needed for orientation [184] or to establish social rankings [183].

Due to the differences stated above between the mouse and human in UVR transmittance, it is concluded that the mouse is not an ideal model for UVR experiments.

The first topic of my studies focused on validating the young adult mouse as a model for ocular surface research by investigating structural similarities and differences between the normal mouse anterior segment and the human. The morphological differences between the two species described in these studies are especially important to take into consideration when extrapolating results from mouse studies to the human. For example, due to the difference in corneal shape, stromal thickness and architecture between the two species, the mouse would most likely not be an ideal model for studying effects of a new refractive surgery method. The results from my studies will also be of importance to researchers starting a new project, mainly to help determine whether the mouse cornea or conjunctiva would be an applicable model for a particular project or if another animal model will be a more suitable choice.

If a researcher is planning to utilize mouse as an animal model for UVR research or transmittance studies it is essential to be aware of the difference in transmittance of the mouse eyes' individual components compared to the human illustrated in my study. The corneal transmittance cut off is similar to the human and the cornea might therefore, be suitable for these types of experiments. It is however, important to be aware of the difference in corneal thickness and proportions compared to the human. The mouse crystalline lens will most likely not be suitable for transmittance studies due to the difference in absorption compared to the human. The above stated studies have given

insight to the importance of experimentally validating an animal model and investigating its applicability to the species of interest before it becomes commonly used.

A second main topic of this research was to assess structural changes occurring in the dry eye. Dry eye is a disease without a cure that affects millions of people world-wide. To one day find an exclusive test for diagnosis, a treatment or a cure for this disease it is important to obtain an enhanced understanding of all aspects of the dry eye e.g. etiology, structural epithelial changes, changes in goblet cell density, tarsal gland secretion etc. My research on this topic contributes to the research community by providing an increase understanding of how the dry eye effects goblet cells and the epithelium.

The studies included in this dissertation only investigated the applicability of the young adult mouse to the human. Since the literature provides limited information on the structure of all ages of the normal mouse anterior segment it would be interesting to investigate how corneal dimensions, and corneal and conjunctival structure changes with age. Is it possible that an older mouse develops dry eye naturally due to aging, as is commonly seen in humans? If so, how would the conjunctival findings of these mice compare to the dry eye model utilized for my studies and to the human? In my transmittance study the C57BL/6, a mouse strain with a heavily pigmented eye was utilized. Would transmittance increase if for example the BALB/c, an albino mouse strain, was used? The transmittance of the human crystalline lens decreases with age. Taking the short lifespan of the mouse into account, does the mouse live long enough to show the same relationship? The above stated questions are only a few examples of areas

where more research is needed to further evaluate the mouse as an animal model for the human.

7.4 Summary of Significant Observations

Cornea:

- The mouse cornea was thicker centrally and thinner peripherally, thus had a shape opposite the human.
- The stroma contributed 2/3 and the epithelium 1/3 to the total corneal thickness.
- Both the epithelium and the stroma showed a decreased peripheral thickness, however, the reduced number of stromal lamellae was the main reason for this thickness loss.
- The difference in number of lamellae between the central and peripheral cornea was explained by a lamellar drop out in the anterior 2/3 of the stroma and suggested, that not all lamellae cross the cornea from limbus to limbus.
- The ALL is composed of randomly oriented collagen fibers but such a corneal layer was not present in the mouse. This is a significant structural variation between the human and the mouse.
- Due to the above stated difference in dimensions and ultratructure between the human and the applicability of the mouse cornea will depend on the research question being investigated.

Conjunctiva & dry eye:

- The mouse conjunctival epithelium had a structure similar to the human.
- There was no difference in number of goblet cells between the superior and inferior conjunctiva.
- The palpebral conjunctival epithelium decreased in thickness in the dry eye. This was associated with a loss of epithelial cells at the junction of the lid margin and the conjunctiva.
- The Vv (approximately 43%) and Sv of granules stayed concordant between the three groups (UT, DS5 and DS10).
- Goblet cell numbers differed depending on technique used. Suggesting that maybe there are different subtypes of goblet cells on the ocular surface.
- In the dry eye the surface access of the goblet cells appeared to be inhibited by the epithelium and this could possibly slow down the ascension of goblet cells towards the conjunctival surface.
- The mouse superior and inferior conjunctiva is an applicable model for human conjunctival and dry eye research.

UVR transmittance:

- The mouse had a transmittance cut off at 280 nm for the cornea and 310 nm for the crystalline lens, which was significantly different to the human where the cornea and the crystalline lens had cut offs at 290 nm and 390 nm respectively, allowing an increased transmittance of UVA and UVB to the retina.
- The mouse eye UVR transmittance renders it a less applicable model in regards to UVR research.

References in Numerical Order

1. Bron AJ, Tripathi RC, Tripathi BJ. The cornea and sclera. *Wolff's anatomy of the eye and orbit*. 8th ed. London, UK: Chapman & Hall Medical, 1997:233-67.

2. Doughty MJ, Zaman ML. Human corneal thickness and its impact on intraocular pressure measures: a review and meta-analysis approach. *Surv Ophthalmol* 2000;44(5):367-408.

3. Alberts B, Johnson A, Lewis J, Raff M, Roberts K, Walter P. Cell junctions, cell adhesion and the extracellular matrix In: Anderson MS, Dilernia B, editors. *Molecular biology of the cell* 4th ed. New York, NY: Garland Science, 2002:1065-127.

4. Bergmanson JP, Horne J, Doughty MJ, Garcia M, Gondo M. Assessment of the number of lamellae in the central region of the normal human corneal stroma at the resolution of the transmission electron microscope. *Eye Contact Lens* 2005;31(6):281-7.

5. Mathew JH, Bergmanson JP, Doughty MJ. Fine structure of the interface between the anterior limiting lamina and the anterior stromal fibrils of the human cornea. *Invest Ophthalmol Vis Sci* 2008;49(9):3914-8.

6. Nishida T. Cornea. In: Krachmer JH, Mannis MJ, Holland EJ, editors. *Cornea*. 2nd ed. Philadelpha, PA Elsevier Mosby, 2005:3-26.

7. Bergmanson JPG. Cornea. In: Bergmanson JPG, Managing editor: Krystal Shulle, editor. *Clinical Ocular Anatomy and Physiology* 18th ed. Houston, TX: Texas Eye Research and Technology Center, 2011:73-100.

8. Prince JH. The rabbit in eye research: Springfield, III., Thomas, 1964:86-134.

9. Smith RS, John SWM, Nishina PM, Sundberg JP. The anterior segment and ocular adnexae In: Smith RS, editor. *Systematic Evaluation of the Mouse Eye, Anatomy, Pathology and Biomethods*. Boca Raton, FL: CRC Press, 2002:3-24.

10. de la Cera EG, Rodriguez G, Llorente L, Schaeffel F, Marcos S. Optical aberrations in the mouse eye. *Vision Res* 2006;46(16):2546-53.

11. Smith RS, Korb D, John SW. A goniolens for clinical monitoring of the mouse iridocorneal angle and optic nerve. *Mol Vis* 2002;8:26-31.

12. Zhang EP, Schrunder S, Hoffmann F. Orthotopic corneal transplantation in the mouse--a new surgical technique with minimal endothelial cell loss. *Graefes Arch Clin Exp Ophthalmol* 1996;234(11):714-9.

13. Jester JV, Ghee Lee Y, Li J, Chakravarti S, Paul J, Petroll WM, et al. Measurement of corneal sublayer thickness and transparency in transgenic mice with altered corneal clarity using in vivo confocal microscopy. *Vision Res* 2001;41(10-11):1283-90.

14. Schulz D, Iliev ME, Frueh BE, Goldblum D. In vivo pachymetry in normal eyes of rats, mice and rabbits with the optical low coherence reflectometer. *Vision Res* 2003;43(6):723-8.

15. Song J, Lee YG, Houston J, Petroll WM, Chakravarti S, Cavanagh HD, et al. Neonatal corneal stromal development in the normal and lumican-deficient mouse. *Invest Ophthalmol Vis Sci* 2003;44(2):548-57.

16. Hazlett LD. Corneal and ocular surface histochemistry. *Prog Histochem Cytochem.* 1993;25(1):2.

17. Rehbinder C. Fine structure of the mouse cornea. *Z Versuchstierk* 1978;20:28-34.

18. Gerlach J, editor. *Von der Cornea. Handbuch der allegemeinen und speciellen gewebelehre des menschlichen körpers*. Mainz: Verlag von Eduard Janitsch, 1854.

19. Avitabile T, Marano F, Uva MG, Reibaldi A. Evaluation of central and peripheral corneal thickness with ultrasound biomicroscopy in normal and keratoconic eyes. *Cornea* 1997;16(6):639-44.

20. Blix M. Oftalmometriska studier, 1879-1880.

21. Gromacki SJ, Barr JT. Central and peripheral corneal thickness in keratoconus and normal patient groups. *Optom Vis Sci* 1994;71(7):437-41.

22. Lam AK, Douthwaite WA. The corneal-thickness profile in Hong Kong Chinese. *Cornea* 1998;17(4):384-8.

23. Prospero Ponce CM, Rocha KM, Smith SD, Krueger RR. Central and peripheral corneal thickness measured with optical coherence tomography, Scheimpflug imaging, and ultrasound pachymetry in normal, keratoconus-suspect, and post-laser in situ keratomileusis eyes. *J Cataract Refract Surg* 2009;35(6):1055-62.

24. Duke-Elder S, editor. *The eye. In: System of ophthalmology. The anatomy of the visual system*. St Louis, MO: Henry Kimpton, 1961.

25. Edelhauser H.F, Ubels JL, editors. *Adler's Physiology of the Eye*. 10th ed. St Louis, MO: CV Mosby, 2003.

26. Klyce SD, Beuerman RW, editors. *Structure and function of the cornea* 2nd ed. Boston, MA: Butterworth-Heinemann, 1998.

27. Thomas CI, editor. *The Cornea*. Springfield, IL: Charles C. Thomas, 1955.

28. Clareus F. Hornhinnans histologi. Upsala University, 1857.

29. Moller-Pedersen T, Ehlers N. A three-dimensional study of the human corneal keratocyte density. *Curr Eye Res* 1995;14(6):459-64.

30. Moller-Pedersen T, Ledet T, Ehlers N. The keratocyte density of human donor corneas. *Curr Eye Res* 1994;13(2):163-9.

31. Doughty MJ, Seabert W, Bergmanson JP, Blocker Y. A descriptive and quantitative study of the keratocytes of the corneal stroma of albino rabbits using transmission electron microscopy. *Tissue Cell* 2001;33(4):408-22.

32. Snyder MC, Bergmanson JP, Doughty MJ. Keratocytes: no more the quiet cells. *J Am Optom Assoc* 1998;69(3):180-7.

33. Cooper LJ, Bentley AJ, Nieduszynski IA, Talabani S, Thomson A, Utani A, et al. The role of dermatopontin in the stromal organization of the cornea. *Invest Ophthalmol Vis Sci* 2006;47(8):3303-10.

34. Alberts B, Johnson A, Lewis J, Raff M, Roberts K, Walter P. Intracellular vesicular trafficing. *Molecular biology of the cell*. 4th ed. New York, NY: Garland Science, 2002:711-66.

35. Johnson ME, Murphy PJ. Changes in the tear film and ocular surface from dry eye syndrome. *Prog Retin Eye Res* 2004;23(4):449-74.

36. Govindarajan B, Gipson IK. Membrane-tethered mucins have multiple functions on the ocular surface. *Exp Eye Res* 2010;90(6):655-63.

37. Macintosh SR. The innervation of the conjunctiva in monkeys. An electron microscopic and nerve degeneration study. *Albrecht Von Graefes Arch Klin Exp Ophthalmol* 1974;192(2):105-16.

38. Dartt DA, McCarthy DM, Mercer HJ, Kessler TL, Chung EH, Zieske JD. Localization of nerves adjacent to goblet cells in rat conjunctiva. *Curr Eye Res* 1995;14(11):993-1000.

39. No authors listed. The definition and classification of dry eye disease: report of the definition and classification subcommittee of the international dry eye workshop in: Report of the international dry eye workshop (DEWS). *The Ocular Surface* 2007;5(2):75-92.

40. Miljanovic B, Dana MR, Sullivan DA, Schaumberg DA. Prevalence and risk factors for dry eye syndrome among older men in the United States *Invest Ophthalmol Vis Sci* 2007;48:E-abstract 4293.

41. Schaumberg DA, Sullivan DA, Buring JE, Dana MR. Prevalence of dry eye syndrome among US women. *Am J Ophthalmol* 2003;136:318-26.

42. No authors listed. The epidermiology of dry eye disease: Report of the epidermiology subcommittee of the international dry eye workshop in: Report of the international dry eye workshop (DEWS) *The Ocular Surface* 2007;5(2):93-107.

43. Dursun D, Wang M, Monroy D, Li DQ, Lokeshwar BL, Stern ME, et al. A mouse model of keratoconjunctivitis sicca. *Invest Ophthalmol Vis Sci* 2002;43(3):632-38.

44. Hodges RR, Raddassi I, Zoukhri D, Toker A, Kazlauskas A, Dartt DA. Effect of overexpression of constitutively active PKCalpha on rat lacrimal gland protein sectretion. *Invest Ophthalmol Vis Sci* 2004;45(11):3974-81.

45. Stewart P, Chen Z, Farley W, Olmos L, Pflugfelder SC. Effect of experimental dry eye on tear sodium concentration in the mouse. *Eye Contact Lens* 2005;31(4):175-78.

46. Barabino S, Shen L, Chen L, Rashid S, Rolando M, Dana MR. The controlled-environment chamber: a new mouse model of dry eye. *Invest Ophthalmol Vis Sci* 2005;46(8):2766-71.

47. Chen W, Zhang X, Zhang J, Chen J, Wang S, Wang Q, et al. A murine model of dry eye induced by an intelligently controlled environmental system. *Invest Ophthalmol Vis Sci* 2008;49(4):1386-91.

48. Bron AJ, Tripathi RC, Tripathi BJ. The ocular appendages: eyelids, conjunctiva and lacrimal apparatus *Wolff's anatomy of the eye and orbit*. 8th ed. London, UK: Chapman & Hall Medical, 1997:30-84.

49. Argueso P, Balaram M, Spurr-Michaud S, Keutmann HT, Dana MR, Gipson IK. Decreased levels of the goblet cell mucin MUC5AC in tears of patients with Sjogren syndrome. *Invest Ophthalmol Vis Sci* 2002;43(4):1004-11.

50. Ralph RA. Conjunctival goblet cell density in normal subjects and in dry eye syndromes. *Invest Ophthalmol* 1975;14(4):299-302.

51. Walsh JE, Bergmanson JP, Koehler LV, Doughty MJ, Fleming DP, Harmey JH. Fibre optic spectrophotometry for the in vitro evaluation of ultraviolet radiation (UVR) spectral transmittance of rabbit corneas. *Physiol Meas* 2008;29(3):375-88.

52. Pitts DG, Kleinstein RN. Ocular effects of radiant energy. In: Pitts DG, Kleinstein RN, editors. *Environmental Vision: Interactions of the eye, vision and the environment*. Boston, MA: Butterworth-Heinemann, 1993:151-220.

53. Boettner EA, Wolter JR-. Transmission of the ocular media. *Invest. Ophthalmol.* 1962;1:776-83.

54. Cooper GF, Robson JG. The yellow colour of the lens of the grey squirrel (sciurus carolinensis leucotis). *J Physiol* 1969;203(2):403-10.

55. Cooper GF, Robson JG. The yellow colour of the lens of man and other primates. *J Physiol* 1969;203(2):411-7.

56. Williams GA, Jacobs GH. Cone-based vision in the aging mouse. *Vision Res* 2007;47:2037-46.

57. Brix F. Determination of the transmission of corneas in situ by means of extinction measurements. *Opthalmic Res* 1977;9:1-8.

58. Schive K, Kavli G, Volden G. Light penetration of normal and photokeratitis induced rabbit cornea. *Acta Ophthalmol. Scand. Suppl.* 1984;62:309-14.

59. Lei B, Yao G. Spectral attenuation of the mouse, rat, pig and human lenses from wavelengths 360 nm to 1020 nm. *Exp Eye Res* 2006;83:610-14.

60. Dillon J, Zheng L, Merriam JC, Galliard ER. Optical properties of the anterior segment of the eye: Implications for cortical cataract. *Exp. Eye Res.* 1999;68:785-95.

61. Doughty MJ, Bergmanson JP, Blocker Y. Shrinkage and distortion of the rabbit corneal endothelial cell mosaic caused by a high osmolality glutaraldehyde-formaldehyde fixative compared to glutaraldehyde. *Tissue Cell* 1997;29(5):533-47.

62. Henriksson JT, McDermott AM, Bergmanson JP. Dimensions and morphology of the cornea in three strains of mice. *Invest Ophthalmol Vis Sci* 2009;50(8):3648-54.

63. Luo L, Li DQ, Doshi A, Farley W, Corrales RM, Pflugfelder SC. Experimental dry eye stimulates production of inflammatory cytokines and MMP-9 and activates MAPK signaling pathways on the ocular surface. *Invest Ophthalmol Vis Sci* 2004;45:4293-301.

64. Howard CV, Reed MG, editors. *Unbiased Stereology Three-Dimensional Measurement in Microscopy.* Oxford, UK: BIOS Scientific Publishers Ltd 1998.

65. Gagen D, Laubinger S, Li Z, Petrescu MS, Brown ES, Smith CW, et al. ICAM-1 mediates surface contact between neutrophils and keratocytes following corneal epithelial abrasion in the mouse. *Exp Eye Res* 2010;91(5):676-84.

66. Petrescu MS, Larry CL, Bowden RA, Williams GW, Gagen D, Li Z, et al. Neutrophil interactions with keratocytes during corneal epithelial wound healing: a role for CD18 integrins. *Invest Ophthalmol Vis Sci* 2007;48(11):5023-9.

67. Ghezzo RH. An introduction to lung morphometry In: Hamid Q, Shannon J, Marin J, editors. *Physiologic Basics of Respiratory Disease.* Lewinston, NY: BC Decker Inc, 2005:769-75.

68. Walsh JE, Koehler LV, Fleming DP, Bergmanson JP. Novel method for determining hydrogel and silicone hydrogel contact lens transmission curves and their spatially specific ultraviolet radiation protection factors. *Eye Contact Lens* 2007;33(2):58-64.

69. Walsh JE, Kavanagh KY, Fennell S, Murphy J, Harmey M. Fibre optic micro-spectrometers for biomedical sensing. . *Trans. Meas. Sci.* 2000(22):355-69.

70. Bergmanson JP. Ocular light and ultraviolet radiation transmission. In: Bermanson JPGMeKS, editor. *Clinical ocular anatomy and physiology*. Houston, TX: Texas Eye Reserach and Technology Center, 2011:69-72.

71. Massof RW, Chang FW. A revision of the rat schematic eye. *Vision Res* 1972;12:793-96.

72. Reader AL, Salz JJ. Differences among ultrasonic pachymeters in measuring corneal thickness. *J Refract Surg* 1987;3(1):7-11.

73. Ward TS, Rosen GD, von Bartheld CS. Optical disector counting in cryosections and vibratome sections underestimates particle numbers: Effects of tissue quality. *Micros Res Tech* 2008;71:60-68.

74. Doughty MJ. Physiological state of the rabbit cornea following 4 degree C moist chamber storage. *Exp Eye Res* 1989;49:807-27.

75. Li HF, Petroll WM, Moller-Pedersen T, Maurer JK, Cavanagh HD, Jester JV. Epithelial and corneal thickness measurements by in vivo confocal microscopy through focusing (CMTF). *Curr Eye Res* 1997;16(3):214-21.

76. Chikama T, Wakuta M, Liu Y, Nishida T. Deviated mechanisms of wound healing in diabetic corneas. *Cornea* 2007;26 (suppl. 1):S75-S81.

77. Madigan M, Holden B. Reduced epithelial adhesion after extended contact lens wear correlates with reduced hemidesmosome density in cat cornea. *invest Ophthalmol Vis Sci* 1992;33(2):314-23.

78. Duke-Elder S, Wybar KC. The anatomy of the visual system. In: Duke-Elder S, editor. *The eye. In: System of ophthalmology* St Louis, MO: Henry Kimpton, 1961:92-131.

79. Bergmanson JPG. Corneal anatomy. In: Begmanson JPG, editor. *Clinical ocular anatomy and physiology*. Houston, TX: Texas Eye Research and Technology Center, 2008:67-94.

80. Hayashi S, Osawa T, Tohyama K. Comparative observations on corneas, with special reference to Bowman's layer and Descemet's membrane in mammals and amphibians. *J Morphol* 2002;254(3):247-58.

81. Watsky MA. Keratocyte gap junctionl communication in normal and wounded rabbit corneas. *invest Ophthalmol Vis Sci* 1995;36(13):2568-76.

82. Bergmanson JPG, Sheldon TM, Goosey JD. Fuchs' endothelial dystrophy: a fresh look at an aging disease. *Ophthal Physiol Opt* 1999;19(3):210-22.

83. Kuwabara T. Current consepts in anatomy and histology of the cornea. *Contact Intraocular Lens Med J* 1978;4:101-32.

84. Bergmanson JPG, Doughty MJ. Anatomy, morphology and electron microscopy of the cornea and conjunctiva. In: Benett E, Weissman BA, editors. *Clinical contact lens practice* Philadelphia, PA: Lippincott Williams & Wilkins, 2005:11-39.

85. Bettelheim FA, Plessy B. The hydration of proteoglycans of bovine cornea. *Biochim Biophys Acta* 1975;381(1):203-14.

86. Castoro JA, Bettelheim AA, Bettelheim FA. Water gradients across bovine cornea. *Invest Ophthalmol Vis Sci* 1988;29(6):963-8.

87. Cristol SM, Edelhauser HF, Lynn MJ. A comparison of corneal stromal edema induced from the anterior or the posterior surface. *Refract Corneal Surg* 1992;8(3):224-9.

88. Edelhauser HF. Endothelial and stromal response to injury: corneal biophysics workshop. *Corneal Biomechanics and Wound Healing NIH* 1989:191-94.

89. Ehlers N, Ehlers D. An apparatus for studies on explanted corneae. *Acta Ophthalmol (Copenh)* 1966;44(4):539-48.

90. Kikkawa Y, Hirayama K. Uneven swelling of the corneal stroma. *Invest Ophthalmol* 1970;9(10):735-41.

91. Lee D, Wilson G. Non-uniform swelling properties of the corneal stroma. *Curr Eye Res* 1981;1(8):457-61.

92. Van Horn DL, Doughman DJ, Harris JE, Miller GE, Lindstrom R, Good RA. Ultrastructure of human organ-cultured cornea. II. Stroma and epithelium. *Arch Ophthalmol* 1975;93(4):275-7.

93. Müller LJ, Pels E, Vrensen GF. The specific architecture of the anterior stroma accounts for maintenance of corneal curvature. *Br J Ophthalmol* 2001;85(4):437-43.

94. Chang SS, Maurice DM, Ramirez-Florez S. Quantitative measurement of corneal haze after myopic PRK. *J Refract Surg* 1996;12(3):412-6.

95. Ramirez-Florez S, Maurice DM. Inflammatory cells, refractive regression, and haze after excimer laser PRK. *J Refract Surg* 1996;12(3):370-81.

96. Meek KM, Tuft SJ, Huang Y, Gill PS, Hayes S, Newton RH, et al. Changes in collagen orientation and distribution in keratoconus corneas. *Invest Ophthalmol Vis Sci* 2005;46(6):1948-56.

97. Bron AJ. Keratoconus - the disease. *Brit J Contact Lens (Proceedings of the Ruben Symposium; London 1983* 1984;7:57-62.

98. Koller T, Seiler T. [Therapeutic cross-linking of the cornea using riboflavin/UVA]. *Klin Monbl Augenheilkd* 2007;224(9):700-6.

99. Wollensak G, Spoerl E, Seiler T. Riboflavin/ultraviolet-a-induced collagen crosslinking for the treatment of keratoconus. *Am J Ophthalmol* 2003;135(5):620-7.

100. McCall AS, Kraft S, Edelhauser HF, Kidder GW, Lundquist RR, Bradshaw HE, et al. Mechanisms of corneal tissue cross-linking in response to treatment with topical riboflavin and long-wavelength ultraviolet radiation (UVA). *Invest Ophthalmol Vis Sci* 2010;51(1):129-38.

101. Martola EL, Baum JL. Central and peripheral corneal thickness. A clinical study. *Arch Ophthalmol* 1968;79(1):28-30.

102. Bron AJ. The architecture of the corneal stroma. *Br J Ophthalmol* 2001;85(4):379-81.

103. Kokott W. Über mechanisch-funktionelle Strukturen des Auges. *A von Graefes Arch Ophthalmol* 1938;138:424-85.

104. Hogan MJ, Alvarado JA, Weddell JE, editors. *Histology of the Human Eye*. Philadelphia, PA: WB Saunders, 1971.

105. Bron AJ, Tripathi RC. The anterior corneal mosaic. *Br J Physiol Opt* 1970;25(1):8-13.

106. McTigue JW. The human cornea: a light and electron microscopic study of the normal cornea and its alterations in various dystrophies. *Trans Am Ophthalmol Soc* 1967;65:591-660.

107. Polack FM. Morphology of the cornea. I. Study with silver stains. *Am J Ophthalmol* 1961;51:1051-6.

108. Salzmann M, editor. *Anatomie und Histologie des menschlichen Augapfels im Normalzustande seine Entwicklung und sein Altern*. Vienna: Franz Deuticke Verlag, 1912.

109. Fine BS, Yanoff M, editors. *Ocular Histology: A Text and Atlas*. 2nd ed. New York/San Francisco/London: Harper and Row, 1979.

110. Maurice DM. The cornea and sclera In: Davson H, editor. *The Eye*. New York and London: Academic Press, 1969:489-600.

111. Meek KM, Blamires T, Elliott GF, Gyi TJ, Nave C. The organisation of collagen fibrils in the human corneal stroma: a synchrotron X-ray diffraction study. *Curr Eye Res* 1987;6(7):841-6.

112. Meek KM, Boote C. The organization of collagen in the corneal stroma. *Exp Eye Res* 2004;78(3):503-12.

113. Meek KM, Boote C. The use of X-ray scattering techniques to quantify the orientation and distribution of collagen in the corneal stroma. *Prog Retin Eye Res* 2009;28(5):369-92.

114. Newton RH, Meek KM. Circumcorneal annulus of collagen fibrils in the human limbus. *Invest Ophthalmol Vis Sci* 1998;39(7):1125-34.

115. Goldman JN, Benedek GB, Dohlman CH, Kravitt B. Structural alterations affecting transparency in swollen human corneas. *Invest Ophthalmol* 1968;7(5):501-19.

116. Müller LJ, Pels L, Vrensen GF. Novel aspects of the ultrastructural organization of human corneal keratocytes. *Invest Ophthalmol Vis Sci* 1995;36(13):2557-67.

117. Hamada R, Giraud JP, Graf B, Pouliquen Y. [Analytical and statistical study of the lamellae, keratocytes and collagen fibrils of the central region of the normal human cornea. (Light and electron microscopy)]. *Arch Ophtalmol Rev Gen Ophtalmol* 1972;32(8):563-70.

118. Morishige N, Wahlert AJ, Kenney MC, Brown DJ, Kawamoto K, Chikama T, et al. Second-harmonic imaging microscopy of normal human and keratoconus cornea. *Invest Ophthalmol Vis Sci* 2007;48(3):1087-94.

119. Morishige N, Takagi Y, Chikama TI, Takahara A, Nishida T. Three-Dimensional Analysis of Collagen Lamellae in the Anterior Stroma of the Human Cornea Visualized by Second Harmonic Generation Imaging Microscopy. *Invest Ophthalmol Vis Sci* 2010.

120. Daxer A, Fratzl P. Collagen fibril orientation in the human corneal stroma and its implication in keratoconus. *Invest Ophthalmol Vis Sci* 1997;38(1):121-9.

121. Sheppard J, Hayes S, Boote C, Votruba M, Meek KM. Changes in corneal collagen architecture during mouse postnatal development. *Invest Ophthalmol Vis Sci* 2010;51(6):2936-42.

122. Quantock AJ, Dennis S, Adachi W, Kinoshita S, Boote C, Meek KM, et al. Annulus of collagen fibrils in mouse cornea and structural matrix alterations in a murine-specific keratopathy. *Invest Ophthalmol Vis Sci* 2003;44(5):1906-11.

123. Aragona P, Puzzolo D, Micali A, Ferreri G, Britti D. Morphological and morphometric analysis on the rabbit conjunctival goblet cells in different hormonal conditions. *Exp Eye Res* 1998;66(1):81-8.

124. Doughty MJ, Bergmanson JPG. Heterogeneity in the ultrastructure of the mucous (goblet) cells of the rabbit palpebral conjunctiva. *Clin Exp Optom* 2004;87(6):377-85.

125. Micali A, Puzzolo D, Pisani A, Arco AM, Bruschetta D, Santoro G, et al. Ultrastructural study of the conjunctival epithelium in the Mongolian gerbil (Meriones unguiculatus). *Ophthalmic Res* 1998;30(4):244-54.

126. Latkovic S. The ultrastructure of the normal conjunctival epithelium of the guinea pig. IV. The palpebral and the perimarginal zones. *Acta Ophthalmol (Copenh)* 1979;57(2):321-35.

127. Micali A, Pisani A, Puzzolo D, Spinella R, Roszkowska A, Aragona P. Effect of Hypothyroidism on Postnatal Conjunctival Development in Rats. *Ophthalmic Res* 2010;45(2):102-12.

128. Setzer PY, Nichols BA, Dawson CR. Unusual structure of rat conjunctival epithelium. Light and electron microscopy. *Invest Ophthalmol Vis Sci* 1987;28(3):531-7.

129. Korb DR, Greiner JV, Herman JP, Hebert E, Finnemore VM, Exford JM, et al. Lid-wiper epitheliopathy and dry-eye symptoms in contact lens wearers. *CLAO J* 2002;28(4):211-6.

130. Korb DR, Herman JP, Blackie CA, Scaffidi RC, Greiner JV, Exford JM, et al. Prevalence of lid wiper epitheliopathy in subjects with dry eye signs and symptoms. *Cornea* 2010;29(4):377-83.

131. Aragona P, Micali A, Paladino G, Ferreri F, Puzzolo D. Effects of tear substitutes on conjunctival epithelium of mice. *Ophthalmic Res* 2007;39(5):265-75.

132. Greiner JV, Henriquez AS, Covington HI, Weidman TA, Allansmith MR. Goblet cells of the human conjunctiva. *Arch Ophthalmol* 1981;99(12):2190-7.

133. Plopper CG, St George JA, Nishio SJ, Etchison JR, Nettesheim P. Carbohydrate cytochemistry of tracheobronchial airway epithelium of the rabbit. *J Histochem Cytochem* 1984;32(2):209-18.

134. Uhlik J, Vajner L, Adaskova J, Konradova V. Effect of inhalation of single dose of beclomethasone on airway epithelium. *Ultrastruct Pathol* 2007;31(3):221-32.

135. Morroni M, Cangiotti AM, Guarino A, Cinti S. Unusual ultrastructural features in microvillous inclusion disease: A report of two cases. *Virchows Arch* 2006;448(6):805-10.

136. Ponce-Macotela M, Gonzalez-Maciel A, Reynoso-Robles R, Martinez-Gordillo MN. Goblet cells: are they an unspecific barrier against Giardia intestinalis or a gate? *Parasitol Res* 2008;102(3):509-13.

137. Dilly PN, Mackie IA. Surface changes in the anaesthetic conjunctiva in man, with special reference to the production of mucus from a non-goblet-cell source. *Br J Ophthalmol* 1981;65(12):833-42.

138. Srinivasan BD, Worgul BV, Iwamoto T, Merriam GR. The conjunctival epithelium II. Histochemical and ultrastructural studies on human and rat conjunctiva. *Ophthalmic Res* 1977;9:59-79.

139. Huang AJ, Tseng SC, Kenyon KR. Morphogenesis of rat conjunctival goblet cells. *Invest Ophthalmol Vis Sci* 1988;29(6):969-75.

140. Fujikawa A, Gong H, Amemiya T. Vitamin E prevents changes in the cornea and conjunctiva due to vitamin A deficiency. *Graefes Arch Clin Exp Ophthalmol* 2003;241:287-97.

141. Nichols BA, Chiappino ML, Dawson CR. Demonstration of the mucous layer of the tear film by electron microscopy. *Invest Ophthalmol Vis Sci* 1985;26(4):464-73.

142. Wanko T, Lloyd BJ, Jr., Matthews J. The fine structure of human conjunctiva in the perilimbal zone. *Invest Ophthalmol* 1964;3:285-301.

143. Kessing SV. Mucous gland system of the conjunctiva. A quantitative normal anatomical study. *Acta Ophthalmol (Copenh)* 1968:Suppl 95:1.

144. Paz HB, Tisdale AS, Danjo Y, Spurr-Michaud SJ, Argueso P, Gipson IK. The role of calcium in mucin packaging within goblet cells. *Exp Eye Res* 2003;77(1):69-75.

145. McKenzie RW, Jumblatt JE, Jumblatt MM. Quantification of MUC2 and MUC5AC transcripts in human conjunctiva. *Invest Ophthalmol Vis Sci* 2000;41(3):703-8.

146. Spurr-Michaud S, Argueso P, Gipson I. Assay of mucins in human tear fluid. *Exp Eye Res* 2007;84(5):939-50.

147. Howard CV, Reed MG. Concepts. *Unbiased stereology three-dimensional measuremt in microscopy*. Oxford, UK: BIOS Scientific Publishers Ltd, 1998:14-15.

148. Diebold Y, Rios JD, Hodges RR, Rawe I, Dartt DA. Presence of nerves and their receptors in the mouse and human conjunctival goblet cell sectetion. *invest Ophthalmol Vis Sci* 2001;42(10):2270-82.

149. Pitts DG, Kleinstein RN. The electromagnetic spectrum. In: Pitts DG, Kleinstein RN, editors. *Environmental Vision: Interactions of the eye, vision and the environment*. Boston, MA: Butterworth-Heinemann, 1993:87-136.

150. (CIE) --CIdE. Ultraviolet radiation: In CIE *CIE Publ. no. 17.4*. International lighting vocabulary, Geneva, 1987.

151. Chaney EK, Sliney DH. Re-evaluation of the ultraviolet hazard action spectrum--the impact of spectral bandwidth. *Health Phys* 2005;89(4):322-32.

152. Bova LM, Wood AM, Jamie JF, Truscott RJ. UV filter compounds in human lenses: the origin of 4-(2-amino-3-hydroxyphenyl)-4-oxobutanoic acid O-beta-D-glucoside. *Invest Ophthalmol Vis Sci* 1999;40(13):3237-44.

153. Bergmanson JPG, Sheldon TM. Ultraviolet radiation revisited. *CLAO J* 1997;23:196-204.

154. Cullen AP, Chou BR, Hall MG, Jany SE. Ultraviolet-B damages corneal endothelium. *Am J Optom Physiol Opt* 1984;61(7):473-8.

155. Doughty MJ, Cullen AP. Long-term effects of a single dose of ultraviolet-B on albino rabbit cornea--II. Deturgescence and fluid pump assessed in vitro. *Photochem Photobiol* 1990;51(4):439-49.

156. Pitts DG, Cullen AP, Hacker PD. Ocular effects of ultraviolet radiation from 295 to 365 nm. *Invest Ophthalmol Vis Sci* 1977;16(10):932-9.

157. Pitts DG, Bergmanson JP, Chu LW. Ultrastructural analysis of corneal exposure to UV radiation. *Acta Ophthalmol (Copenh)* 1987;65(3):263-73.

158. Bergmanson JP, Soderberg PG. The significance of ultraviolet radiation for eye diseases. A review with comments on the efficacy of UV-blocking contact lenses. *Ophthalmic Physiol Opt* 1995;15(2):83-91.

159. Widmark EJ. Über den Einfluss des Lichtes auf die Vorderen medien des Auge. *Scand Arch Physiol* 1889;1:264-80.

160. Widmark EJ. Über die Durchdringlichkeit der Augenmedien für Ultraviolette Strahlen. *Scand Arch Physiol* 1892;3:14-46.

161. Coroneo MT. Pterygium as an early indicator of ultraviolet insolation: a hypothesis. *Br J Ophthalmol* 1993;77(11):734-9.

162. McCarty CA, Fu CL, Taylor HR. Epidermiology of pterygium in Victoria, Australia. *Br J Ophthalmol* 2000;84:289-92.

163. Walsh JE, Bermanson J.P.G, Wallance D, Saidana G, Dempsey H, Mcevoy H, et al. Quantification of ultraviolet (UVR) radiation field in the human eye in vivo using novel instrumentation and the potential benefits of UVR blocking hydrogel contact lens. *Br J Ophthalmol* 2001;85:1080-85.

164. Mott R. A haplotype map for the laboratory mouse. *Nat Genet* 2007;39(9):1054-6.

165. Gorgels TG, van Norren D. Spectral transmittance of the rat lens. *Vision Res* 1992;32(8):1509-12.

166. Siebeck UE, Marshall NJ. Transmission of ocular media in labrid fishes. *Philos Trans R Soc Lond B Biol Sci* 2000;355(1401):1257-61.

167. Jacobs GH, Neitz J, Deegan JF, 2nd. Retinal receptors in rodents maximally sensitive to ultraviolet light. *Nature* 1991;353(6345):655-6.

168. Lyubarsky AL, Falsini B, Pennesi ME, Valentini P, Pugh EN, Jr. UV- and midwave-sensitive cone-driven retinal responses of the mouse: a possible phenotype for coexpression of cone photopigments. *J Neurosci* 1999;19(1):442-55.

169. Gouras P, Ekesten B. Why do mice have ultra-violet vision? *Exp Eye Res* 2004;79(6):887-92.

170. Löfgren S, Michael R, Ayala M, Söderberg PG. Does eye pigment and small pupil size protect agains UVR cataract. *Protection against the hazards of UVR*, 1999.

171. Ambach W, Blumthaler M, Schöpf T, Ambach E, Katzgraber F, Daxecker F, et al. spectral transmission of the optical media of the human eye with respect to keratitis and cataract formation. *Doc Ophthalmol* 1994;88:165-73.

172. Norren DV, Vos JJ. Spectral transmission of the human ocular media. *Vision Res* 1974;14(11):1237-44.

173. Smith RS, John SWM, Nishina PM, Sundberg JP. Selection of controls. In: Smith RS, editor. *Systematic evaluation of the Mouse Eye, Anatomy, Pathology and Biomethods*. Boca Raton, FL: CRC Press, 2002:77-80.

174. Smith RS, John SWM, Nishina PM, Sundberg JP. Ocular Development. In: Smith RS, editor. *Systematic Evaluation of the Mouse Eye, Anatomy, Pathology and Biomethods* Boca Ration, FL: CRC Press, 2002:45-63.

175. Lerman S. Susceptibility of ocular tissues to radiant energy. *Radiant enery and the eye*. New York, NY: MacMillian Publishing Co. Inc., 1980:29-114.

176. Bergmanson JPG. Ocular light and ultraviolet radiation transmission. In: Bergmanson JPG, editor. *Clinical Ocular Anatomy and Physiology*. 16th ed. Houston, TX: Texas Eye Research and Technology Center, 2009:63-66.

177. Pitts DG, Cameron LL, Jose JG, Lerman S, Moss E, Varma SD, et al. Optical radiation and cataracts. In: Waxler M, Hitchins VM, editors. *Optical Radiation and Visual Health*. Boca Raton, FL CRC Press, 1986:5-42.

178. Land MF, Nilsson D-E. Lens eyes on land. *Animal Eyes*. New York, NY: Oxford University Press, 2002:81-87.

179. Schmucker C, Schaeffel F. A paraxial schematic eye model for the growing C57BL/6 mouse. *Vision Res* 2004;44:1857-67.

180. Bergmanson JPG. Cornea. In: Bergmanson JPG, editor. *Clinical Ocular Anatomy and Physiology* 17th ed. Houston, TX: Texas Eye Research and Technology Center, 2010:69-96.

181. Muller LJ, Pels L, Vrensen GF. Novel aspects of the ultrastructural organization of human corneal keratocytes. *Invest Ophthalmol Vis Sci* 1995;36(13):2557-67.

182. Henriksson JT, Bergmanson JP, Walsh JE. Ultraviolet radiation transmittance of the mouse eye and its individual media components. *Exp Eye Res* 2010;90:382-87.

183. Desjardins C, Maruniak JA, Bronson FH. Social rank in house mice: differentiation revealed by ultraviolet visualization of urinary marking patterns. *Science* 1973;182(115):939-41.

184. Chavez AE, Bozinovic F, Peichl L, Palacios AG. Retinal spectral sensitivity, fur coloration, and urine reflectance in the genus octodon (rodentia): implications for visual ecology. *Invest Ophthalmol Vis Sci* 2003;44(5):2290-6.

Appendix A - Protocols in Alphabetical Order

Alcian blue (pH 2.50)

1. For paraffin-embedded tissue, remove paraffin with xylenes and hydrate through decreasing concentrations of alcohol as described in “paraffin removal from slides”.
2. Incubate slides in Acetic Acid for 3 minutes.
3. Incubate slide in Alcian Blue (pH 2.5) solution for 15 minutes at 31 degrees Celsius on the “long” hot plate.
4. Rinse briefly in Acetic acid solution to remove excess Alcian Blue.
5. Rinse for 2 minutes in running tap water followed by 2 changes of distilled water.
6. Stain slide in neutral fast-red solution for 5 minutes.
7. Rinse for 2 minutes in running tap water followed by two changes of distilled water.
8. Dehydrate in 2 x 1.5 minute changes of 95% alcohol.
9. Dehydrate in 2 x 1.5 minute changes of 100% alcohol.
10. Clear through 2 x 5 minute changes of xylene.
11. Mount with 1-2 drops of Permount and coverslip.

Immunohistochemistry(IHC) MUC5AC antibody (SC-20118 Santa Cruz)

1. For paraffin-embedded tissue, remove paraffin with xylenes and hydrate through decreasing concentrations of alcohol as described in “paraffin removal from slides”.

Heat induced antigen retrieval

2. Leave slide rack in tap water.
3. Add the antigen retrieval buffer solution: Sodium Citrate Buffer (10mM Sodium Citrate, 0.05% Tween 20, pH 6.0) 1000-1500 ml into the microwaveable vessel and place in the microwave.
4. Wait until the solution comes to a boil (approximately 5-10 minutes), add the slide rack with slides.
5. Boil for 20 minutes. The solution will evaporate, so make sure the vessel is big enough to hold enough buffer to keep the slides covered with solution at all times.
6. When 20 minutes has elapsed, remove the vessel and run cold tap water into it for 10 minutes.
7. Proceed to IHC.

IHC: MUC 5AC using NovaRed DAB.

1. 5 min Wash slides in PBS
2. 5 min Blot dry. Wax slides. Add PBS (5 min) **Never let the samples dry out!!!** Work slides 2 by 2. *Prepare blocking solution = (20% Goat).*
3. 10 min Incubate **EYES ONLY** in 0.3% H_2O_2 in PBS (quench endogenous peroxidases) Prepare 75mL of PBS + 0.75ml of 30% H_2O_2. Copplin jar.
4. 5 min Wash in PBS.

5. 10 min Apply 2 drops/section of Avidin block. Timer is counting up. Do not rinse. Aspirate it out.
6. 10min Apply 2 drops/section of Biotin block, work slides 2 by 2.
7. 3 min Rinse with PBS
8. 30 min, RT Block with 20% Goat serum in PBS. *Prepare 1° Antibody.*
9. Aspire it out the GS, blot around the tissue. Work slides 2 by 2.
10. 60 min, RTApply 1° Antibody in 5% Goat serum-PBS (or O/N, 4°C).
11. 5 min x 3Wash in PBS. *Prepare 2° Ab*
12. *Prepare Vectastain ABC Solution (to stand at RT at least for 30 min prior to use): 5ml PBS + 2 drops A +2 drops B*
13. Aspire it out the 1° Atb, blot around the tissue. Work slides 2 by 2.
14. 30 min, RT Apply 2° Antibody: see below (in 5% GS-PBS)
15. 3 min x 3 Wash in PBS.
16. 30 min Blot around tissue. Incubate in ABC reagent. Work slides 2 by 2.
17. 3 min x 3 Wash in PBS.
18. *Prepare DAB solution (NovaRed substrate kit, Vector, CN SK-4800, red stain) right before use: 5 mL* ***glass*** *ddH_2O + 3 drops Reagent 1 (mix) + 2 drops reagent 2 (mix) + 2 drops Reagent 3 (mix) + 2 drops* H_2O_2. **FRESH!!!!!**
19. Look at scope Blot around tissue. Add DAB solution to develop.
20. MUC 5AC:2 min. **THIS STEP IS CRUSIAL FOR TIME. MAKE SURE EXACTLY 2 MINUTES!!!!**
21. 1 x Terminate reaction with rinse in distilled H_2O in rack.
22. 5 min x 2 Wash in ddH_2O.

23. 2min Counterstain with Mayer's Hematoxylin

24. Rinse in tap H_2O in rack. This step is performed 4X in different beakers

25. 1 min x 2 95% EtOH

26. 1 min x 2 100% EtOH

27. 5 min x 1 Xylene (100%)

28. 5 min x 1 Xylene (100%)

29. Add 1-2 drops of Cytoseal solution (or permount) and attach 22x50 coverslip. Let it dry before using the microscope for at least 40~60 mins at room temperature, in a flat surface.

Antibody	Stock concentration	Exp conc	Ab + 5% GS-PBS
Rabbit α-human MUC 5AC (n=4)	SC-20118. Santa Cruz. 200ug/ml	1:200	2µL+ 398µL (=400 µL)
Biotin Goat α-rabbit (n=4)	BD Pharmingen CN 550338. 0.125mg/ml	0.5ug/mL (1:50)	8µL+ 392 µL (=400 µL)

Blocking solution: 20% Goat serum: 1 ml goat serum + 4 ml PBS. Can be stored at 4C for 2-3 weeks then throw out.

To make 5% GS- PBS: Take 1 ml from the 20% Goat serum and add 3 ml of PBS.

Important for the antibodies: Count how many individual sections that are going to be stained (normally 4 per slide). You need approximately 50-75 µl per section.

Depending how many sections that are being stained 400 µl might not be enough. It could be necessary to double or tripple the antibody recipe.

IgG control: Use normal rabbit serum instead of the 1º antibody and make sure to use the same concentration = (1:200).

Periodic acid schiff (PAS) stain (0.5%)

1. For paraffin-embedded tissue, remove paraffin with xylenes and hydrate through decreasing concentrations of alcohol as described in “paraffin removal from slides”.
2. Rinse in tap water 2 x 10 minutes.
3. Oxidize 10 minutes in 1% periodic acid.
4. Wash 5 minutes in running tap water.
5. Immerse 5 minutes in Schiff’s reagent.
6. Pass directly into 3 successive washes of 2 minutes each in 0.25% sodium meta-bisulfite (2.5g in 1000 ml H_2O).
7. Wash 10 minutes in running tap water.
8. Stain 90 seconds in acid hematoxylin.
9. Briefly rinse in two changes of H_2O.
10. Counter stain 1 minute in 1% aqueous Orange G (2g in 200 ml H_2O).
11. Water wash 10 dips.
12. Dehydrate in 2 x 1.5 minute changes of 95% alcohol.
13. Dehydrate in 2 x 1.5 minute changes of 100% alcohol.
14. Clear through 2 x 5 minute changes of xylene.
15. Mount with 1-2 drops of Permount and coverslip.

Removal of paraffin from slides

	Solvent	Repetition x Duration
1.	Xylene	3 X 5 minutes
2.	100% Ethanol	2 X 3 minutes
3.	95% Ethanol	2 X 3 minutes
4.	80% Ethanol	2 X 3 minutes
5.	70% Ethanol	2 X 3 minutes

6. Rinse in running tap water for 5 minutes.

Uranyl acetate (3.5%) and Reynold's lead citrate staining

1. Put copper grids in small tubes, (3-4 grids per tube).
2. Cover grids with uranylacetate.
3. Put the small tubes with grids in the oven at 60 degrees Celsius for 20 minutes.
4. Rinse grids with distilled water with pipette 4 times.
5. Keep rinsing with distilled water by putting grids in a beaker. Rinse 4-5 times.

Make CO2 free chamber

1. Use paraffin paper to make wells, (3-4 grids per well).
2. Put lead citrate into these wells.
3. Add sodium hydroxide to make CO2 free chamber.
4. Let chamber sit for about 5 minutes.
5. Dab grid on filter paper, (non section side towards the paper).
6. Put grids in CO2 free chamber, section side down.
7. Leave grids in chamber for 10 minutes.
8. Rinse 3-4 times in a beaker with distilled water.
9. Dab grid on filter paper and put back.